TASK RELATED NEUROMAGNETIC ACTIVITY UNDERLYING THE VISUAL PERCEPTION OF VELOCITY CHANGE: A MEG STUDY

SHENG HUA WANG

A THESIS SUBMITTED TO THE FACULTY OF GRADUATE STUDIES
IN PARTIAL FULFILMENT OF THE REQUIREMENTS
FOR THE DEGREE OF
MASTER OF ARTS

GRADUATE PROGRAM IN PSYCHOLOGY
YORK UNIVERSITY,
TORONTO, ONTARIO

SEPTEMBER 2011

Library and Archives Canada

Published Heritage Branch

395 Wellington Street
Ottawa ON K1A 0N4
Canada

Bibliothèque et Archives Canada

Direction du Patrimoine de l'édition

395, rue Wellington
Ottawa ON K1A 0N4
Canada

Your file Votre référence
ISBN: 978-0-494-91758-9

Our file Notre référence
ISBN: 978-0-494-91758-9

TASK RELATED NEUROMAGNETIC ACTIVITY UNDERLYING THE VISUAL PERCEPTION OF VELOCITY CHANGE: A MEG STUDY

by **Sheng Hua Wang**

By virtue of submitting this document electronically, the author certifies that this is a true electronic equivalent of the copy of the dissertation approved by York University for the award of the degree. No alteration of the content has occurred and if there are any minor variations in formatting, they are as a result of the conversion to Adobe Acrobat format (or similar software application).

Examination Committee members:
1. Joseph F.X. DeSouza
2. Mazyar Fallah
3. J. Douglas Crawford
4. Denise Y. P. Henriques

ABSTRACT

In the first part of this project, we showed moving dots to subjects to investigate whether the fast and slow velocity would trigger different spatial and temporal dynamics in the brain signals. In the second part, we increased or decreased velocity of the moving dots and asked the subjects to report the perceived velocity change with button press. We intended to use this paradigm to investigate the decision-making processing, namely when and where in the brain a visual perception is transformed into the signal for motor responses. When examining the visual motion evoked fields (VEF), we found that the cuneus activated earlier than the V3A and MT+ sources with significantly higher amplitude. However, the motion velocity had no effect on spatial and temporal dynamics. When exploring the signals underlying the decision-making process, we found that only the correct response trials showed frontoparietal activations after the velocity change. Furthermore, in the correct trials, the parietal sources demonstrated significantly more β band event related desynchronizaiton (ERD) from 200 to 400 ms after the velocity change. In addition, the sensorimotor sources also showed significantly more β band ERD in the correct responses after the velocity change, and this ERD increased its amplitude after 400 ms. The parietal β band ERD from 200 to 400 ms reflects the process of sensory evidence accumulation before the selection of a response, and the increased sensorimotor ERD after 400 ms implies the motor command for a response is prepared after the decision is made.

Table of Contents

List of Figures

List of Tables

List of Appendices

Introduction - Part 1

Motion Velocity and Motion Perceptions

Vision is an important sense upon which our impressions about the world are formed, and our memories, imaginations, and even illusions rely heavily on vision. Among various aspects of visual perceptions, understanding motion is crucial not only for daily life, but also for the survival of an organism. For example, a fast approaching object from the periphery often signals an imminent danger (e.g. a truck or a predator) and a quick decision for a reaction substantially increases the chance of survival for an organism (e.g. not get run over by the truck or killed by the predator). In contrast, lesions to the motion processing regions severely impair one's capability to perceive motion stimuli and to perform visuomotor tasks (Billino, Braun, Bohm, Bremmer, & Gegenfurtner, 2009; Haarmeier, Thier, Repnow, & Petersen, 1997). From the perspective of neuroscience, visual motion perception is a process of inferring the speed and direction of moving objects in a visual scene which involves multiple cortical areas including parietal, temporal, and frontal regions as well as multiple subcortical structures of the brain (Boussaoud, Ungerleider, & Desimone, 1990; Maunsell & Newsome, 1987). In this thesis, my first research question concerns the velocity-dependent motion perception. Therefore, I will begin by reviewing the visual system and the neural pathways for conveying and processing the visual motion stimulus. I will also

cover the important components of the motion perception pathways such as the MT+ and empirical evidence on velocity-dependent perception.

The Visual System and the Visual Pathways

One main function of the visual system is to process the attended visual stimulus by transforming information from light into an internal representation of objects and their context for the guidance of action. The importance of the visual system can be reflected by its large cortical representation. For example, over half of the neocortex of the macaque monkey is devoted to processing visual information (Van Essen & Gallant, 1994) (see Figure 1). The processing of the visual information starts in the retina where a dynamic view is transduced to neuronal signals by the retinal photoreceptors and the relevant information is conveyed to multiple visual areas in the brain for further processing. These neuronal signals include different features of vision such as form, color, depth, and motion. The visual system contains parallel pathways for processing various visual information, and all the pathways begin with the retinal photoreceptors that project onto bipolar or amacrine cells, which in turn synapse on retinal ganglions cells (for a review see Merigan & Maunsell, 1993). It has been suggested that different sets of the visual signals that transduced in the retina remain separated up to the highest levels of the visual cortex through these pathways (considering the importance of the photoreceptors in visual perception, I shall discus them in more detail in the following subsection). Moreover, the retinal ganglion cells can be physiologically categorized into various types according to their receptive field

properties. A group of ganglion cells has been recently reported to respond to light spots moving in specific direction within their receptive field, and the cholinergic amacrine cells are thought be the key input to these direction-selective ganglion cells (Borg-Graham, 2001; Fried, Münch, & Werblin, 2002). The axons of the ganglions cells form the optic nerve and project to different layers in the lateral geniculate nuclei (LGN) in the thalamus, which in turn project into the primary visual cortex (V1) and other extrastriate and subcortical areas.

In humans and other primates, the LGN contains six layers of cell bodies separated by intralaminar layers of axons and dendrites. The layers are numbered from 1 to 6 from ventral to dorsal. Axons of the magnocellular (M) and parvocellular (P) retinal ganglion cells remain segregated in the lateral geniculate nucleus (LGN). The two most ventral layers of the nucleus, the magnocellular layers, contain relatively large cells and their major input is from parasol retinal ganglion cells. The four dorsal layers in LGN are known as the parvocellular layers and receive input from the midget retinal ganglion cells. Both the magnocellular and parvocellular layers include on- and off-center receptive field (RF) cells, which are similar to the on- and off-center ganglion cells in the retina. The importance of the M and P pathways within the visual pathways can be inferred from the fact that they are comprised of approximately 90% of retinal axonal output (Silveira & Perry 1991) and that little vision remains when these pathways are selectively lesioned (Schiller, Logothetis, & Charles, 1990).

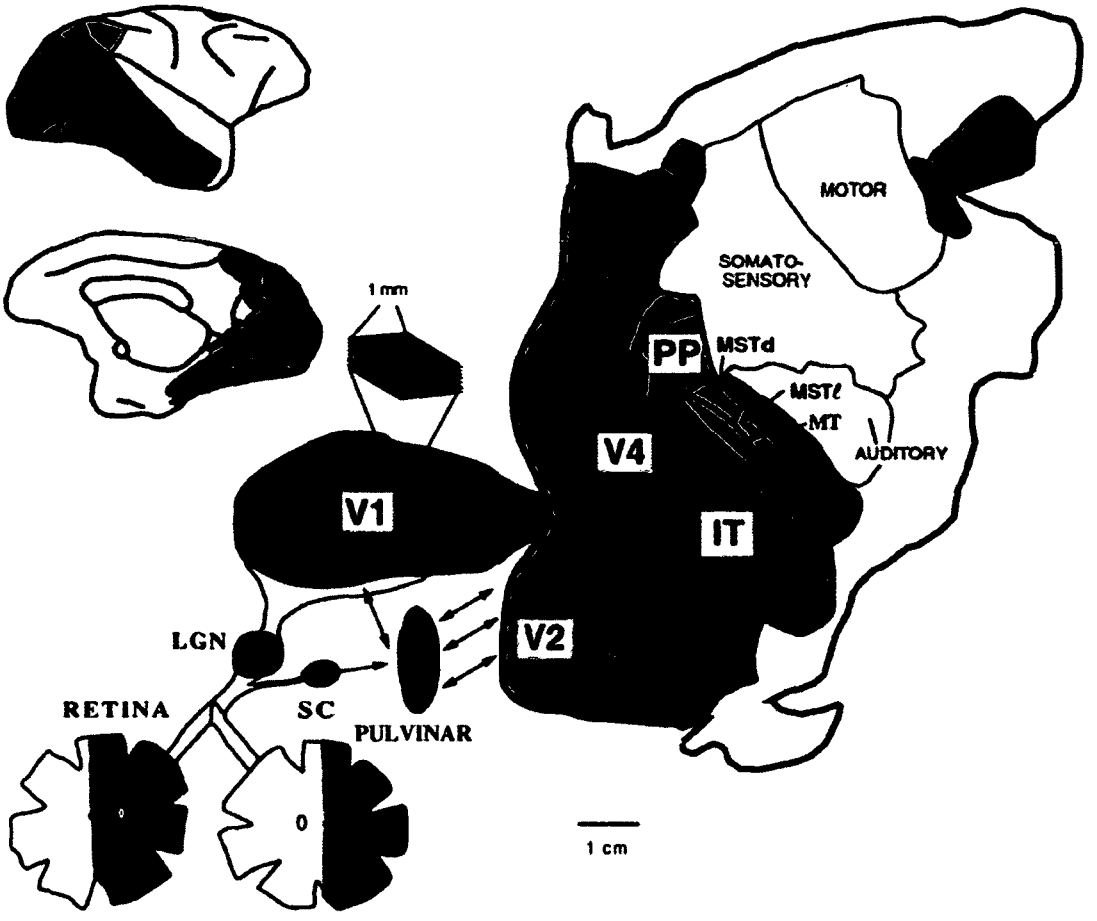

Figure 1. Schematic drawing showing the mapping from the right hemi-retinal to the right V1 cortex as well as subcortical and some of the extrastriate cortex in the macaque monkeys. For simplicity, only some regions of the visual system are shown here. The blobs, interblobs zones, and layer 4B in V1 are coloured as blue, green, and red respectively. In V2, red, blue, and green areas stand for thick and thin stripes, and interstripes zones. (Van Essen & Gallant, 1994).

The primary visual cortex (V1) consists of six layers of cells, and the principal layer for receiving inputs from the LGN is layer 4, which can be further divided into four sublaminae as 4A, 4B, $4C_{\alpha}$, and $4C_{\beta}$ (Lund, 1988). Like the LGN and superior colliculus, the primary visual cortex in each cerebral hemisphere receives information exclusively from the contralateral half of the visual field. Beyond V1 lie the extrastriate cortices for specific feature processing. Based on anatomical and

functional evidence, along with lesion studies, it has been proposed that the extrastriate visual areas in monkeys are organized into the dorsal "where" pathway and the ventral "what" pathway (Mishkin & Ungerleider, 1982). This "what" and "where" model was later modified by Goodale and Milner (1992) in which they proposed that the ventral and dorsal streams are specialized in processing "perception" and "action" signals respectively. The motion signals are processed in the dorsal pathway which starts in V1 and extends to the middle temporal and the parietal cortices. In addition, the dorsal pathway is also sensitive to depth, spatial locations, and is mostly involved in the sensorimotor transformations for visually guided actions directed at objects. To better understand motion perception in the visual system, it is important to look at the retina where the neuronal signals for various visual features begin to differentiate.

Visual Signals in the Retina

Visual signal processing begins in the retina when light passes through the cornea and is projected onto the back of the eye, where it is transduced into an electrical signal by the retina (for a review see Lagnado & Baylor, 1992). There are two types of photoreceptors: rods and cones. The human retina contains approximately 7 million cones and 120 million rods. The cones are concentrated in the foveal region which covers approximately two degrees of the visual field (Fairchild, 2005; Horton & Hoyt, 1991), whereas the rods are dominant in the retinal periphery. The size and shape of the foveal and peripheral visual field are shown in Figure 2. Cones and rods are different in several aspects. Cones require

significantly brighter light than the rods in order to produce outputs, and so they are much less active than the rods in dim light. Cone-mediated foveal vision is of higher acuity than rod-mediated vision of the visual periphery and provides better temporal resolution of changes in visual images (i.e. performs better in detecting slow motion). On the other hand, rods work better than cones in detecting visual stimulus in dim light because they contain more photosensitive pigment than the cones and thus a small number of photons can evoke a response in a rod. Moreover, the rod system is highly convergent that many rods synapse onto one target interneuron (bipolar cell), and this spatial summation of the input amplifies the input thereby increasing the possibility of detecting a stimulus in dim light.

Between the photoreceptors and the ganglion cells, there are three types of interneurons (bipolar, horizontal, and amacrine cells), and the axons of the ganglion cells form the optic nerve, namely the major output of the retina. Although there are at least five types of ganglion cells, two are essential to forming the major visual pathways. They are the parvocellular (P) ganglions that project to the P layers of the lateral geniculate neuclei (LGN), and the parasol retinal ganglions that project to the M layers of the LGN (Figure 3). The majority of the cells in the LGN P layers receive inputs from the midget ganglion cells, each of which is linked to one cone through one midget bipolar cell (Hugh, Edward, & Perkins, 2008). On the other hand, the M ganglions receive inputs from many rods and cones, and they have fast conduction velocity. Because of the input convergence, the M ganglions have much larger receptive fields.

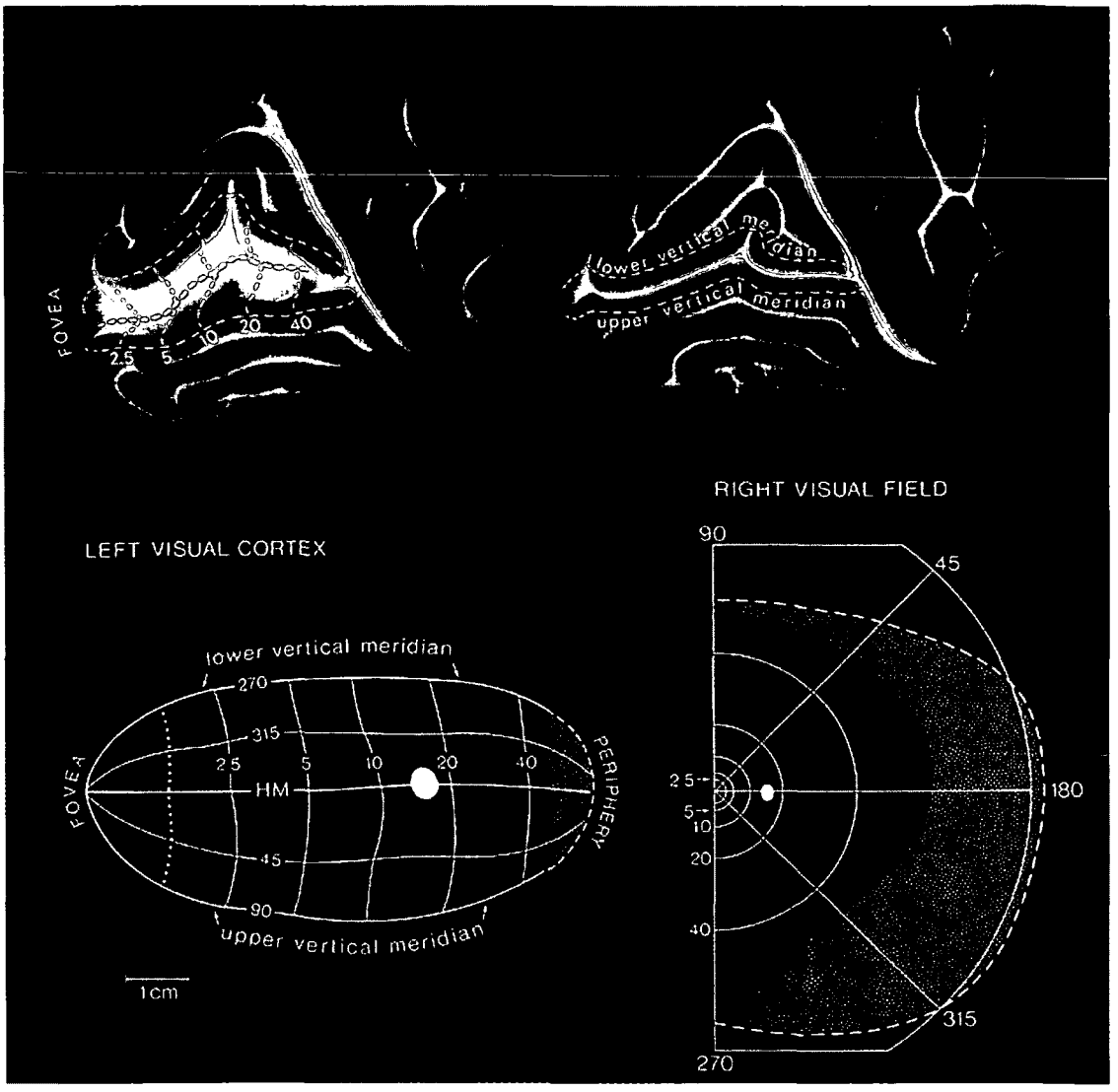

Figure 2: Retinotopic map of the human striate cortex. Upper right shows left occipital lobe with most part of the primary visual cortex buried in the Calcarine fissure. Upper left shows the fissure is opened and overlaid with an eccentricity map of the visual field (in degrees) with regard to the foveal region. The horizontal meridian (HM) lies along the base of the Calcarine fissure. Lower left is the flattened map with dotted line depict occipital pole. The central 1° of the visual field is located on the lateral convexity with some possible individual variability. The oval area on the HM line is a proximal size of the blind spot, and stippled zone corresponds to the monocular crescent. (Horton & Hoyt, 1991).

An important notion for understanding motion stimulus' effects on the retina is the receptive field (RF) of the ganglion cells (for a review see Schiller, 1992). A ganglion cell's RF is determined by the area of the retina that the ganglion cell monitors, and the shape of the RF is proven roughly circular. The RF of the most ganglion cells can be divided into a circular RF center, and a surrounding area of the center. The ganglion cells can be categorized by their responses to a small spot of light applied to their RF. The on-center ganglion cells are excited when light is shed into the center of their RF, and they are inhibited if light applied to the surround of the RF. The off-center ganglion cells are inhibited by shedding light into the center of the RF, but the firing rate will increase for a short period of time after the central light disappears. The off-center ganglions are also excited when light is applied to the surround of their RF.

Thus, when a small moving light spot passes through the RF center of a ganglion cell, it would evoke one or two burst of signals depending on the type of the ganglion cell: (A) when the light spot enters the surrounding area of the RF of an on-center ganglion cell, the increase of the luminance will inhibit the cell. The cell will be excited after the light spot enters the center, and will be inhibited again when the light spot exits its RF center. (B) When the light spot enters the surrounding area of the RF of an off-center ganglion cell, it will excite the cell. The cell will be inhibited after the dot enters the surround, and will be excited again when the light dot leaves the RF center. Therefore, when a field of light dots moves through the RF of a ganglion cell, it will produce a train of signal

resembling the pattern described above depending on the cell type. Furthermore, different motion velocity will influence the duration of the bursts and the interval between the bursts. Thus, the difference in motion speed will influence the output dynamics of the retinal ganglions.

The Magnocellular (M) and Parvocellular (P) Pathways

In the previous section, we discussed that the P ganglions, which correspond to the foveal vision, project to the P layers in the LGN, whereas the M ganglions, which correspond to peripheral vision, project to the M layers of the LGN (Figure 3). Hence, the visual information highway from the retina to the visual cortices is composed of the magnocellular (M) and parvocellular (P) pathways. The M and P pathways relay at the corresponding layers in the LGN before feeding into the striate and extrastriate cortex (Shapley & Perry, 1986; Silveira & Perry, 1991). In the current study, the motion stimuli were displayed in the visual periphery, thus, the motion signals would be mostly processed in the M pathway. To provide a better understanding of the constituent features of the visual pathways, I shall briefly discuss the M and P pathways.

Evidence from anatomical and physiological studies has suggested a direct correspondence between the M and P pathways and the dorsal and ventral pathways (Livingstone & Hubel 1987; Maunsell, 1987). It has been shown that the M and P pathways remain largely segregated in the visual cortex, and each dominates one of the cortical pathways as the M pathway and the dorsal pathway form one subsystem, and the P pathway and the ventral pathway form the other

(Figure 3). Specific visual information, such as motion, depth, colour, and form, is transmitted and processed in a specific subsystem (for a review see Merigan & Maunsell, 1993). Physiologically, the P and M pathways are very different that the P pathway is much more sensitive to colour and high spatial frequencies due to the high cell density of the cones in the fovea (Kulikowski, Robson, & Murray, 2002). On the other hand, the M pathway is faster in signal conducting speed and much more sensitive to moving stimuli, low luminance and contrast (Gouras 1969; Kaplan & Shapley 1982; Schiller & Malpeli 1978). Furthermore, the contrast sensitivity of M cells is typically many times that of P cells. P cells rarely respond well to luminance contrasts below 10%, whereas M cells often respond to stimuli with contrasts as low as 2% (Purpura, Kaplan, & Shapley, 1988; Sclar, Maunsell, & Lennie, 1990; Shapley, Kaplan, & Soodak, 1981). In addition, M pathway are often reported to be responsive to higher temporal and lower spatial frequencies than P pathway (Derrington & Lennie, 1984; Hicks, Lee, & Vidyasagar, 1983).

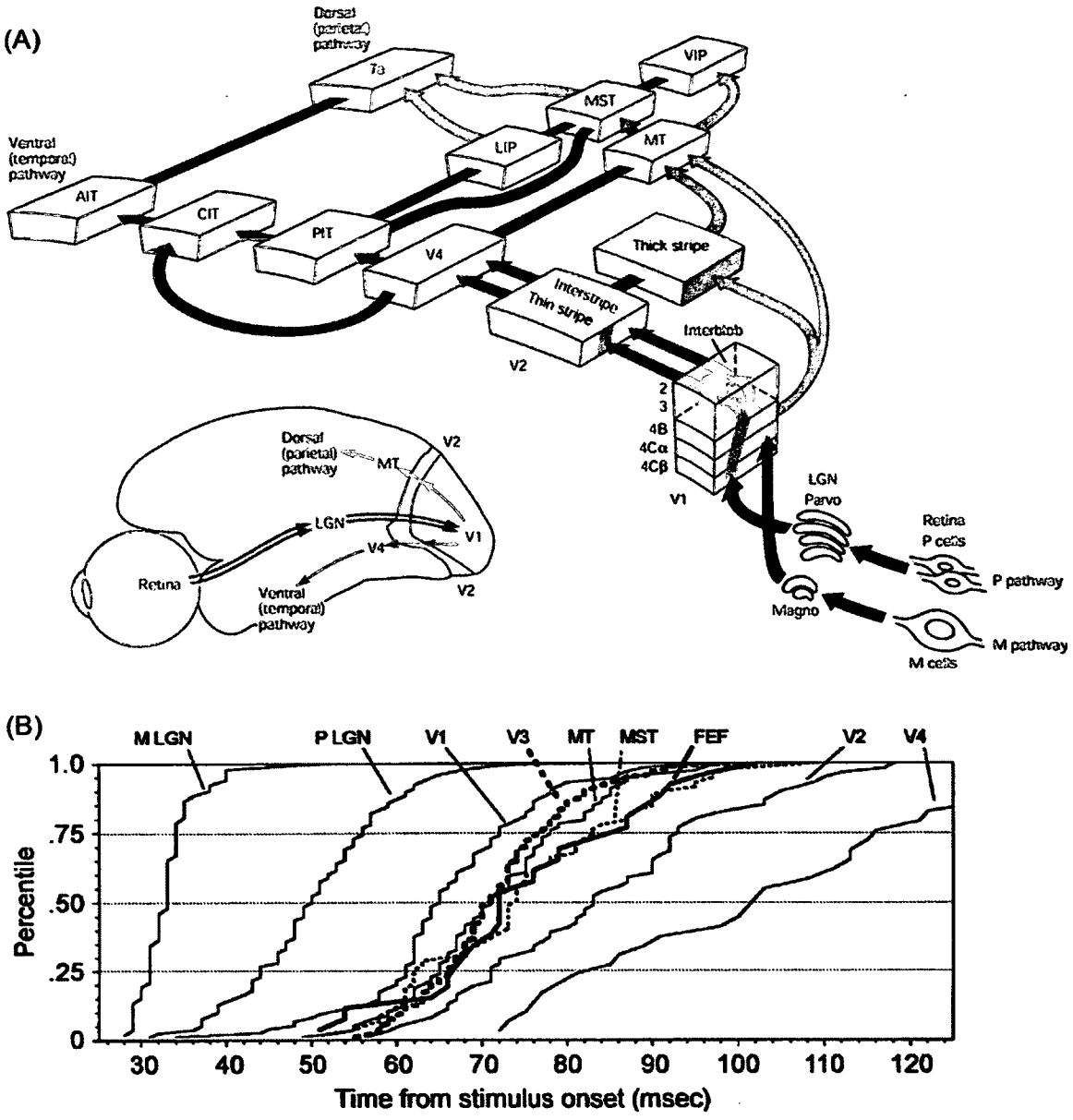

Figure 3. (A) The M and P pathways arise from the retinal ganglions and directly project to V1 and some extrastriate areas after relaying at LGN. The two pathways remain mostly separated in the visual cortex with some interconnection occurs in several temporo-parietal sub-regions. AIT: anterior inferior temporal area; CIT: central inferior temporal area; LIP: lateral intraparietal area; Magno: magnocellular layers of the LGN; MST: medial superior temporal region; MT: middle temporal region; Parvo: parvocellular layers of the lateral geniculate nucleus; PIT: posterior inferior temporal area; VIP: ventral intraparietal area. (Kandel et al., 2000). (B) The accumulative distribution of percentiles of the neuron population that started to respond to a visual stimulus were plotted against time from the stimulus onset. M LGN: magnocellular layers in the LGN. P LGN: parvocellular layers in the LGN. (Schmolesky et al., 1998).

All these aforementioned properties make the M pathway a preferable route for fast changing motion signals. Evidence supporting this idea can be found in a lesion study by Merigan, Byrne, and Maunsell (1991). They reported that the selective lesion to the M pathway causes a dramatic decrease in luminance contrast sensitivity for stimuli of higher temporal frequency and lower spatial frequency, which results in a reduced perception of rapidly moving or rapidly flickering stimuli. This result indicated that the dorsal pathway to the MT and the parietal cortices included a predominance of M pathway inputs (Figure 4).

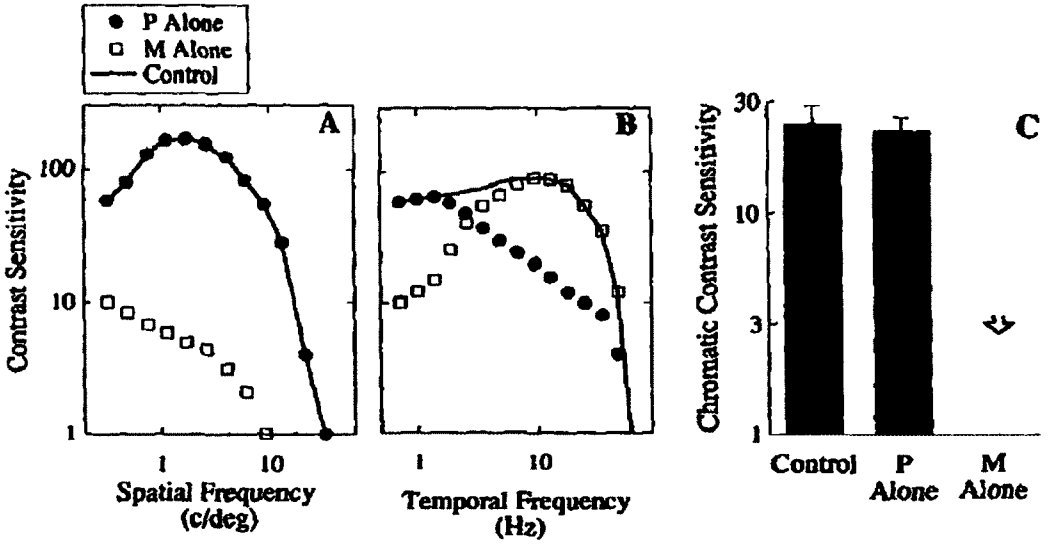

Figure 4. The contrast sensitivity after selective lesions to the P and M pathways. Contrast sensitivity is the inverse of the lowest stimulus contrast that can be detected by the animal. In (A) and (B), the solid line shows sensitivity of the intact monkey (control). Filled circles show the contribution of the P pathway in task (lesion to the M pathways). Boxes show the contribution of the M pathway in the task (lesion to the P pathway). Temporal contrast sensitivity was measured at a low spatial frequency. (C) shows the colour contrast sensitivity was severely impaired in animals that had lesion to the P pathway. (Merigan et al, 1991).

Although evidence has shown that the M and P pathways are not functionally

exclusive of each other, whether there are cross connections that allow one cortical pathway to modulate activity in the other is still not clear. However, the M pathway has been suggested to play a crucial role in orienting visual attention (Egeth & Yantis,1997; Khoe, Mitchell, Reynolds, & Hillyard, 2005; Steinman, Steinman, & Lehmkuhle, 1997), in visual searching tasks (Cheng, Eysel, & Vidyasagar, 2004), and neglect patients are shown more impaired in processing visual information of the M pathway (Harvey et al., 2006; Pitzalis, Di Russo, & Spinelli, 2005).

Direct Pathways to MT

Besides the input of M and P pathways to the motion-selective region MT, it has been recently proposed, albeit still under considerable debate, that there are two direct thalamic inputs that bypass V1 and feed information into MT in nonhuman primates (Warner, Goldshmit , & Bourne, 2010). These pathways are speculated to account for the residual visual capability following the lesions to the M and P pathway or to V1. One of these two direct pathways is relayed through the medial portion of the inferior pulvinar nucleus (Adams, Hof, Gattass, Webster, & Ungerleider, 2000; Cusick, Scripter, Darensbourg, & Weber, 1993; Lin and Kaas, 1980; Stepniewska, Qi, & Kaas, 1999) and the other is the retino-thalamic-cortical direct pathway from LGN to MT, in which the constituent neurons were found to be mostly koniocellular cells (Nassi, & Callaway, 2006; Sincich, Park, Wohlgemuth, & Horton, 2004). Sincich et al. (2004) reported that the koniocellular cells in this pathway send almost no collateral axons to V1 and are equivalent to

approximately 10% of the V1 projection to MT. They suggested that, although the functional role of this direct pathway was still unclear, the koniocellular pathway might account for the residual motion perception after V1 lesions.

The Pulvinar

In addition to the cortical ventral and the dorsal stream, another important visual pathway involves the thalamic pulvinar nuclei that has been postulated for visual attention, perception, eye movements, and actions (for a review see Grieve, Acuna, & Cudiero, 2000; Shipp, 2003; Stepniewska, 2003). The pulvinar and the LGN together constitute the thalamic complex of the visual system (although the pulvinar is also involved in other sensory modalities), and the pulvinar is especially found to be well-developed and differentiated into distinct nuclei in humans and other primates. Anatomically, the pulvinar lies posterior, medial, and dorsal to the LGN, and covers the underlying superior colliculus (SC) and forms a larger and more diffuse mass around the brachium of the SC. At the cellular level, the pulvinar is similar to the LGN in that it is mainly composed of relay neurons and interneurons (Ogren & Hendrickson, 1979; Wong-Riley, 1972). The majority of the input to the pulvinar comes from the cortex and the only output from the pulvinar projects back to the cortex (Figure 5). Therefore, the pulvinar is often regarded as an "associative" thalamic nucleus (Sherman & Guillery 1996). The medial and anterior (oral) pulvinar is involved mainly in multisensory and somatosensory functions. More relevant to my research interest in motion processing for a motor response, I shall discuss the ventral and posterior part of

the pulvinar, also known as the "visual pulvinar".

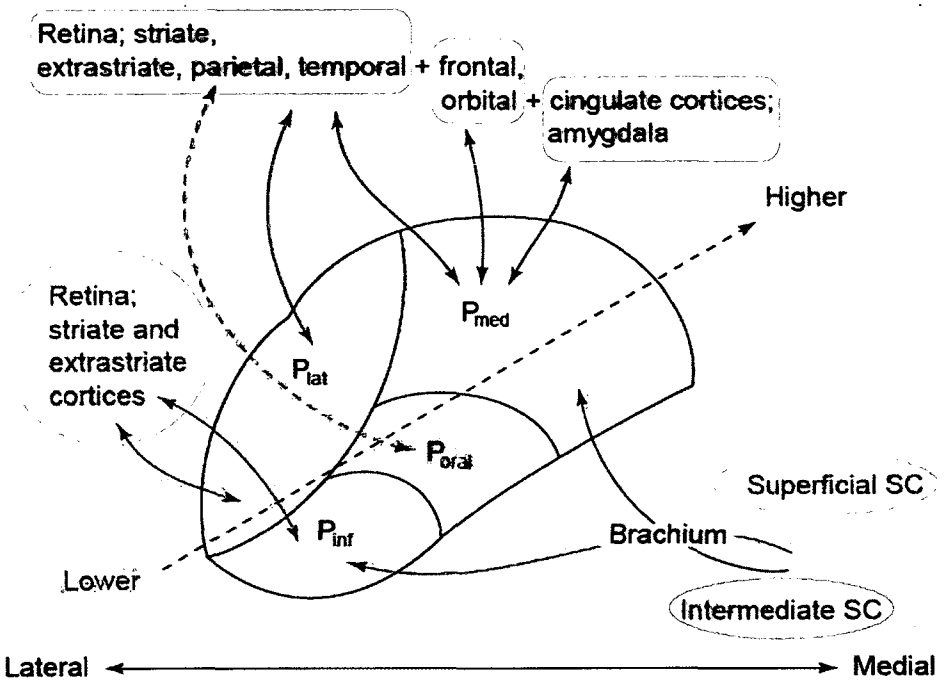

Figure 5. Schematic drawing of major cortical and sub-cortical connections with the pulvinar nuclei. The sub-divisions in the inferior and lateral pulvinar are thought to be retinotopically organized. P_{inf}: inferior pulvinar; P_{lat}: lateral pulvinar; P_{med}: medial pulvinar; P_{oral}: oral pulvinar; SC: superior colliculus. (Grieve et al., 2000)

The "visual" pulvinar consists of the medial, lateral and inferior pulvinar nuclei, which is demarcated by the reciprocal connections to the visual cortices and the superior colliculus (Itaya & Van Hoesen 1983; Kaas & Lyon, 2007; Nakagawa & Tanaka 1984; O'Brien et al. 2001). There is also retinal input to the pulvinar, but it is not as substantial compared to the LGN. Evidence has shown that the visual pulvinar plays an important role in the motion perception. Three distinct fields of connection between the ventral pulvinar and the cortical motion-sensitive area V5/MT have been identified (Ungerleider, Desimone, Galkin, & Mishkin, 1984). A recent study on non-human primate found that the pulvinar neurons output to MT

had similar activation pattern to the neurons receiving SC inputs, whereas those receiving input from MT frequently showed directional selectivity as does MT (Berman & Wurtz, 2008). Villeneuve, Kupers, Gjedde, Ptito, & Casanova (2005) also revealed a significant activation of the pulvinar in the coherent motion condition supporting the notion that the human pulvinar is functionally connected to MT+ and involved in higher-order motion processing such as plaid pattern. Furthermore, the thalamus and in particular the pulvinar are thought to be the necessary components of the computational network subtending complex motion integration, and all levels of motion processing have been described in the pulvinar (Villeneuve et al., 2005). Because of its extensive connection with the motion areas, it is likely that the pulvinar nuclei complex could actively influence in- and out-going cortical signals within the motion network. Therefore, the pulvinar could be regarded as a coordinator of the neural representations in area MT/V5 (Shipp, 2003).

Motion-sensitive Areas

Motion stimulus is processed primarily in the dorsal pathway through the M pathway, and one key component in the motion network is the MT/V5 region (for a review see Born & Bradley, 2005). In the primary visual cortex (V1) of macaque monkeys, motion-selective cells are found to form three parallel pathways (Gur & Snodderly, 2007). One population of neurons in layer 4B and the other in layer 6 send parallel direct outputs to area MT in the dorsal cortical stream. Neurons in 4B were reported to have smaller RF and are more selective for orientation than

those in layer 6. The input to MT are believed to be dominated by the cortical inputs, most prominently the M pathway that originates from layer 4B of V1; however, MT+ receives inputs from many other cortical and subcortical sources (Figure 6). In monkeys, most MT neurons are found to be direction-selective (Albright, 1984; Maunsell & van Essen, 1983a, 1983b; Zeki, 1974), and like V1, MT also has a retinotopic map of the contralateral visual field, but the RF of a MT cell is about 10 times larger than that of V1 RFs. Similar to V1, the MT cells with similar directional specificity are organized into vertical columns from the surface of the cortex to the white matter. Each part of the visual field is represented by a set of columns in which cells respond to different motion directions in that part of the visual field. Many MT cells respond to motion of spots or bars of light by detecting contrasts in luminance, and some cells also respond to moving forms by difference only in texture or coloured edges. On the other hand, stimulation of MT neurons can influence animals' behavioural outcome during motion direction discrimination tasks (Salzman, Britten, & Newsome, 1990; Salzman, Murasugi, Britten, & Newsome, 1992), and MT lesions impair motion perception (Azzopardi, Fallah, Gross, & Rodman, 2003; Newsome & Pare, 1988; Newsome, Wurtz, & Dürsteler, 1985; Pasternak & Merigan, 1994). The human motion-sensitive area has been identified at the junction of the parietal, temporal and occipital cortices by several research groups using neuroimaging techniques (Anderson, Holliday, Singh, & Harding, 1996; Cornette et al., 1998; Dukelow et al., 2001; Greenlee, 2000; Martinez-Trujillo, Cheyne, William, Simine, & Tsotsos, 2006; Morrone et al.,

2000; Schoenfeld, Heinze, & Woldorff, 2002; Schoenfeld et al., 2003; Smith, Greenlee, Singh, Kraemer, & Hennig, 1998; Tootell et al. 1995; Watson et al. 1993; Zeki, Friston, Kennard, & Frackowiak, 1991) and histological studies of postmortem human brains (Malikovic et al., 2007; Wilms et al., 2005).

MT is architectonically different from neighbouring regions with its lower cell density in layer IV and VI and heavy myelination in deeper layers (Allman & Kaas, 1971). The human motion area is often referred to as MT+ since it embraces the MT area and other adjacent motion-sensitive areas, including the medial superior temporal (MST) area. Some researchers also suggested that the MT+ has functional lateralization as the left hemisphere attends to contralateral stimuli whereas the right hemisphere attends to contralateral and ipsilateral stimuli (Heilman & van den Abell, 1980; Marshall & Fink, 2001; Wilms et al., 2005). These researchers postulated that this disparity could be based on the well-established right hemispheric dominance for visual attention.

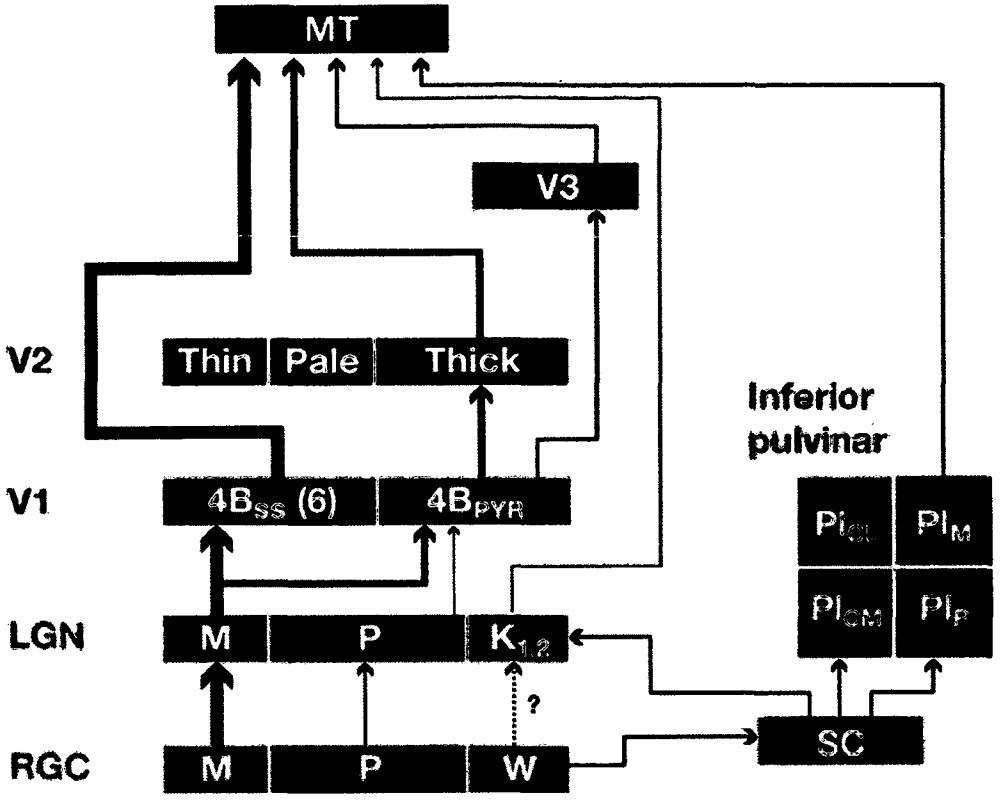

Figure 6. A schematic map showing the inputs to MT. Line thickness roughly reflects the number of the input neuron and synapse strength. The thickest lines represent the direct cortical M pathway originates from layer 4B in V1. For simplicity, some of the feed forward cortical inputs of lesser magnitude (e.g. V3A, VP, PIP) and some subcortical inputs are omitted. The precise nature of the retinal inputs to LGN koniocellular layers ($K_{1,2}$) is still not understood. $4B_{SS}$: spiny stellate neurons in layer 4B. $4B_{PYR}$: pyramidal neurons in layer 4B. LGN: lateral geniculate nucleus. M: M pathway. P: P pathway. $K_{1,2}$: koniocellular layers. PI_{CL}: central lateral nucleus of the inferior pulvinar. PI_{CM}: central medial nucleus of the inferior pulvinar. PI_M: medial nucleus of the inferior pulvinar. PI_P: posterior nucleus of the inferior pulvinar. RGC: retinal ganglion cells. SC: superior colliculus. (Born & Bradley, 2005).

The third visual complex (V3) in the monkey brain is another important visual area that contains neurons that are selective to motion and motion direction (Felleman & Van Essen, 1987; Gegenfurtner, Kiper, & Levitt, 1997; Zeki, 1978). Recently, several subdivisions in the V3 complex have been demarcated in the human brain as dorsal and ventral V3, V3A and V3B by using neuroimaging

techniques (Smith et al., 1998; Tootell et al., 1997; Wandell, Dumoulin, & Brewer, 2007; Zeki, Perry, & Bartels, 2003). Among these subdivisions, V3A has been suggested as the most important structure for processing of motion signals (Maus, Weigelt, Nijhawan, & Muckli, 2010; McKeefry, Burton, & Morland, 2010; McKeefry, Burton, Vakrou, Barrett, & Morland, 2008; Seiffert, Somers, Dale, & Tootell, 2003; Smith et al., 1998; Tootell et al., 1997).

Motion Velocity and Anatomy

As mentioned earlier, MT has been considered as a key structure for motion perception by its direction- and speed-tuned neurons (for review see Albright, 1993; Born & Bradley, 2005). Behavioral studies have suggested that temporal stimulus context can affect the perception of the direction and speed of motion (Williams et al., 1986). Several groups have shown that activity in MT plays a key role in the perception of speed using microstimulation, neurophysiology, and lesion in monkeys (Liu & Newsome, 2005; Krekelberg, Van Wezel, & Albright, 2006a & b; Maunsell & Van Essen, 1983a; Mikami, Newsome, & Wurtz, 1986; Newsome, Wurtz, & Dürsteler, 1985; Orban, Saunders, & Vandenbussche, 1995; Pasternak & Merigan, 1994; Rodman & Albright, 1987; Rudolph & Pasternak, 1999).

The indirect evidence of speed-specific pathways for fast and slow speed in humans can be found in studies with healthy normal subjects using neuroimaging and TMS and in the double dissociation of fast and slow motion perception in blindsight and motion-blind patients (Beckers, G., & Zeki, S. 1995; ffytche, Guy, &

Zeki, 1995; Laycock, Crewther, Fitzgerald, & Crewther, 2007). When a patient with damage to the primary visual cortex, known as "cortical-blind", is able to detect, localize, and discriminate visual stimuli such as motion in the scotoma, the patient is said to have blindsight (for review see Cowey, 2010). For example, Barbur, Ruddock, and Waterfield (1980) reported the most well-known blindsight patient GY who had unilateral V1 lesions was able to detect motion stimuli faster than 10°/s in the scotoma, whereas another "motion-blind" patient LM with bilateral lesions to MT+ and adjacent parietal region could only detect motion stimuli slower than 6°/s (Zihl, von Cramon, & Mai, 1983).

The 36-year-old patient GY acquired extensive left V1 lesion at the age of 7, but he showed high sensitivity to fast moving stimuli that were faster than 10°/s (Barbur et al., 1980). His velocity discrimination in the scotoma was normal, but he was unable to discriminate object shape or size. In a later PET study, Barbur, Watson, Frackowiak, and Zeki (1993) found that motion stimuli displayed in GY's scotoma activated V5, V3 and area 7 ipsilateral to the lesioned V1. Barbur et al. (1993) concluded that although the major corticocortical input from V1 to ipsilateral MT+ was absent, other pathways were sufficient for both the discrimination and the conscious awareness of the motion stimulus. More recently, Bridge, Thomas, Jbabdi, and Cowey (2008) used diffusion tensor imaging (DTI) to further investigate GY's cortical and subcortical connectivity that might account for his blindsight. They found that both controls and patient GY had a neural pathway between LGN and ipsilateral MT+ that bypasses V1. However, due to the

limitation of the technique used, it is difficult to conclude whether this pathway between V1 and ipsilateral MT+ composed of corticofugal feedback or the koniocellular pathway described by Sincich et al. (2004) or both pathways. More interestingly, Bridge et al. (2008) found that GY had two unique pathways: a geniculocortical tract connecting the right LGN to the left MT+ (ipsilateral to V1 lesion), and another corticocortical tract connecting bilateral MT+. However, given the poor spatial resolution of the DTI imaging, it is difficult to tell the subcortical pathway arises from the LGN or the pulvinar. The behavioural and DTI data suggest that the alternative cortical and subcortical pathways to MT+ could be strengthened as a result of neural plasticity following cortical damage in early stages of development.

On the other hand, the motion-blind patient LM reported by Zihl and colleagues (1983) had lesions to bilateral temporo-occipital regions and showed substantial impairment in discriminating temporal frequency above 6 Hz and motion direction above 6°/s. LM could only discriminate stationary from moving objects in the visual periphery and detect motion slower than 10°/s around central visual field (Hess, Baker, & Zihl, 1989), and she was only able to reach for objects moving at 0.5 m/s or slower (Schenk, Mai, Ditterich, & Zihl, 2000) . Hess et al. (1989) speculated that the residual motion perception in LM might be due to the "rudimentary" function of the parallel pathways because of complete disruption of the primary motion pathway due to the lesion, and this parallel pathway is thought to be the P pathway routed from LGN to V1 to V4.

The dissociation of pathways for fast and slow velocity is also supported by evidence from neurophysiology that directional selectivity of MT neurons was reported to be preserved after lesions to the striate cortex (Girard, Salin, & Bullier, 1992; Rodman & Albright,1989). This indirectly proved the existence of other cortical or subcortical motion pathways from LGN to region MT, such as a colliculo-pulvinar route as suggested by Rodman, Gross, and Albright (1990).

Research Question and Hypothesis for Part 1

Dukelow, DeSouza, Bhanji, Gati, Menon, and Vilis (1997) previously attempted to use fast and slow translating boxes to inspect the modulation of different speeds in the MT+ complex using fMRI. However, by using fMRI, it is difficult to investigate the spatial and temporal dynamic for fast and slow velocity simultaneously. In the current study, the motion stimulus was displayed with 3.1° to 9.1° eccentricity in either the left or right visual field, and thus we hypothesized that the monochrome motion stimuli would stimulate the M ganglions in the visual periphery but not the P ganglions in the foveal region (for the human retinotopic map see Figure 2). Thus, the motion signals were mostly processed within the M pathways in the visual system. During the experiment, twelve healthy subjects viewed translating motion stimuli with a slow velocity of 4°/s and a fast velocity of 20°/s while undergoing Magnetoencephalography (MEG) recording. I used an linearly constrained minimum-variance (LCMV) event-related beamformer algorithm (Cheyne, Bostan, Gaetz, & Pang, 2007) to explore the cortical sources of motion velocity-dependent MEG signals, and attempted to differentiate the

spatial and temporal profiles of the neuromagnetic dynamics in the human brain during the perception of slow and fast motion.

In Part 1 of the thesis, I hypothesized that passively viewing the moving dots of fast motion velocity will evoke an early MT+ response approximately 50 ms after stimuli onset, and this early response will not be observed in the slow motion subset of the task. With the high temporal resolution of the MEG data (625 Hz sampling rate) and high 3D spatial resolution (up to 1 mm) of the event-related beamformer, it would be possible to investigate the cortical sources as well as the neural dynamics with more improved detail than our predecessors.

Introduction - Part 2

Decision-making/Motor Intention

The second research question concerns the motor intention for goal-directed actions following the perceptual decision-making of a velocity change (increment or decrement) in the motion stimuli. In our experiment, a perceptual decision was formed based on the detection of a thresholded velocity change in the motion stimuli. The thresholded velocity change made this experiment an attention-demanding visual task, and it also inevitably yielded many trials in which the subjects did not made correct responses. Thus, we would be able to compare the neural dynamics between the correct and incorrect responses. The decision-making process depends heavily on the central executive functions to perform online analyses and evaluation of the continuous sensory inputs for making a commitment of a rule-based behavioural output (Everling & DeSouza, 2005). This process could be described by the probability theory of decision-making proposed by Gold and Shadlen (2007) as illustrated in Figure 7.

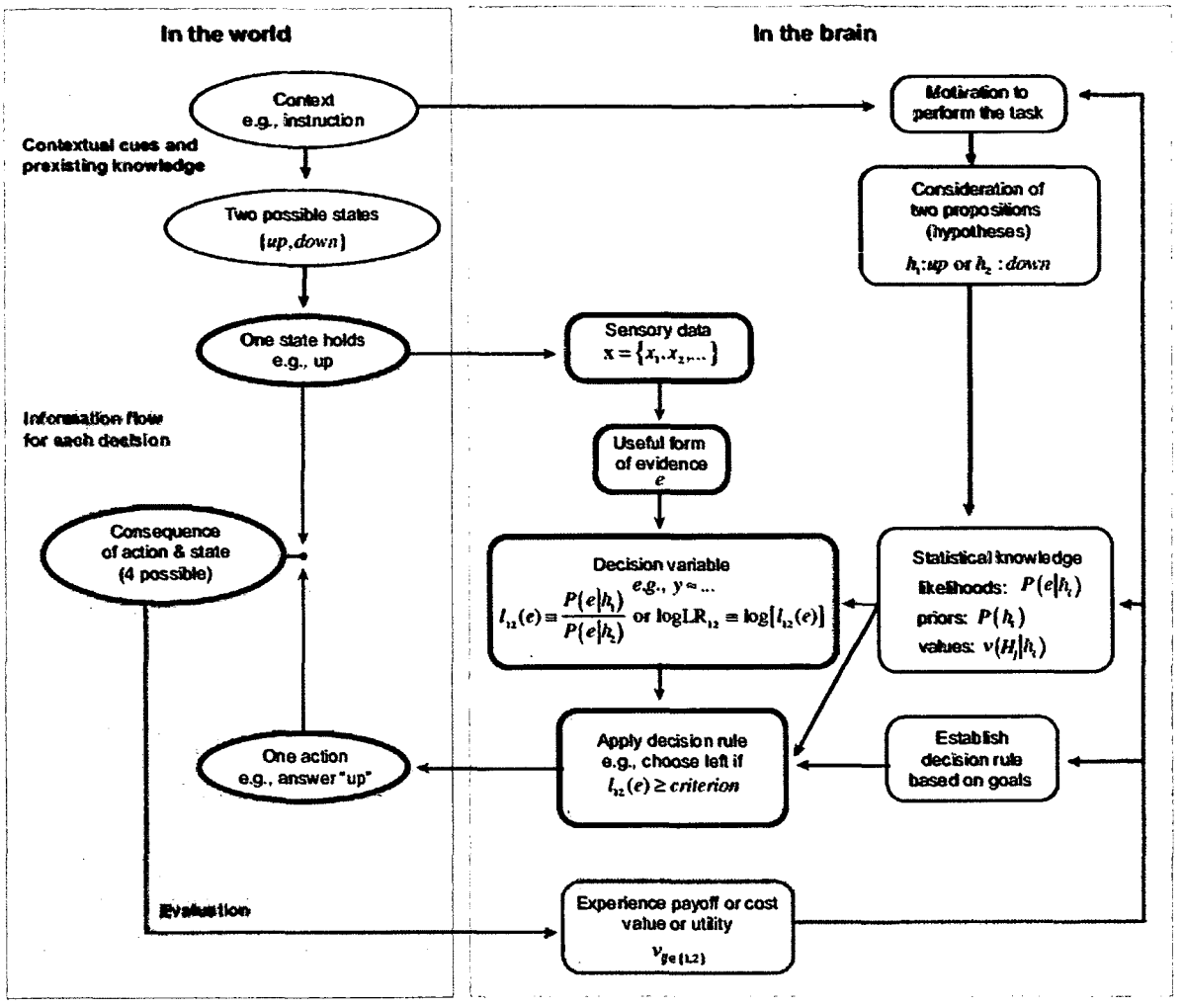

Figure 7. The elements of a simple decision-making processes between two alternatives (motion direction of the dots: h_1 = up or h_2 = down). The grey panel shows elements of the real world, and the yellow panel shows how the elements of the decision process are represented in the brain. Items in the black boxes define the context. Red elements form the decision. Blue elements evaluate and possibly update the decision-making process (Gold & Shadlen, 2007).

In this model, prior probability P(h_i) is the prediction of seeing a particular stimulus or inferred from its relative frequency of occurrence on previous trials (a Bayesian inference). Evidence (*e*) stands for the sensory information that can lead to the commitment of decision for a particular hypothesis (e.g. the neural activity that represents the remembered attributes of the velocity change is used

as evidence). The output of the likelihood function $P(e \mid h_i)$ is thus determined by evidence when h_i is true. Value (v) is an output of the decision-making process and could be the subjective costs and/or benefits being estimated. Value can be manipulated (e.g. given as an explicit feedback cue for a human or a drop of juice for a monkey). The decision variable (DV) represents the Gestalt sum of the priors, evidence, and value, which is measured by the decision rule to produce a final choice. The decision rule defines when and how to utilize the DV in order to determine the particular alternative H_i, and the goal of a decision is to achieve the most desired outcomes (the best choice associated with h_i) and avoid to choose the undesired (wrong) options.

Neurophysiological evidence has shown that the neurons in the monkey PPC regions represent the decision variable (DV) which reflected the accumulation of stochastic sensory evidence during visual tasks when the monkeys need to detect the motion direction in moving random dots (Churchland, Kiani, Chaudhuri, Wang, Pouget, & Shadlen, 2011; Gold et al., 2007; Roitman & Shadlen, 2002; Shadlen & Newsome, 2001). Moreover, the PPC neurons in the monkey brain were also thought to reflect the termination of the decision-making process when their firing rates reach a critical level (Churchland, Kiani, & Shadlen; 2008; Kiani, Hanks, & Shadlen, 2008; Roitman et al., 2002). In addition, when the difficulty level of the stimulus detection varied, the time-dependent firing rates of the PPC neurons were reported to correlate with the confidence level of the decisions (or choices certainty) in a graded fashion (Kiani, & Shadlen, 2009). Based on the

aforementioned studies, it could be concluded that the neurons in the PPC regions are crucial to the different stages of the decision-making process when the monkey needs to determine the best choice between two or more discrete options based on sensory evidence.

The Neural Basis of Decision and Motor Intention

Motor intention can be conceptualized as a cognitive plan for movements to achieve a goal based on a previous decision (Desmurget & Sirigu, 2009b). Thus, finding the neural correlates of the motor intention will provide important information pertaining to the connection between the decision-making processes and behavioural outputs. The first series of research on motor intentions in humans were conducted by Benjamin Libet and his colleagues by using a self-initiated movement paradigm (Libet, Gleason, Wright, & Pearl, 1983), and they found the motor intention of "wanting to move" (W judgment) occurred approximately 200 ms prior to the behavioural responses. Libet et al. (1983) also found that the EEG readiness-potential (RP) started to build up around 800 ms before the W judgment, which could be a crucial indicator of early movement preparation prior to motor intention. In a later study, Haggard and Eimer (1999) used a modified Libet's Paradigm in which subjects could freely decide to respond with either the left or right index finger. They postulated that a "lateralized" RP (LRP) was a more specific marker of early motor preparation before motor response than RP. Haggard and Eimer (1999) suggested that LRP is the unconscious cause of the conscious state upon which W judgment depends, and

motor intention emerged after the initial stage of this unconscious early motor preparation. In the current study, subjects were asked to detect a velocity change in the motion stimulus and make responses with right hand button press. I intended to inspect the brain signals following the velocity change to investigate when and where in the brain the successful detection of the velocity change is transformed into the signals for motor responses. In order to investigate this question, it is first necessary to understand the anatomical-functional relations between the brain regions that are involved in the motor intention and motor preparation, specifically the posterior parietal cortex (PPC), premotor cortex (PM), and the supplementary motor area (SMA).

The Posterior Parietal Cortices (PPC)

The PPC region has been proven crucial to the formation of intention and motor command preparation for eye, hand, and limb movements (Andersen & Cui, 2009; Baumann, Fluet, & Scherberger, 2009; DeSouza et al., 2000; DeSouza, Menon, & Everling, 2003; Kurata & Tanji, 1986; Medendorp, Goltz, Crawford, & Vilis, 2005; Murata, Gallese, Luppino, Kaseda, & Sakata, 2000; Rizzolatti, Fogassi, Gallese, 1997; Rushworth, Ellison, Walsh, 2001; Rushworth, Johansen-Berg, Göbel, & Devlin 2003; Sakata, Taira, Kusunoki, Murata & Tanaka, 1997; Vesia, Yan, Henriques, Sergio, & Crawford, 2008). Historically, the PPC has been seen as the association cortex that receives and integrates multiple sensory modalities. However, studies by Mountcastle, Lynch, Georgopoulos, Sakata, and Acuna (1975) and Hyvärinen (1982) showed that the PPC not only serves as a

multisensory association cortex, but also codes motor actions and provides the representations of these motor actions with specific sensory information. Most relevant to my research interest, several groups have reported the involvement of the PPC region in selective attention, visual-motor integration, decision-making, and motor intention (Andersen,1987; Andersen & Buneo, 2002; Behrmann, Geng, & Shomste, 2004; Burnod et al., 1999; Colby & Goldberg, 1999; Desmurget, Reilly, Richard, Szathmari, Mottolese, & Sirigu, 2009a; Fogassi et al., 2005; Grossberg & Pilly, 2008; Hesse, Thiel, Stephan, & Fink, 2006; Johnson, Ferraina, Bianchi, & Caminiti. 1996; Kalaska, Scott, Cisek, & Sergio, 1997; Lacquaniti, Guigon, Bianchi, Ferraina, & Caminiti, 1995; Patel, He, & Corbetta, 2009; Rizzolatti et al., 1997; Rushworth et al., 2001, 2003).

The Frontal region and Supplementary motor area (SMA)

The frontal region and PPC are intensively interconnected, and they work together during generation of intention and motor commands (Cavada & Goldman-Rakic, 1989; Corbetta, 1998; Geyer, Matelli, Luppino, & Zilles, 2000; Luppino, Murata, Govoni, & Matelli, 1999; Marconi et al., 2001; Padberg et al., 2007; Strick & Kim, 1978; Tanne-Gariepy, Boussaoud, & Rouiller, 2002; Wise, Boussaoud, Johnson, Caminiti, 1997). Anatomically, the supplementary motor area (SMA) and its adjacent areas have been suggested as a likely source for LRP during the formation of motor intention (Eimer, 1998; Ikeda, Lüders, Burgess, & Shibasaki, 1992). Other evidence comes from several electrical stimulation studies in patients during brain surgery. Fried and colleagues (1991) reported that

stimulating the SMA area triggered a compulsive desire in the patients to make very precise movement such as to "move the right leg inward", or "lift the right elbow". Fried et al. (1991) also found that increased stimulation intensity caused the movements to actually occur. In contrast, although simulation to the PPC also evoked strong urges to make movements, these motor intentions seemed to be more "general", and the patients were sometimes unable to specify what movement they wanted to perform (Desmurget et al., 2009a). Interestingly, when the intensity of the PPC stimulation increased, the patients believed that they had already moved even though no eletromyographic response was detected. Moreover, Desmurget and colleagues (2009a) also found that stimulation to the premotor cortices triggered actual movements, but the patients were unaware of these movements.

The Frontoparietal Network of Motion Intention and Awareness

The PPC is extensively interconnected with the premotor and M1 region (Matelli, Camarda, Glickstein, & Rizzolatti, 1986; Petrides & Pandya, 1984), and together they play an important role in planning, executing, and comprehending actions (Andersen et al., 2002 & 2009 ; Fogassi et al., 2005; Rizzolatti et al., 1997). It has been reported that the electrical stimulations to various locations in the premotor and PPC regions can induce either simple or complex movements that involved multiple joints and with specific pattern in monkeys (Stepniewska, Fang & Kaas, 2005 Stepniewska, Cerkevich, Fang & Kaas, 2009) and in humans (Desmurget et al., 2009a; Fried et al., 1991).

In addition to the anatomical and functional evidence, Desmurget and Sirigu (2009b) proposed a general model for understanding motor intention and awareness that involves the PPC, PM, primary motor cortex (M1), and ACC regions. Desmurget and Sirigu (2009b) postulated that the motor intention generated in the PPC is likely independent of movement execution per se, while SMA triggers precise movement by suppressing the inhibitory signal exerted on the M1 as reported by Ball and colleagues (1999). Desmurget (2009b) suggested that an initial unconscious intention to act (prior intention) emerges within a wide frontoparietal network, and this prior intention causes an unspecific activation of the motor system. For example, the frontal RP (or readiness field in MEG studies) buildup occurs around 1 to 1.5 s before motor output (Cheyne, Bakhtazad, & Gaetz, 2006; Eimer, 1998; Haggard & Eimer, 1999; Libet et al., 1983). Progressively, starting from around 800 ms prior to the muscle contraction, this RP becomes lateralized, which is specified by the side of motor output. Conscious intention emerges around 250 ms before the movement onset.

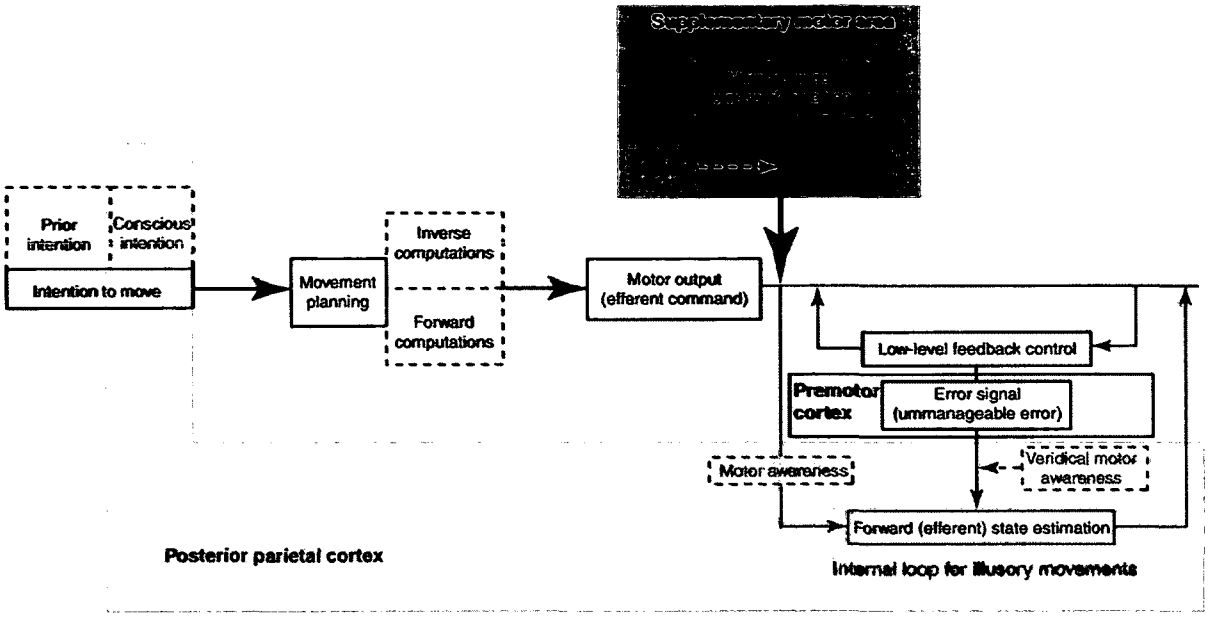

Figure 8. A general anatomo-functional framework for motor intention and awareness. (Desmurget et al., 2009b).

Desmurget et al. (2009b) speculated that the increases in PPC activity underlie the emergence of conscious motor intention, and during the last 250 ms or so before the movement onset, a specific motor command output is planned within a parietal-motor network. When the motor command is ready to be issued, the SMA releases it by suppressing the inhibitory output to M1, which generates a conscious experience of intentional urge to move (Fried et al., 1991). A few dozen milliseconds after, the effector muscle contraction begins. Additionally, the movement awareness seems to be associated with increased PPC activity. Other studies have provided evidence in support of Desmurget's claim that the formation of intentions includes the evaluation of the potential motor significance of the sensory inputs as well as the selection of actions but it is independent of

action execution in primates (Andersen & Buneo, 2002; Calton, Dickinson, & Snyder, 2002; Gnadt & Andersen, 1988; Snyder, Batista, & Andersen, 1997) and in humans (Rushworth et al., 2001, Toni, Thoenissen, & Zilles, 2002).

Research Question and Hypothesis for Part 2

The main interest of this study is to investigate the spatial and temporal activation pattern of the fronto-parietal network when the central executive functions need to evaluate external sensory stimuli in order to make rule-based decisions for a response. To answer this question, we measured neuromagnetic activities in an attention-demanding visual task where the subjects were required to respond with right hand button press after the velocity change in a motion stimulus was detected. First, we were interested in exploring when and where in the brain a perceived visual stimulus is transformed into a signal for a behavioural response. Furthermore, in order to inspect the neural correlates of motor intention during decision-making, a delayed motor response paradigm was used to temporally separate the neural responses due to visual perception and decision from that due to movement execution. My hypothesis was that the neural correlates of motor intentions will emerge from the frontoparietal network during the delay period before the actual button press. The frontoparietal dynamics should be in line with the predictions of Gold & Shadlen's decision model (2007) and Desmurget's intention model (2009b) that the PPC, SMA, and PMC will be involved when the subjects could perceive the velocity change and the PPC will be a key structure in the formation of motor intention during decision-making.

Methods

Subjects

Subjects' motion detection thresholds were obtained prior to the MEG session to assure that they could understand the task and the velocity change stimulus met the MEG experimental requirements. 22 healthy adult volunteers (9 males and 13 females, all right handed, mean age (±SD) = 25.6 ± 4.7 years old) were tested for their motion detection thresholds. All the subjects had normal or corrected-to-normal vision and were all screened for MRI and MEG safety. Twelve from these twenty-two subjects (6 males and 6 females, mean age = 27.1 ± 4.6 years) participated the MEG experiment with their informed consent at York University and Toronto Hospital for Sick Children. This research was approved by both institutions' ethics review boards.

Motion Detection Threshold

Prior to the MEG scan, the subjects were tested for their perceptual thresholds for the fast and slow baseline velocity. The experiment used a block design with a staircase procedure. There were thirty blocks, and each block had eight randomized trials of either increment or decrement from the baseline velocity. Each trial started with center fixation, and white dots (7 dots/degree^2, each dot's

diameter = 5 pixels) would be translating downwards in the right visual field with 100% motion coherence on a black background beneath an apertural mask. The aperture was 6.1° in diameter and had no visible border. The moving dots were first translating at 4 or 20°/s for a random interval between 0.75 to 1.25 s, and the velocity was increased or decreased. This change in velocity lasted for 200 ms, and the stimulus velocity returned to the baseline. The stimulus was displayed for another 1 second before it disappeared, and the subjects used right hand button press to report the perceived velocity change was either a decrease (index finger: left button press) or an increase (middle finger: right button press) in the motion velocity. The value of velocity change in the next block was adjusted to a larger or smaller velocity value according to subjects' performance in the current block (correct rate (CR) >= 75%: smaller velocity change; CR = 50%: no change; CR < 50%: larger velocity change). The entire threshold experiment took approximately 45 ~ 50 minutes, and the subjects were given a break in the middle of the experiment. Stimuli were displayed on a flat LCD screen, and the subjects sat upright in a dark room with both eyes open and their chins in a head rest. The stimulus was generated with Matlab (ver.2007a The MathWorks, Natick, United States) with Psychophysics Toolbox extensions (Brainard, 1997; Pelli, 1997).

Paradigm and MEG Recording

During the MEG recording session, the subjects sat upright in the dark MEG scanner room, and the stimulus was projected onto a screen in front of the subjects through a set of mirrors from outside of the room. Padding was used to

minimize the head motion during MEG recording. The viewing distance was 75 cm, and the stimulus was the same as the one used in the perceptual threshold experiment except for some modification in parameters (Figure 9). In each trial, the stimulated visual field (left or right), the motion direction (left, right, up, and down), the baseline velocity (4 or 20 °/s), and the velocity change (increment or decrement) were randomly determined, and the velocity change was set according to each subject's perceptual thresholds measured before and confirmed on site at the MEG laboratory in the first 6 subjects. The thresholds were confirmed to be identical to those acquired prior to the MEG session and therefore not verified in the rest of the subjects. The motion stimulus was displayed for 2.2 seconds in total with a random onset of motion change from 0.75 to 1.25 s after stimulus onset, and the subjects were required to respond with right hand button press as soon as the stimulus disappeared. Throughout the whole trial, subjects were instructed to maintain fixation on a white square located in the center of the screen while attending to the stimulus in the visual periphery. The events of interest (e.g. stimulus onset and velocity change onset) were coupled with the luminance changes in one corner of the screen that were invisible to the subjects. The luminance changes were captured by a photo-resistor circuit that in turn sent a transistor digital pulse to the data acquisition computer to synchronize the visual stimuli with the MEG recording.

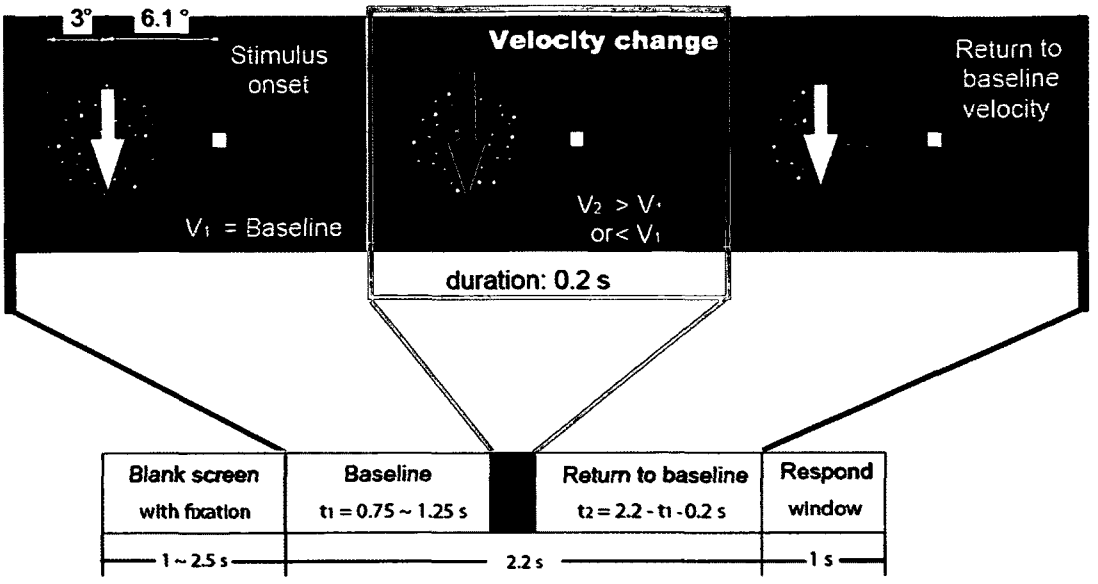

Figure 9. Each trial starts with a center fixation. After a delay of 1 ~ 2.5s, a stimulus consisting of moving white dots is displayed in either the left or right peripheral visual field (only left display is shown for simplicity). The dots are translating in one of four primary directions (up, down, left or right) at a baseline velocity of 4 or 20 °/s. After a delay of 0.75 ~ 1.25s, the stimulus velocity increases or decreases (according to each subject's perceptual thresholds) for 0.2 seconds. As soon as the stimulus disappears, the subjects are required to respond to the speed change by pressing the appropriate button (index finger button: decrease, middle finger button: increase).

Neuromagnetic fields were recorded with a 151 channel whole-head CTF MEG system (VSM MedTech, Ltd, Coquitlam, BC, Canada) at a sampling rate of 625 Hz with an online bandpass filter of 0 to 200 Hz. Subjects' head position was recorded by using three fiducial reference coils (nasal, left and right temporal) at the beginning and end of the MEG recording session. Three of the twelve subjects had to participate for a second time due to equipment errors during their first MEG session or excessive head movement (> 10 mm). T1-weighted structural magnetic resonance images (MRI) (axial 3D spoiled gradient echo sequence) were obtained for each participant using a 1.5 Tesla Signal Advantage system

(GE Medical Systems, Milwaukee).

Preprocessing

In order to investigate the research questions regarding motion perception and motor intention, four events of interest were identified as (A) motion stimuli onset, (B) motion velocity change, (C) stimulus offset (the GO cue for response), and (D) button press for creating subset of the MEG data. The timestamp of these four events were extracted from the event log file of each subject's MEG recording by in-house Matlab program, and separate datasets were epoched for further analyses. The alignment of these events and the duration of the datasets are shown in Figure 10.

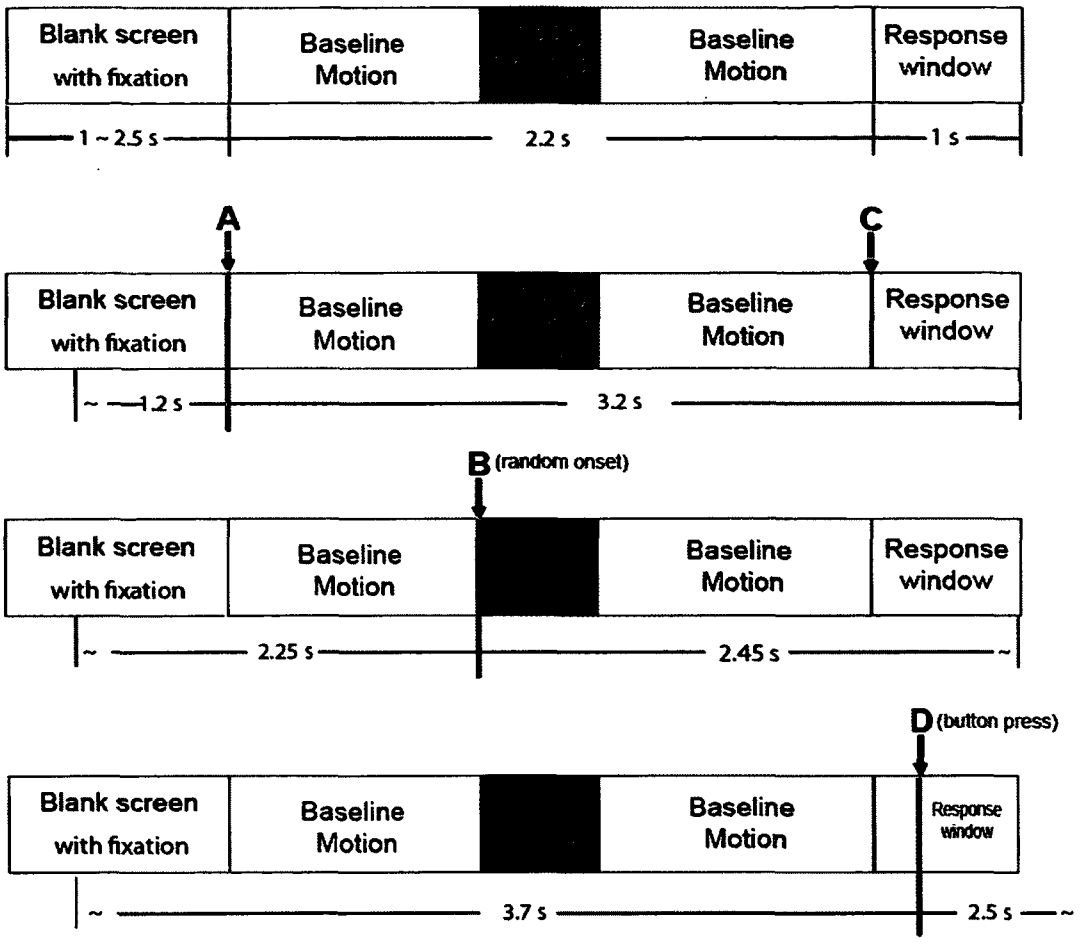

Figure 10. Events of interest. The visual stimulus was displayed for 2.2 second in total, and the onset of velocity was randomized from 0.75 ~ 1.25 after the onset of the stimulus. Event A: the onset of motion stimulus. Event B: the velocity change that lasted for 0.2 second. Event C: the offset of the motion stimulus, which was also the cue for making a response. Event D: button press. The datasets were epoched based on the interval indicated by the number before and after the event of interest (the thick red line).

The motion stimulus onset was used as a localizer for mapping the motion network in the brain. Considering the lateralization of the motion-sensitive regions, we extracted event markers based on left and right visual display. To investigate the velocity effects on the temporal and spatial dynamics, we separated fast and slow motion stimuli for both visual displays. Thus, each subject's motion onset

data was epoched into four datasets of motion stimuli as follows: (1) left visual fast, (2) left visual slow, (3) right visual fast, and (4) right visual slow motion. The trials in which subjects did not make a response were excluded for analysis. On average, the number of no-response trials was 5.6 ± 6.5 in the left visual field, and 5.8 ± 5.6 in the right visual field. Continuously recorded MEG data were epoched into single trials of 4 s duration based on the event markers. Each trial in these datasets included 1.2 s preceding and 3.2 s following the visual stimulus onset. The motion stimulus was displayed for 2.2 seconds from the onset till offset (Figure 9), and therefore this dataset included 1 s of data after the stimulus offset, which was the GO cue for motor response.

The onset of velocity change (B – see figure 10) was defined as an event of interest for mapping the brain areas that are involved in decision-making and motor intention for a correct response. In order to generate enough statistical power for comparing the neural dynamics of the correct with the incorrect responses, trials of left and right visual fields were combined. The trials in which the subjects made no responses were excluded from analysis (the average no-response rate was 1.8% ± 2.5%). The MEG data were epoched into single trials of 4.7 s duration for the correct and incorrect conditions. Each trial in the correct or incorrect condition included 2.25 s preceding and 2.45 s following the motion change onset.

The onset of button press (D – see Figure 10) was used as localizer for mapping the motor field and motion evoked fields as described by Cheyne et al

(2006). For the button press, event markers for correct and incorrect responses were separated, and the MEG data were epoched into single trials of 6.2 s duration for the correct and incorrect conditions. Each trial included 3.7 s preceding and 2.5 s following the button press.

Source Localization

The MEG datasets were first averaged for inspecting evoked responses in individual subjects. Each subject's global field power was computed based on the root mean square (RMS) of the averaged sensor data. For source localization in the brain space, the datasets were first co-registered to the subject's structural MR images in CTF system's fiducial-defined 3D space (x axis: anterior and posterior, y axis: medial and lateral, z axis: inferior and superior). A multiple sphere conductor head model (Lalancette, Quraan, & Cheyne, 2011) was created for each subject based on an inner skull surface mesh derived from the subject's MR image using the FSL BET2 and BETSURF tools (Jenkinsen et al., 2004; Smith, 2002). An event-related beamformer (erSAM) algorithm (Cheyne et al., 2007) based on individual multiple-sphere head model was then used to create source images for evoked neuromagnetic activity over the source space of the whole brain with a 2.5 mm spatial resolution. The covariance matrix and beamformer weights were calculated based on 0 to 1 s interval of the single trial data after bandpassed from DC to 30 Hz with a baseline window from -1 to 0 s and a temporal resolution of 10 ms. This event-related beamformer performs a voxel-by-voxel searching over the whole brain space by applying a linearly

constrained minimum-variance (LCMV) beamformer algorithm that estimates a single optimal current orientation at each voxel, which is obtained by first computing a vector beamformer with two orthogonal dipole sources at each location (Cheyne et al. 2007). The dominant orientation is then given by the eigenvector associated with the maximum eigen value of the vector beamformer output integrated over all data segments. The RMS peaks in the subjects were used as time references for finding peaks in their three-dimensional beamformer images. Nine of the twelve subjects had good signals from the MEG channels (see subject DA in Figure 11), while three subjects had low signal-to-noise ratio and thus the group mean for the sensor data and global field power were not calculated. However, the event-related beamformer showed its great noise reduction capability in sources localization for these three subjects as shown in previous studies (Cheyne et al., 2006; Cheyne et al., 2007). The reported Talairach coordinates of the ROIs were visually confirmed within each subject's anatomical data to assure the correct locations were picked.

To find the group activation peaks, the subjects' beamformer images and structural MRI were spatially normalized into the Talairach space using SPM2 (Welcome Institute of Cognitive Neurology, London, UK) and in-house Matlab scripts (http://www.mathworks.com/). The average source power was computed in the Talairach and Tournoux (1988) coordinates, and the thresholds for the average beamformer time series were determined with an omnibus permutation test of the mean voxel value (Nichols & Holmes, 2002). The beamformer images

were visually scanned for group average peaks that had the maximum power within the evoked-response time window. For peak locations of activation in the erSAM images, averaged time series (virtual sensor) waveforms were reconstructed for the entire epoch in order to examine source activity as a function of time. Group average virtual sensor waveform data were normalized and compared for conditions such as fast and slow motion, or correct and incorrect response for different events of interest.

Time-frequency Analysis

For viewing the phase-locked as well as the non-phase-locked oscillatory brain activity from the sources and for comparing the activation patterns between conditions (e.g. correct and incorrect responses), we conducted a time by frequency analysis across our events (A,B,C,D see Figure 10). For finding the individual erSAM peaks for time-frequency (TFR) analysis, a group erSAM source peak was unwarped from Talairach coordinates into CTF coordinates, and this group peak was used as the center for searching the voxel with maximal source power with a 10 mm searching radius at the latency when the group peak was reported. The single trial data at the individual peak was then extracted, and the oscillatory activity of evoked and induced response was computed for the peak by convolving a Morlet wavelet with the single trial data (Tallon-Baudry et al., 1997). Group average full spectrum TFR images were plotted for the correct and incorrect responses for an ERB peak, and the mean difference between correct and incorrect responses across all the subjects were tested for significance with a

nonparametric unpaired permutation test of the mean pixel values (Maris et al., 2007). The oscillatory activities that showed significant difference ($P<0.05$) between the correct and incorrect responses are shown as the outlined areas on the group averaged TFR plots.

Results

Behavioural

The subjects' responses recorded in the MEG event log were verified with the responses in the psychophysical recording and categorized into three types: correct, incorrect and no-response. A correct response occurred when the subject pressed only one button that was consistent with the velocity change shown in the motion stimuli (e.g. pressed "faster" button when the change was velocity increment). An incorrect response occurred when the response was inconsistent with the velocity change, or when the subject pressed both buttons, or pressed any one of the buttons more than once. For the MEG data analyses, we excluded all the trials in which the subject made no response or the subject made eye movements. Subjects' responses were next compared across velocity and stimulated visual field.

The correct response rate (±SD) for fast velocity was 70.0%±13.8% and for slow velocity was 66.7%±10.6% (see Table 1). A two-sample t-test was conducted to compare the correct response rate between the fast and slow baseline

velocities, and no significant difference between the fast (M=167.92, SD=33.10) and slow (M=160.00, SD=25.43) baseline velocity was found, $t(22)=0.66$, $P=0.52$. Moreover, a series of two-samples t-test showed that the subjects made more correct (M=167.92, SD=33.10) than incorrect (M=67.67, SD=28.79) responses for the fast velocity, $t(22)=7.92$, $P<0.01$, and made more correct (M=160.00, SD=25.43) than incorrect (M=75.67, SD=21.33) responses for the slow velocity, $t(22)=8.80$, $P<0.01$.

The correct response rate (±SD) in the left visual display was 69.0%±11.2% and in the right visual display was 67.7%±12.7% (see Table 2). A two-sample t-test was conducted to compare the correct response rate between the left and right visual displays, and no significant difference between the fast (M=165.50, SD=26.81) and slow (M=162.42, SD=30.39) baseline velocity was found, $t(22)=0.26$, $P=0.79$). Moreover, a series of two-samples t-test showed that the subjects made more correct (M=165.50, SD=26.81) than incorrect (M=70.25, SD=22.93) responses in the left visual display, $t(22) = 9.35$, $P<0.01$, and made more correct (M=162.42, SD=30.39) than incorrect (M=73.08, SD=25.58) responses in the right visual display, $t(22) = 7.79$, $P<0.01$.

In the total 480 trials, the average correct responses rate was 68.3%±11.7%, the average incorrect responses rate was 29.9%±9.9%, and the average no-response-trial rate was 1.8%±2.5%. A two-sample t-test was conducted to compare the button press latencies (ms) between the correct and incorrect responses, and no significant difference between the latencies of correct

(M=520.00, SD=160.00) and incorrect (M=640.00, SD=230.00) responses was found, $t(22)=-1.52$, $P=0.14$.

Source Localization

Motion perception

All of our subjects showed remarkable visually evoked responses after the motion stimulus onset for the fast and slow motion in both stimulated visual fields. Figure 10 shows an example of subject DA's sensor data and global field power data. The global field power data is represented by the root mean square (RMS) of the average sensor data. The top two average sensor plots illustrated the visually evoked field in femtotesla (fT) as a function of time aligned to motion stimulus onset in milliseconds with all the MEG channels superimposed. These two average sensor plots showed that both the fast and slow motion stimuli evoked a neuromagnetic response that lasted about 200 ms and reached its peak approximately at 100 ms after the stimulus onset. The RMS, the quadratic mean of average sensor data, is a statistical measure of the overall magnitude change of the sensor data as a function of time. The RMS data showed that the visually evoked response began at 60 ms and peaked at 100 ms for both fast and slow motion. The evoked response lasted for about 200 ms. The RMS also showed a second peak approximately at 150 ms.

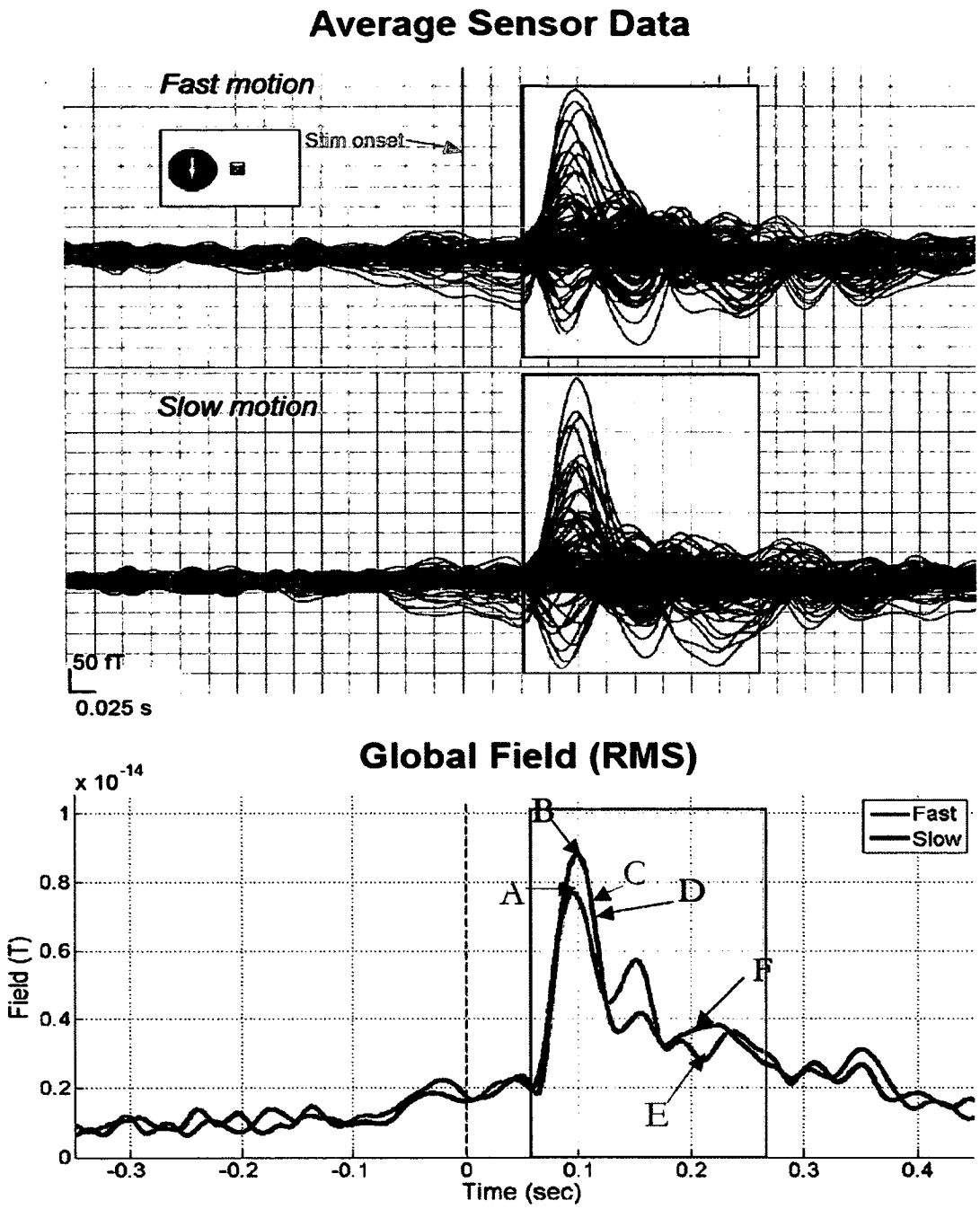

Figure 11. An example of sensor data analysis from one subject (DA). Top two figures showed the average sensor data for fast and slow motion onset in the left visual field (sensors space: blue = left hemisphere; green = right hemisphere, light blue = central channels). The boxes indicate the evoked response that began approximately at 60 ms and terminated at 260 ms. The M1 peak was found at 100 ms when the contralateral cuneus showed highest amplitude in the erSAM time series (A & B in Figure 12). The erSAM peaks for V3A (C & D) and MT+ (E & F) are shown in Figure 12. The M2 peak was found approximately at 150 ms when cuneus and V3A both showed a second erSAM peak after M1.

Individual source localization was based on the sensor global field power and erSAM images with temporal resolution of 10 ms. Each subject's erSAM images were visually scanned within the subject's evoked response window, and the RMS peak latencies were used as time reference for localizing erSAM peaks. Based on individual beamformer analysis, we identified three regions of interest as the contralateral cuneus, V3A, and the MT+ complex. We successfully localized these three peaks for fast and slow motion onset in both visual fields for all the twelve subjects except for: subject PD did not show the cuneus peaks for both fast and slow motion onset in the left visual field; JD did not show the V3A peaks for both fast and slow motion onset in the right visual field; CM did not show MT+ peaks for left slow motion onset; ST did not show MT+ peaks for right slow motion onset; and SW did not show MT+ peaks for right fast motion onset. An example subject's cortical source localization is shown in Figure 11 and 12. The subject's erSAM images were thresholded to spatially separate the top three peaks for each time point along the time series (Cheyne et al., 2006). Within the time window of evoked response (blue box in the RMS plot in Figure 11), peaks were found in contralateral cuneus, V3A, and MT+ approximately at 100 ms, 110 ms and 210 ms after the stimulus onset respectively in subject DA (Figure 12). The cuneus peak was coincident with the RMS peak at 100 ms, whereas the V3A peak was located when the RMS started to decrease. The MT+ activation was not as readily apparent on the RMS plot, which indicated its small signal amplitude and relatively smaller contribution to the global field power than the cuneus and V3A sources.

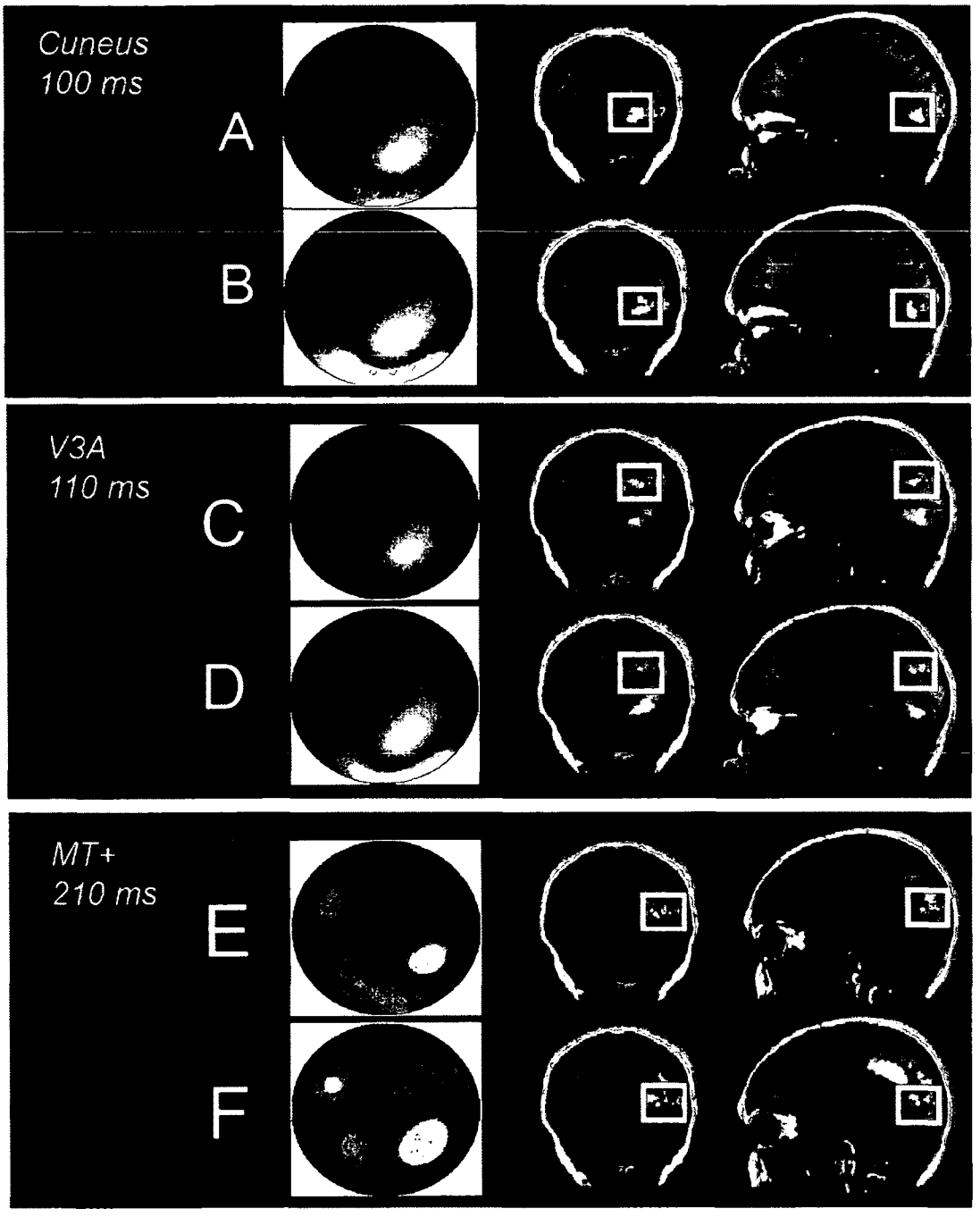

Figure 12. An example of source localization from subject DA based on the sensor analysis (see Figure 11). The second and third column demonstrate the erSAM peaks in contralateral cuneus, V3A, and MT+ that are corresponding to the time points shown in DA's RMS plot (labeled as A ~ F in Figure 11). The sensor maps at specified time points in the first column are generated based on the averaged sensor data, and they confirm the lateralization as well as the intensity of the signal peaks reported in the erSAM series. The MT+ peaks were localized after the activation amplitude in cuneus and V3A decreased, which also can be inferred from the RMS plot (after time point C & D in Figure 11).

The individual contralateral MT+ locations for all twelve subjects are shown in Figure 13. For comparison, the group MT+ locations (see Figure 14) are also plotted here as larger markers. The boundary of the blue dotted line box in every plot was defined based on the MT+ coordinates reported in previous studies (see Table 3). In each plot, the green ellipse is the standard error of the MT+ coordinates for fast motion, and the black ellipse is the standard error for slow motion. The group MT+ location showed 4 to 6 mm difference in the Talairach space, but the MT+ errors showed remarkable overlap between fast and slow motion in both visual fields. A Hotelling's T^2 test for two multivariate independent samples was used to examine the effect of velocity on individual MT+ source locations in the Talairach coordinates (x, y, and z coordinates), but no significant result was found.

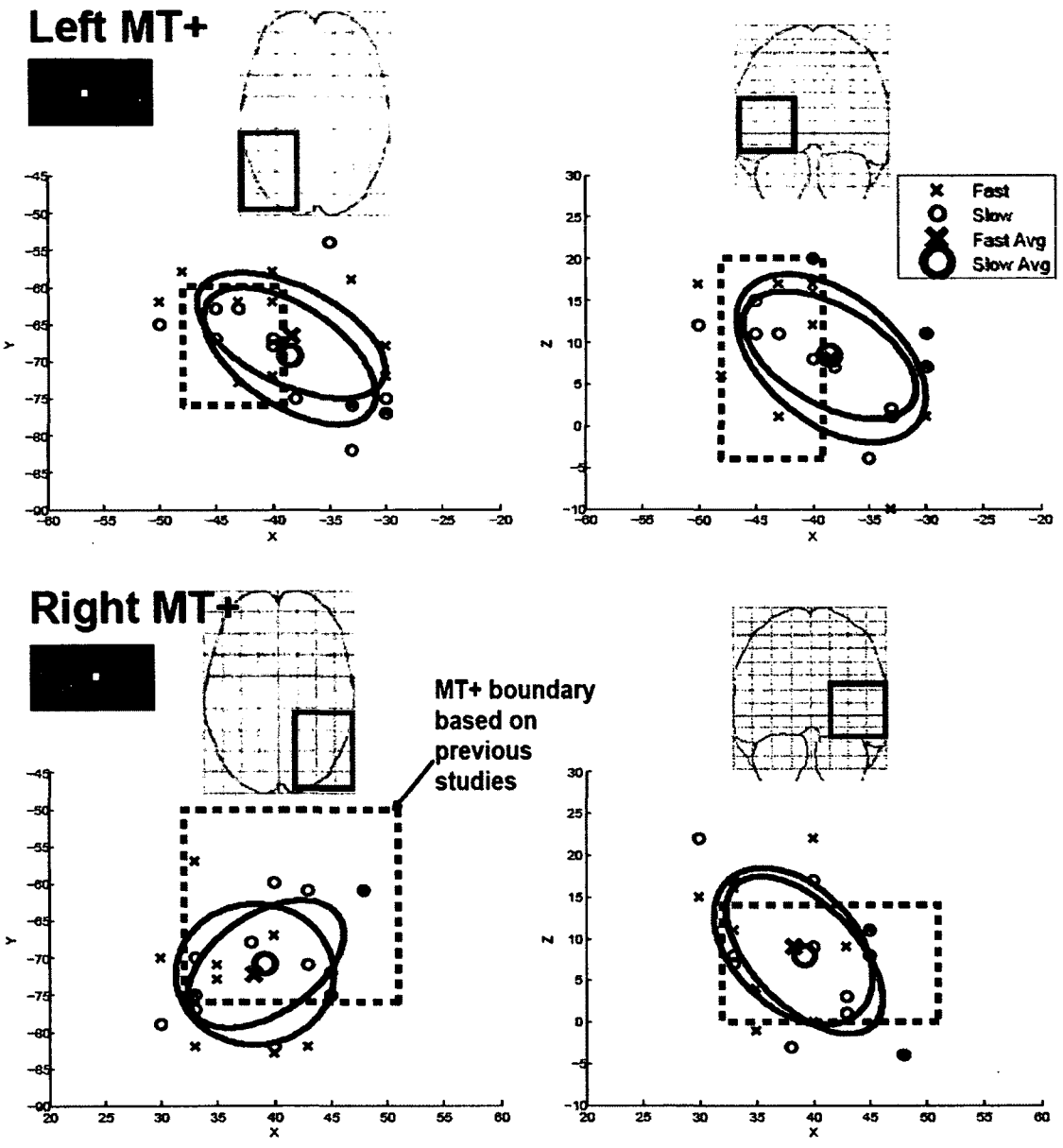

Figure 13. Individual and average MT+ locations. The Talairach coordinates of the individual MT+ peaks in axial and coronal view are plotted and compared with the MT+ locations reported in previous studies. The error of the MT+ coordinates is plotted as ellipses for fast and slow trials to illustrate the relationship of the two clusters of MT+ locations. The boundaries of the blue dotted line boxes are derived from the MT+ location reported in previous studies (see Table 3).

In order to inspect the commonly activated MT+ peak locations (instead of the mean x, y, z coordinates) evoked by the motion stimulus, a group analysis was conducted by averaging subjects' erSAM images at selected latencies in the Talairach space (see Methods section). The thresholds of each erSAM image in the time series were determined by an omnibus permutation test ($P<0.05$). When the averaged erSAM images were computed by aligning to the latency after stimulus onset, no above-threshold group MT+ activations were reported for fast and slow motion in both visual fields. However, when the averaged erSAM images were computed by aligning to the individual peak latencies, the fast and slow stimuli in both visual fields showed significant contralateral MT+ peaks (Figure 14).

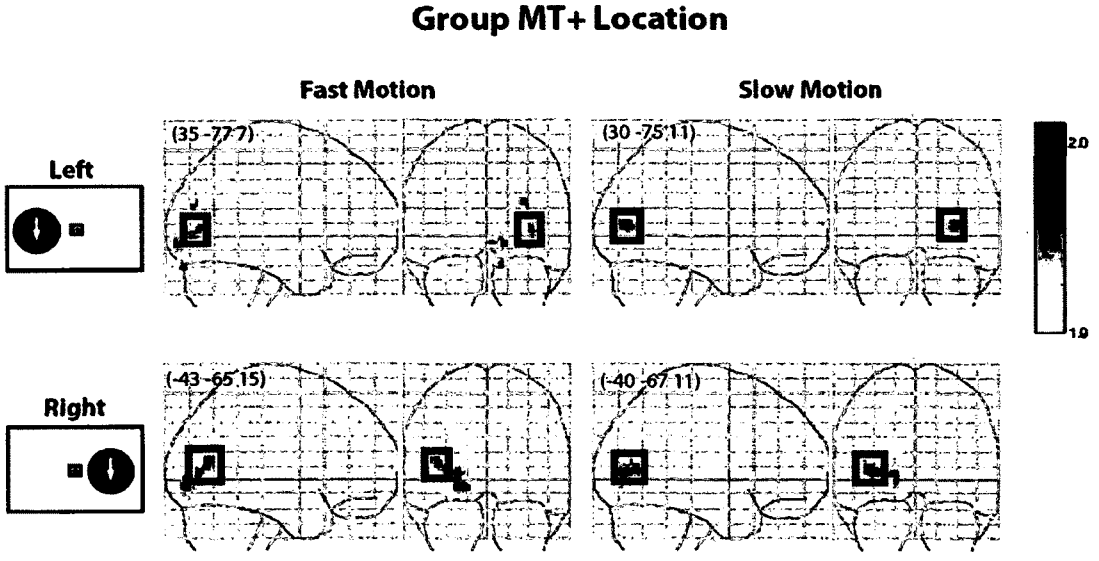

Figure 14. The group erSAM images showing MT+ peaks that are contralateral to the stimulated visual field. The group erSAM images were calculated by aligning the individual MT+ peak images. Top row: left visual display. Bottom row: right visual display. The Talairach coordinates of the group peak were displayed on the left top corner of the sagittal view. The erSAM averaging method was unable to capture these peaks when aligned to the latencies after stimulus onset, which was due to the large individual variability in peak latency as shown in Figure 15 & 18.

The ROI peak locations were picked based on the erSAM images with temporal resolution of 10 ms. Therefore, the amplitude and latency reported in the downsampled erSAM data did not necessarily represent the real data accurately (625 Hz sampling rate). In order to find the exact peak latency and activation amplitude (pseudo-Z), each subject's averaged waveform data were extracted from the individual virtual sensors for cuneus, V3A, and MT+. However, because the polarity of the dipole at each voxel (neuronal current flowing away or towards the cortical surface) is unknown, the sign of the beamformer waveform data could be arbitrarily determined during 3D source reconstruction, (Cheyne et al., 2007). This uncertainty is due to the fact that orientation is derived from source power independently for each voxel and the plus and minus sign may be randomly assigned for neighboring voxels. Therefore, absolute value of the waveform signal must be used for further analyses to avoid adding unnecessary variability into the data (Cheyne et al., 2007).

The activation peaks were searched in each subject's absolute waveform signals within the evoked response window (from 40 to 300 ms after motion onset) for the fast and slow motion in both visual fields. During this process, one subject (WW) showed unacceptable noisy virtual sensor data that were much lower in activation amplitude (pseudo-Z) and sometimes the visually evoked responses were invisible (see Appendix A & B). Therefore, subject WW was identified as an outlier and excluded from further virtual sensor analysis (see the outlier in Figure 17). In addition, we noticed that the beamformer demonstrated its

great capability in noise reduction during signal sources localization for subject WW (see Appendix C & D), and therefore we did not exclude WW's data in the group average erSAM images (Figure 13 & 14). The peak latencies are shown in boxplot form in Figure 15. There was an evident trend that the cuneus had the earliest peak with small individual variability, and its peak was followed by V3A and MT+ peaks. Note that the MT+ source showed relatively larger latency variability than the other two sources, and this may account for the result of no significant MT+ peaks reported in the group average when the erSAM images were aligned to the latency after stimulus onset.

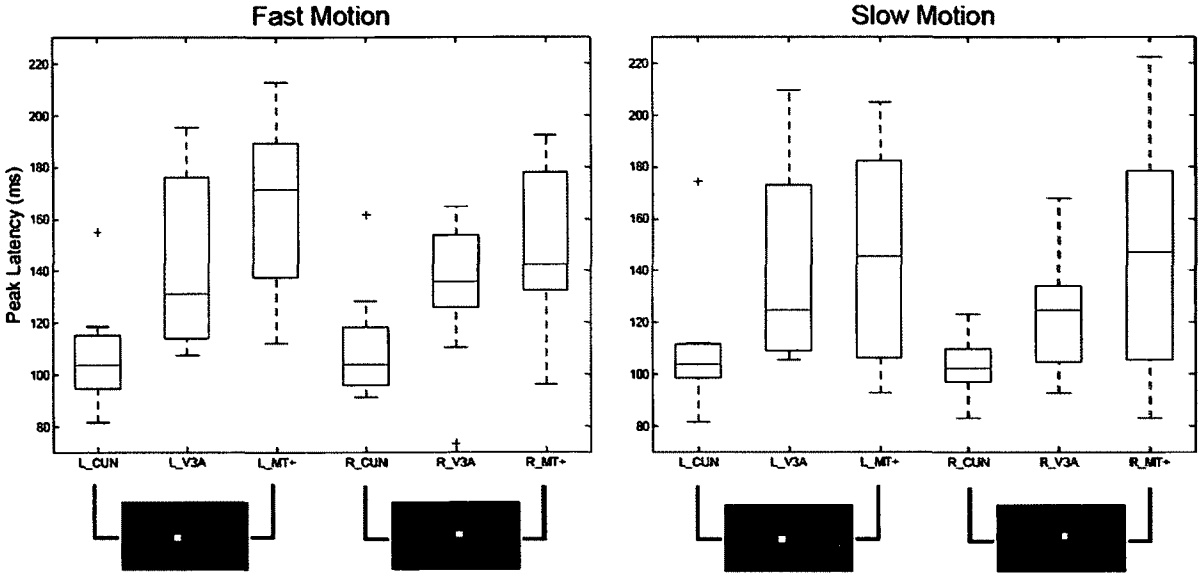

Figure 15. Box plots of individual virtual sensor peak latencies. Only the contralateral sources are plotted here for the fast and slow velocity. The boxes show the interquartile of the individual latencies. Red line is the median. Whiskers are the most extreme values within 1.5 times the interquartile range from the ends of the box. Those outside of the 1.5 interquartile range were displayed as "+". Subject WW's data was excluded. Source name are shown in short form (e.g. L_CUN: left cuneus, R_CUN: right cuneus).

Because individual variability in signal amplitude (pseudo-Z) may bias the grand average virtual sensor data, absolute virtual sensor waveform signals were normalized within each subject by first finding the largest amplitude among the four conditions (fast and slow motion velocity in both stimulated visual fields). The subject's waveform data of each of the four conditions were then divided by this largest amplitude value which resulted in activation of zero to one unit space. The average sensor waveform data and mean difference were plotted in Figure 16 to compare how the signals changed over time for fast (green curve) and slow (black curve) motion in both stimulated visual fields. The difference between the fast and slow motion for each ROI was tested by a Lilliefors permutation test with a significant level of 0.05 (Conover, 1980), and the significant mean differences were shown as red dots along the difference curve (blue). Cuneus and V3A both showed a clear main peak from 100 to 120 ms and a less obvious second peak from 180 to 200 ms. The main peak latency difference between cuneus and V3A was approximately 20 ms. In contrast, MT+ showed more sustained activity from 60 to 260 ms, but it seemed to have two separate peaks.

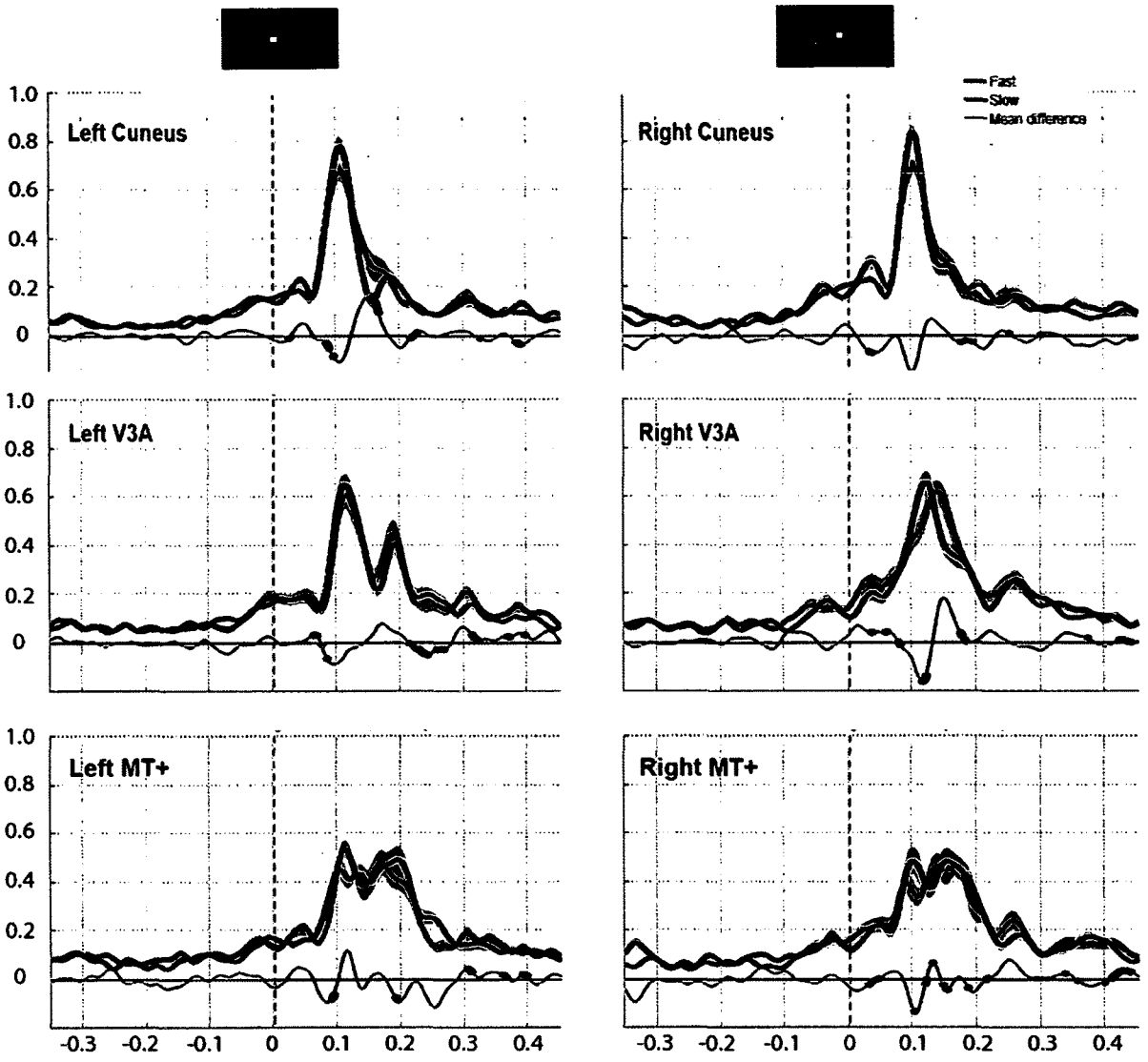

Figure 16. Grand average sensor data (normalized) from cuneus, V3A, and MT+ contralateral to the stimulated visual field (red dotted line: the onset of motion stimulus). Each column of figures shows the average data for one visual display as indicated by the icon on the top (left column: right visual field; right column: left visual field). The standard error of the mean is plot as shaded area along the curves (most are too small to be visible). The significant mean differences between fast and slow motion were determined by a Lilliefors permutation test, and the differences are shown as red dots ($P < 0.05$).

To inspect the effect of the motion velocity and stimulated visual field on ROI peak latency and amplitude, a three-way ANOVA was conducted for factors as follows: (1) fast and slow baseline velocity, (2) left and right visual display, (3) selected regions of interest (cuneus, V3A, and MT+). The results showed a main effect of ROI on peak latency, $F(2, 134)=8.92$, $P<0.05$, and a main effect of ROI on normalized amplitude, $F(2, 134)=18.79$, $P<0.05$. There were no significant effects found for velocity and the side of stimulated visual field, and there were no significant interactions between these three main factors. However, there was a marginally significant effect of velocity on ROIs' peak latency, $F(1, 134) = 3.00$, $P<0.07$. Matlab multiple comparison tests showed that the cuneus had significantly earlier peak latency and higher amplitude than V3A and MT+. To have a better overview of the amplitude and latency of the three ROIs, the pseudo-*Z* amplitude, normalized amplitude, and peak latency were collapsed across fast and slow velocity and stimulated visual field for each individual and plotted in Figure 17. Among the twelve subjects, three subjects (3, 4, and 9) showed relatively high pseudo-*Z* amplitudes. Both pseudo-*Z* and normalized amplitude demonstrated a pattern of descending staircase from cuneus to V3A, and to MT+. Conversely, the peak latency demonstrated a pattern of ascending staircase from cuneus to V3A, and to MT+ within each subject.

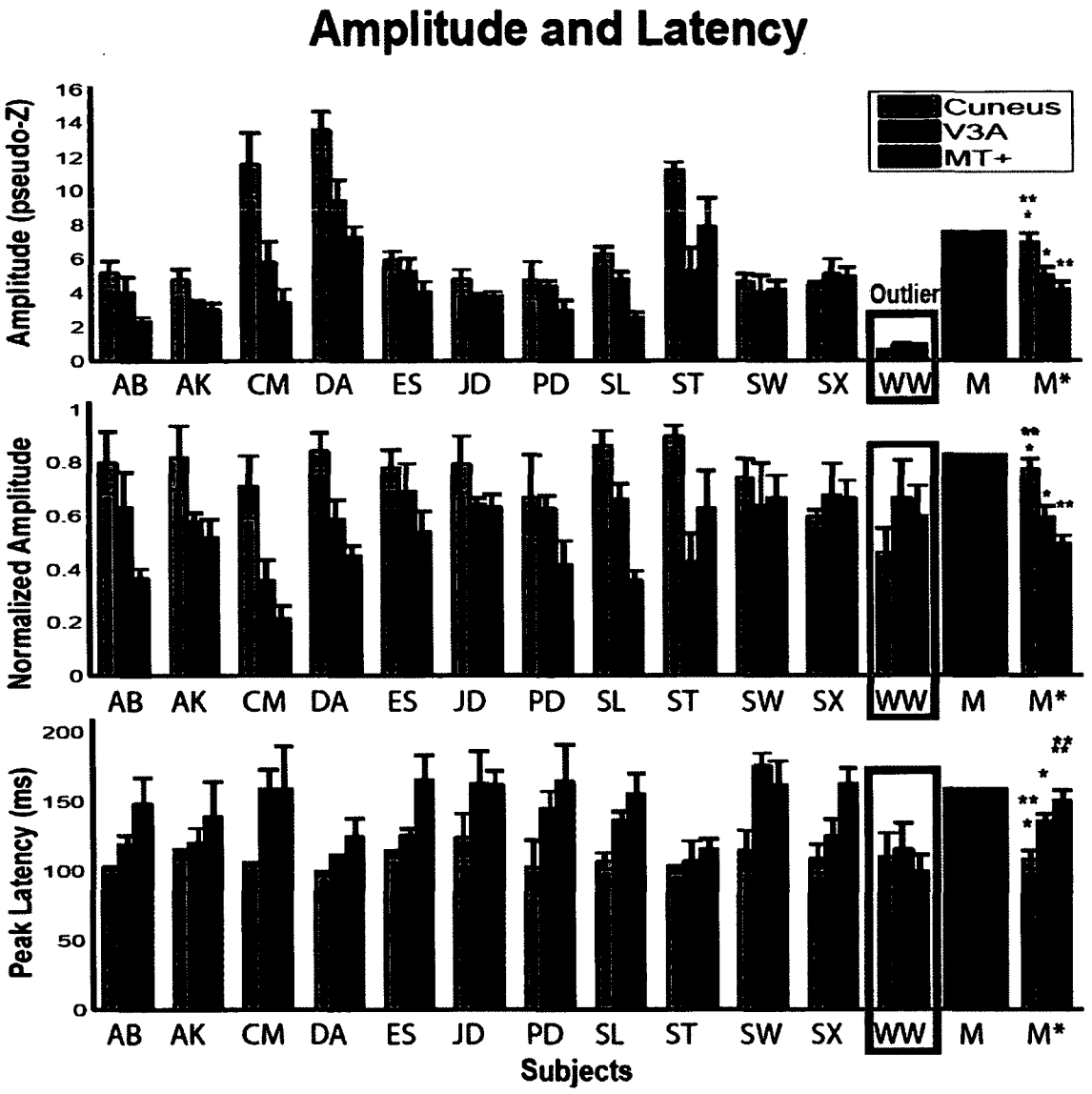

Figure 17. Average amplitude and latency collapsed across the stimulated visual field and motion velocity. Error bars were the standard deviation within each subject. Subject CM, DA, and ST had larger peak amplitude (pseudo-Z) than the other subjects. Subject WW was identified as outlier (see Appendix A & B). M: the group mean when subject 12 was included. M*: the group mean with subject WW's data excluded from averaging.

Figure 18 was next plotted for showing an overview of the ROI peak amplitude against latency. The cuneus source showed highest amplitude and earliest latency, and the data were much more tightly clustered than the V3A and MT+ sources. The average MT+ latency varied from 110 to 170 ms, and the amplitude was relatively lower compared to the cuneus and V3A sources. A general pattern was evident that the sources having early latencies showed higher amplitudes, and the sources having lower peak amplitudes were observed to have more variable latencies.

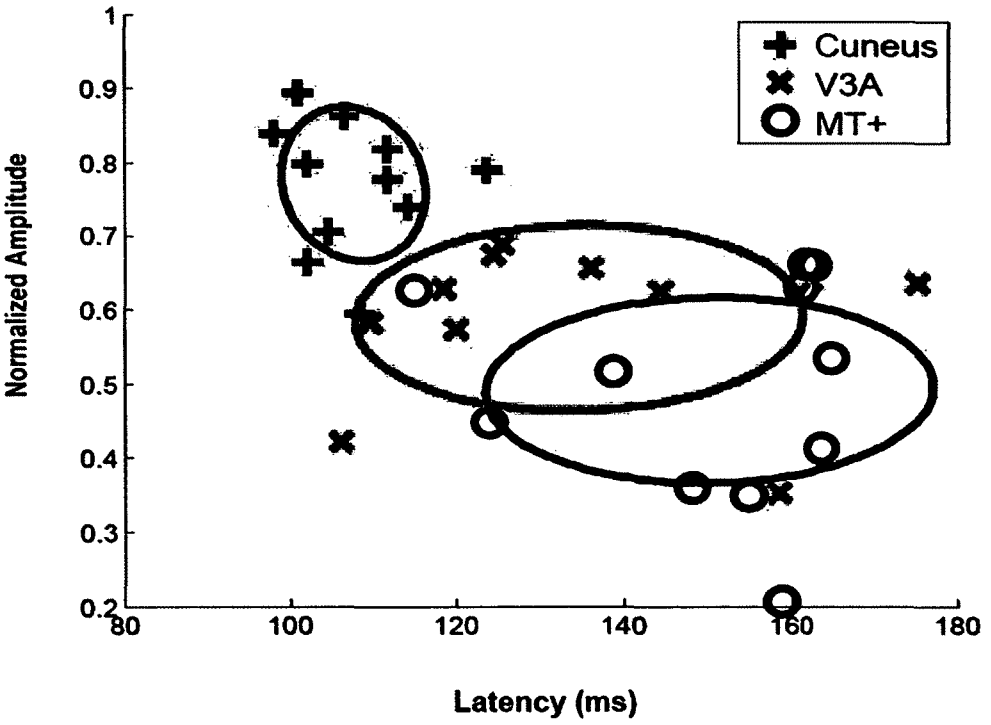

Figure 18. ROI peak latencies were plotted against normalized peak amplitude. Each item in the plot stands for the averaged data for one subject's ROI. Error ellipse was plotted for each ROI.

Motor Intention

In order to investigate the neural correlation of decision-making and motor intention, left and right visual field display trials were combined and aligned to the onset of velocity change. Although a previous study (Martinez-Trujillo et al., 2006) has shown remarkable evoked response and located individual MT+ and parietal sources after a motion change in translating dots, we expected a weak evoked response in the motion-processing network in the current study. First, Martinez-Trujillo et al. (2006) used a very salient direction change of 40° from the baseline, which was about ten times above the detection threshold of motion direction in healthy and normal subjects (Watamaniuk & Sekuler, 1992). Moreover, it has been shown by Amano, Nishida and Takeda (2006) that the MEG signals are correlated to the change in motion speed. Not surprisingly, three out of twelve subjects showed visible evoked response for correct and incorrect responses. Because of the low signal-to-noise ratio of evoked response data, we defined our time window from 40 to 300 ms and regions of interest in the frontoparietal network based on well-established motion detection theories (Burr, 1981; Watson & Nachmias, 1977) and data from previous ERP/MEG and neurophysiology studies (Amano et al., 2006; Bach & Hoffmann, 2000; Kaneoke, 2006; Schmolesky et al., 1998).

Group average erSAM images were visually inspected within 40 to 300 ms window after the velocity change onset (for an explanation of the paradigm, see Figure 9 & 10). Multiple peaks in the frontoparietal regions were found within 300

ms after the velocity change at various time points in the correct trials (see left column in Figure 19). However, the incorrect trials showed almost no above-threshold activations in the frontoparietal network except for activations reported as the left medial frontal gyrus (MFG/ACC) at 50 ms after velocity change (see right column in Figure 19). In the correct responses, at 50 ms after the velocity change, there were activations in the frontal and parietal regions. At 120 ms, two left frontal peaks were found respectively in the premotor (BA9) and somatosensory cortex (SMC). The frontal activations were then followed by a peak in the left inferior parietal lobule (pIPL) at 220 ms, and this peak continued moving forward to a more anterior site within the left IPL from 220 to 280 ms. The thresholds of each erSAM image in the time series were determined by an omnibus permutation test ($P<0.05$). The erSAM image at 50 ms of both the correct and incorrect trials showed relatively lower source power (pseudo-Z) compared to the erSAM images at other time points in Figure 19. For better viewing of this figure, its original threshold (0.6) was used instead of using a more conservative threshold scale (0.7).

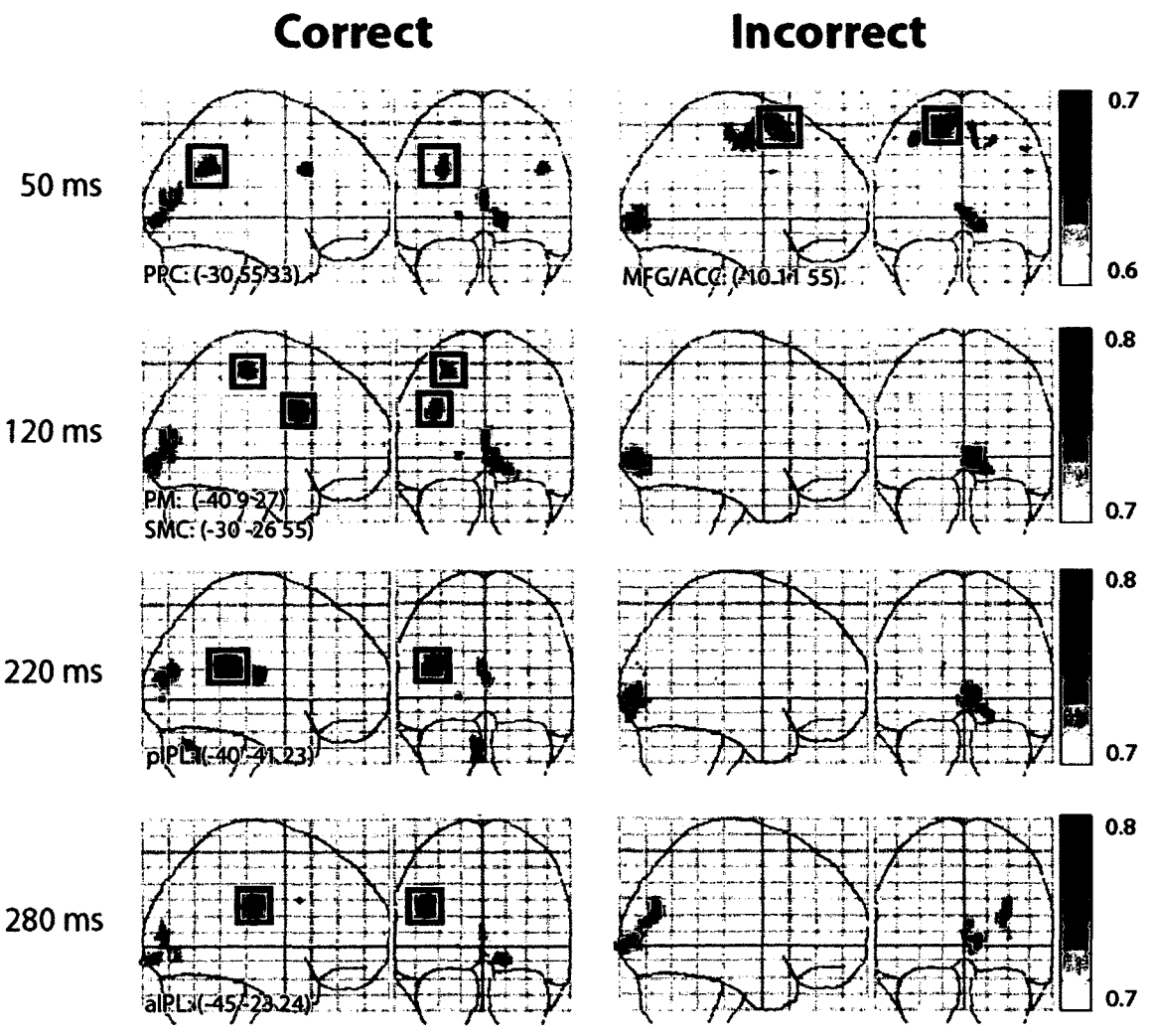

Figure 19. Source localization after velocity change. In the correct trials, group *erSAM images show more frontoparietal activations after the change onset as* follows: at 50 ms, peaks were found in the left PPC and right premotor (PM); at 120 ms, peaks were found in left SMC and PM; at 220 ms, a peak were reported in the left pIPL, and this signal peak moved to a more anterior site within the left inferior parietal region (aIPL) at 280 ms. In the incorrect trials, a left MFG/ACC peak was reported at 50 ms, and the frontoparietal network had no significant evoked responses. The colour bars indicated the pseudo-*Z* value of the activation. The original threshold (0.6) of the erSAM at 50 ms was used for plotting because of its relatively low signal-to-noise ratio. (PM: premotor cortex. PPC: posterior parietal SMC: *sensory motor cortex. pIPL: posterior site in the inferior parietal lobule. aIPL:* anterior site in the inferior parietal lobule)

Button press

Group erSAM time series for button press were visually inspected to localize the ROIs that are involved in the motor preparation and execution. In order to differentiate a task-dependent cortical activation map, we compared the erSAM image of correct and incorrect trials. According to a previous study, a pre-movement motor field (MF) for button press typically starts from 500 ms and reaches maximal amplitude approximately 50 to 60 ms prior to movement onset (Cheyne et al., 2006). They also reported that the signal sources of button press MF is bilaterally distributed over the precentral gyrus, and the stronger peak is localized to the hand area of contralateral precentral gyrus. The pre-movement MF is followed by a peak in the contralateral postcentral gyrus at 40 ms after movement onset, corresponding to the first movement-evoked field (MEFI). The MEFI is then followed by a second activation of the precentral gyrus at a latency ranging from 130 to 160 ms, corresponding to the second movement-evoked field (MEFII). Thus, the peaks of the movement related fields (MF, MEFI, and MEFII) followed a spatial sequence from precentral, to postcentral, and return to the precentral region (Cheyne et al., 2006). In addition, the left inferior parietal was found to be activated prior to the movement no matter which hand was used for button press.

The group erSAM images of our data showed that the timing of the erSAM peaks in the sensorimotor region was consistent with the previous studies;

however, the peaks were different for MEFI and MEFII. The pre-movement MF peak was found at 60 ms in correct responses and at 70 ms in incorrect responses prior to the movement onset. The major sources of the MF were reported as the bilateral precentral gyrus (BA 4) for both correct and incorrect trials, and the contralateral precentral gyrus showed stronger amplitude (Figure 20). The MEFI component was found at 40 ms for both correct and incorrect trials as a highly dipolar field pattern over the contralateral hemisphere, which is the feature of the first movement-evoked field (MEFI) component following movement onset (Cheyne et al., 2006). The group MEFI peak was found to be slightly posterior to the MF peak, and it was localized within the contralateral precentral gyrus (BA 4). The MEFII peak was found at a latency of 150 ms in the correct trials and 130 ms in the incorrect trials, and the peak was localized to the contralateral postcentral gyrus (BA3). Our results show that the peaks of the movement related fields (MF, MEFI, and MEFII) followed a spatial sequence from an anterior site to a more posterior site within the precentral, and moved to the postcentral region. The correct and incorrect responses demonstrated no spatial differences in these sources. In addition, the nature of MF, MEFI, and MEFII determined large difference in pseudo-*Z* amplitude and threshold value (Cheyne et al., 2006). If the same threshold scale was used in Figure 20 (the largest threshold as a conservative measure), the MF and MEFII would show no above-threshold activations. Therefore, in this plot, each erSAM image used its original threshold that was determined by omnibus permutation test ($P<0.05$).

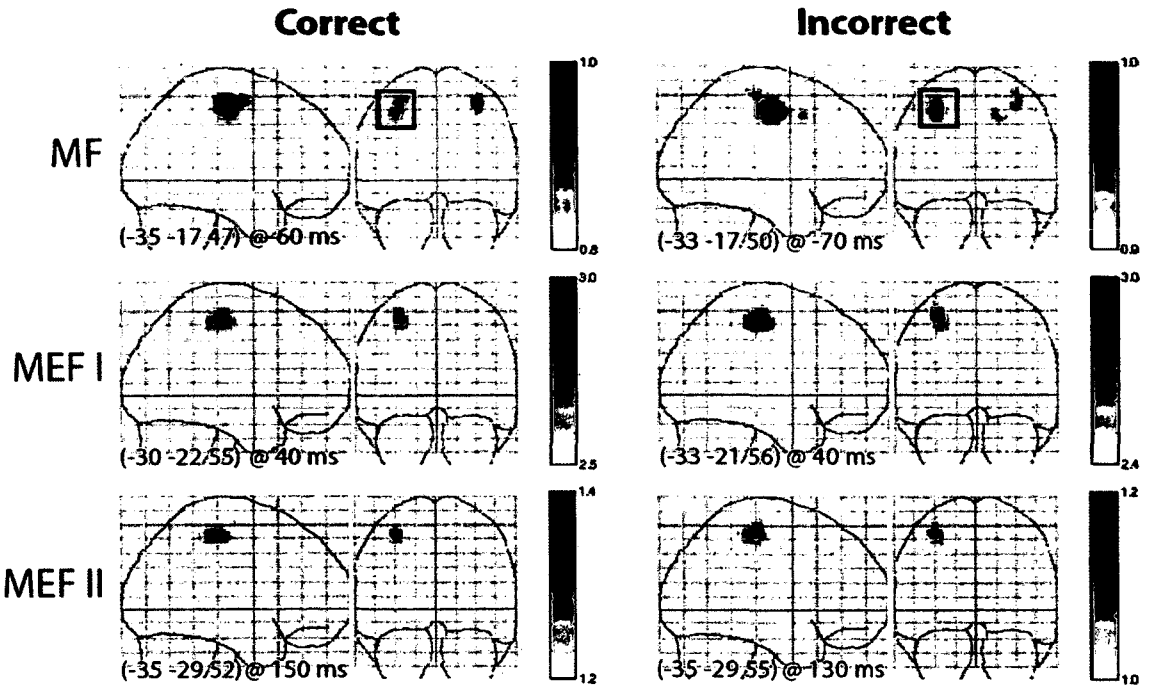

Figure 20. Source localization for motor responses. The Talairach coordinates and latency of the peaks are shown on the bottom of each panel. For all the motor related fields, the correct and incorrect trails showed similar activation pattern with slightly different latencies. The MF showed bilateral precentral gyrus activation with stronger source in the contralateral hemisphere (in the black boxes). The strongest signals generated in the SMC region were found to be the MEFI which occurred at 40 ms after the movement for both correct and incorrect responses. The MEFII was generated in the postcentral gyrus and more posterior to the MEFI source. (MF: motor field. MEFI: first movement-evoked field component. MEFII: second movement-evoked field component. SMC: sensorimotor cortices).

Time-frequency (TFR) analysis

The full spectrum time-frequency representation (TFR) plots were derived from beamformer single-trial data from the virtual sensors to examine phase-locked as well as the non-phase-locked oscillatory activity. The TFR plots represent the percent change in the total source power during the epochs with respect to the baseline period in the frequency range from 1 to 100 Hz. We only

showed source power increase (red) and decrease (blue) in the frequency range from 1 to 40 Hz in Figure 21 because our TFR analysis data did not show significant γ band activity.

The TFR plots in the left column illustrated the oscillatory activities of the whole trial for the correct and incorrect responses (baseline: 0.5 to 1 s prior to the stimulus onset during fixation, see Figure 10). The motion stimulus was displayed for 2.2 seconds in total, and the onset of velocity change was randomized from 0.75 to 1.25 s after the stimulus onset. Our main interest was to inspect the signals related to decision-making processes by comparing the oscillatory activities of the correct responses with incorrect responses time-locked to the velocity change (shown in the right column, baseline: 0 to 0.5 s prior to the velocity change). The mean difference between responses was tested with an unpaired permutation test for each pixel, and the significant differences ($P<0.05$) were encircled in highlighted dots and shown in the plots for incorrect responses.

The first and second plots in the right column showed that, after velocity change, the left premotor region demonstrated more sustained high β band event-related desynchronization (ERD) in the correct trials, and a significant high β band difference was found between the correct and incorrect trials within 200 ms ($P<0.05$) as shown in the magenta boxes. The third and fourth plots in the right column showed that the left SMC demonstrated a distinctive high β ERD in the correct trials immediately following the velocity change, and the amplitude of this ERD increased after 400 ms (shown in the green boxes). This high β band power

difference between the correct and incorrect trials could be observed in the whole trial TFR data as well (in the third and fourth plots in the left column). More importantly, the left pIPL showed β band ERD approximately from 200 to 400 ms following the velocity change in the correct responses (shown in black boxes in the fifth rows in the right column), and after 400 ms, the correct and incorrect responses demonstrated no differences in oscillatory pattern. In addition, the left pIPL demonstrated significantly more α band ERS in the whole trial data for the incorrect trials (shown in the sixth plot in the left column). Overall, we observed more β band ERD time-locked to the velocity change in the correct responses from the left frontoparietal sources, and the low α and θ band activities following the velocity change observed in these main sources confirmed that the velocity change evoked low signal-to-noise response observed in the average sensor data.

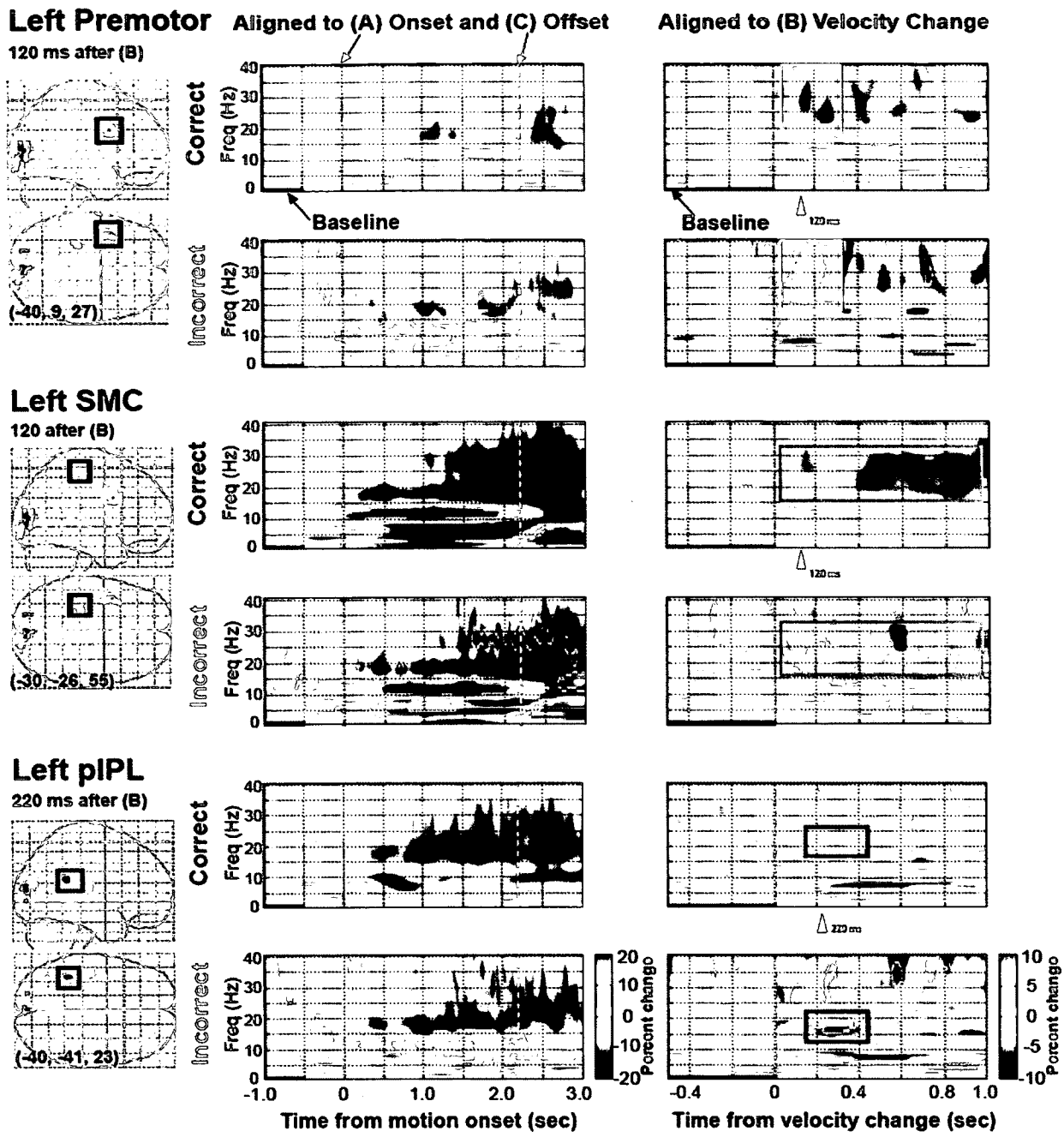

Figure 21. The first and second rows in the right column show that within 200 ms of the (B) velocity change, left premotor showed high β band differences (in magenta boxes). The third and fourth rows in the right column show that the left SMC demonstrated sustained high β ERD in the correct trials after the velocity change, which increased amplitude after 400 ms (in green boxes). The last two rows in the right column illustrate that from 200 to 400 ms, the left pIPL showed α band power differences between correct and in correct trials (in black boxes). The significant differences (determined by a nonparametric unpaired permutation test, $P<0.05$) were encircled in highlighted dots. The red arrows indicated the latencies when the peaks were selected (Figure 19).

Another key structure, the left MFG/ACC, also showed different oscillatory activity patterns between the correct and incorrect responses (Figure 22). In the correct trials, the MFG/ACC had stronger β band ERD over the time course of the whole trial (shown in the first and second plots in the left column). The first and the second row in the right column are the TFR representations for velocity change onset. To inspect the effect of velocity change to the oscillatory activities, they were computed based on a 500 ms baseline window prior to the change onset when the motion stimulus was being displayed. The TFR analysis showed that, after the velocity change, the MFG/ACC demonstrated two β band ERD components similar to what was observed in the left SMC (see Figure 21, third and fourth raw in the right column). The first β band ERD component started from 100 ms and terminated at 300 ms (shown in the first box), and the second component began after 400 ms (shown in the second box). These two plots showed relatively low amplitude compared to other plots (this was also consistent with the low amplitude of evoked-response observed in the sensor data). However, the β band oscillatory power following velocity change did show power differences ($P<0.05$) between correct and incorrect responses (shown in the black boxes in first and second plots in the right column). The third and fourth row in the left column are TFR representations for stimulus offset (GO instruction) which was computed based on a 500 ms baseline from 1.4 to 1.9 s prior to the offset. Because the motion stimulus was displayed for 2.2 s, we chose the baseline window from 300 s after the motion onset to avoid including evoked response in

the baseline period. After the GO instruction, the correct trials showed a significantly stronger β ERD beginning at 200 ms and ending near 600 ms, and this β ERD was coupled with α band ERD. The termination of the β ERD at 600 ms after the GO instruction in the correct trials was close to the latency of button press (±SD) = 520 ± 160 ms for the correct responses. The third and the fourth rows in the right column are the TFR representations for correct and incorrect trials aligned to button press events which were computed based on a 500 ms baseline from 2 to 2.5 s prior to the button press. The latency for button press was 520±160 ms and 640±230 ms for correct and incorrect response respectively, and 2 to 2.5 s prior to the button press was a 500 ms time window started near 300 ms after the motion onset. Thus, the visual evoked-response was excluded in this baseline period. The TFR analysis showed that the pre-movement α band synchronization was more consistent in the correct trials (shown in the boxes in third plot in the right column). Moreover, both the correct and incorrect trials showed clear motor evoked-response below 7 Hz, but the correct trials demonstrated significantly stronger β band ERD. In addition, after the button press, the MFG/ACC showed a post movement β band rebound in both correct and incorrect trials. Overall, the β band ERD time-locked to the velocity change, and the pre-movement α band ERS differentiated the TFR representation of the correct and incorrect response.

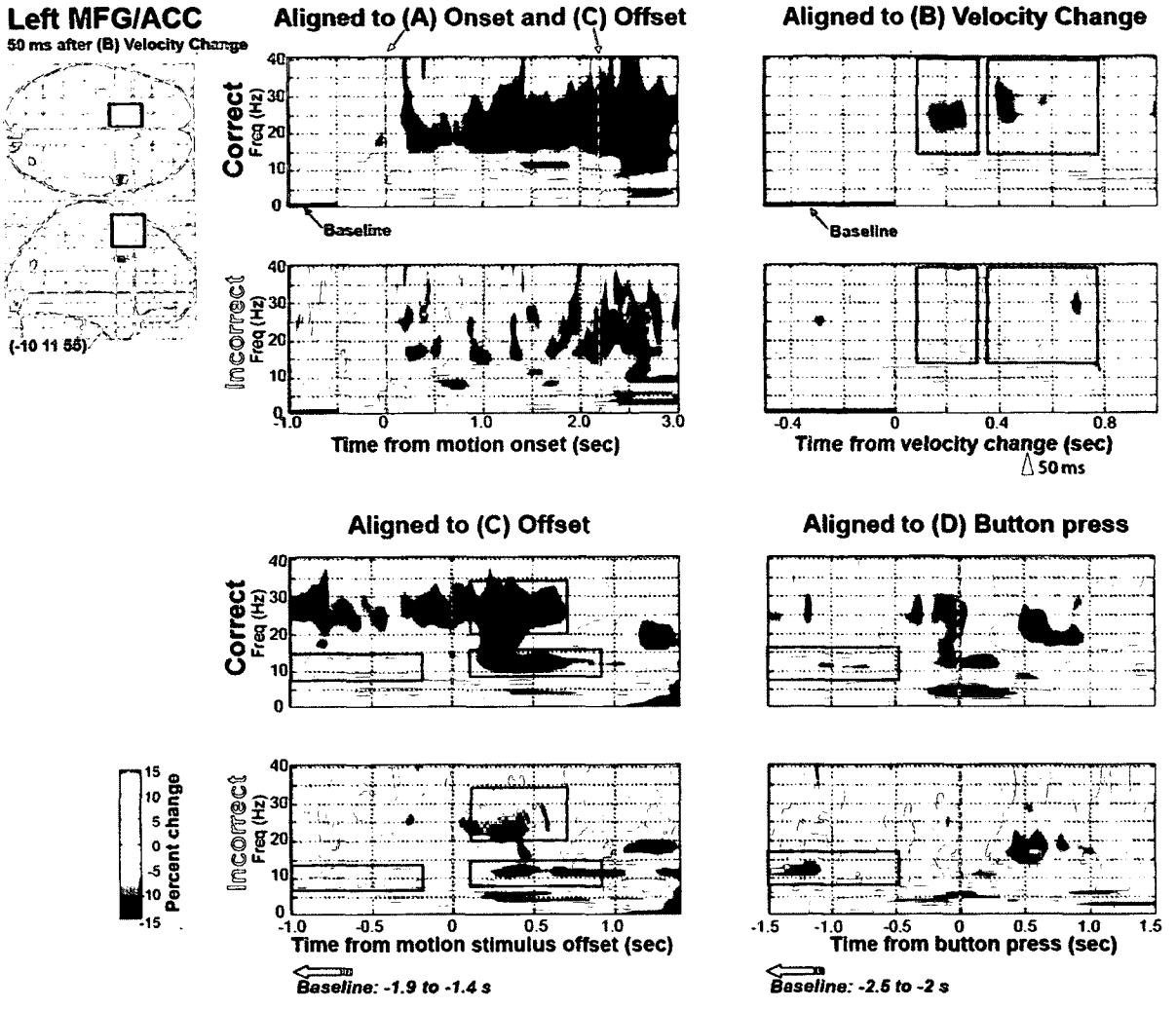

Figure 22. The MFG/ACC showed more visible high β band ERD throughout the whole trial after (A) stimulus onset. Two very distinctive high β band post-stimulus ERD components were observed after the (B) velocity change (shown in the black boxes). The high β band ERD differences continued until 600 ms after the (C) GO instruction. A clear pre-movement α band synchronization was only observed in the correct trials prior to the (D) button press (shown in the black boxes). The significant differences between the correct and incorrect trials were determined by a nonparametric unpaired permutation test ($P<0.05$), and the different areas were encircled in highlighted dots. The red arrows indicated the latencies when the peaks were selected (Figure 19).

Discussion

To date, this is the first study that uses MEG to examine velocity-dependent signals in the human motion processing network. The data from our study showed that the motion stimulus onset evoked strong neuromagnetic response in all of our subjects. We used an event-related beamformer (erSAM) and successfully localized the motion signals in cuneus peaked near 100 ms, and in MT+ peaked approximately from 110 to 170 ms, while the V3A source latencies were more variable. Our results were consistent with previous studies that the highest MEG peak (M1) was generated not only by the cuneus, but also partially by V3A and MT+. However, we were unable to find the evidence to support to our first hypothesis that fast motion velocity would evoke an early MT+ response approximately at 50 ms. We did not find the velocity-dependent spatial dynamics in the MT+ either.

An interesting result was that after the velocity change in the motion stimulus, the frontoparietal network was found active at various time points only in the correct trials. Moreover, the correct and the incorrect trials demonstrated different α and β band oscillatory power from these frontoparietal sources. The differences in spatial dynamics and oscillatory activity pattern from the frontoparietal region implied that different neural populations in this ensemble could be recruited during the accumulation of sensory evidence for the formation of a decision. Moreover,

the erSAM signal sources were mostly localized within the left hemisphere, which suggested a functional asymmetry in directing visuomotor attention and in the formation of a perceptual decision. The results supported our second hypothesis that the motor intentions would emerge during the delay period in the frontoparietal network (in areas such as PPC, SMA, and PMC) when the subjects could perceive the velocity change and that the PPC will be a key structure in the formation of motor intention during decision-making.

Motion processing of velocity signals

Previous studies using EEG/MEG have showed that P1/M1 and N2/M2 reflected the properties of the motion stimulus (Bach & Ullrich, 1994; Kuba & Kubova, 1992; Kubova, Kuba, Hubacek, & Vit, 1990; Kubova, Kuba, Spekreijse, & Blakemore, 1995; Nakamura & Ohtsuka, 1999; Niedeggen & Wist, 1999; Prieto et al., 2007). After the motion stimulus onset, P1/M1 peak varied from 100 to 140 ms while N2/M2 emerged approximately from 150 to 200 ms post-stimuli (Kuba & Kubova, 1992; Kubova et al., 1990 & 1995). Our data confirmed previous findings that the motion stimulus onset did evoke a clear electromagnetic response peaked at 100 ms and lasted approximately 200 ms. We also found that the M1 component was generated not only by the cuneus source, but also partially by V3A and MT+. The temporal shifting of the erSAM peaks in the cuneus, V3A, and MT+ supports the idea that a feed forward connection and close functional relation exist between these structures in the early processing of a motion stimulus (Bullier, 2001). In addition, the average MT+ virtual sensor (Figure 16)

seemed to show two peaks with similar amplitude, and the second peak observed in MT+ was very close to the second peaks reported in cuneus and V3A. This implied a feedback projection from MT+ to the cuneus and V3A, which induced a second peak around 200 ms. This implied that during motion processing, cuneus, V3A and MT+ were activated repeatedly through forward and feedback connections and contribute to the different peaks observed in the global field power.

Latencies of Cuneus and MT+

In the current study, the motion stimuli were displayed in left or right visual periphery with 3.1° to 9.1° eccentricity, and thus the motion signals were mostly processed and transported by the M pathways (See Figure 2 & 9). However, we were not able to observe the effects of motion velocity on activation amplitude and latency in the region of interests for fast and slow velocities. In addition, we were unable to differentiate the cortical representation for fast and slow velocity in MT+. One reason could be the low signal-to-noise ratio of the early response (around 50 ms) for the "fast" signal in the visual network. As described by Bullier (2001) in the integrated model of visual processing, subregions in parieto-temporal area such as MT+ were very rapidly activated by visual inputs through the direct M pathway from the magnocellular layers of LGN. The computation results from these regions were rapidly sent back to V1 and V2 through feedback connections to modulate processing of parvocellular and koniocellular pathway information. Given the relatively small number of this M pathway input compared to the major

input to MT+, it is reasonable to infer that event-related averaging methods, namely the erSAM with a conservative omnibus permutation test, were not sensitive enough to detect this early signal in MT+, even if it does exist.

Furthermore, our results showed no effects of velocity on MEG signal latencies from the sources of interest which showed some resemblance to a previous study by Azzopardi et al. (2003) in which MT and MST neurons were recorded in macaques with unilateral V1 lesion while motion stimuli were shown in normal and defected visual field. They reported that motion velocity (4 or 20°/s) showed no effect on neuronal response latency in the MT contralateral to the lesioned V1. Moreover, V1 lesions did result in reduced response magnitudes and increased latencies in the ipsilateral MT, but the effects were irrespective of the motion velocity or where the stimuli were displayed (in scotoma or unaffected visual field). Azzopardi et al. (2003) also found that the V1 lesion did not selectively impair MT responses to slow motion as that has been seen in blindsight patient GY (Barbur et al., 1980; Zihl et al., 1983). Although the double dissociation reported in patients and the evidence in monkey literature (Girard et al., 1992; Rodman et al., 1989 & 1990) both support the existence of separate pathways for fast and slow motion, Azzopardi et al. (2003) reasoned, first, it has been shown that the MT neurons in monkeys with striate cortex lesions were not able to differentiate the motion direction of random dots but they were able to discriminate the motion direction of light bars (Azzopardi, Fallah, Gross, & Rodman, 1998). A similar phenomenon was also reported in patients with striate

cortex lesions (Azzopardi & Cowey, 2001; Barton & Sharpe, 1997; Cowey & Azzopardi, 2001). Azzopardi et al. (2003) concluded that moving bars could have confounded motion processing with relative position of the bars.

Moreover, the extensively studied blindsight patient GY might not be a good representation of the general population. Blindsight is not common among patients with large striate cortex damage. Patient GY acquired the unilateral striate cortex lesion at age of seven, and he began to participate in the experiments after the age of thirty six. It was possible that the alternative cortical and subcortical pathways connecting the LGN to MT+ has been strengthened as a result of neural plasticity over the decades following the deafference of major M and P pathways to V1. Bridge et al. (2008) in a DTI study on GY found that he had two unique pathways: one geniculocortical tract projecting from right LGN to the left MT+ (ipsilateral to V1 lesion), and another corticocortical tract connecting bilateral MT+. These two pathways might account for the blindsight in patient GY.

In addition, the sequence of the peak latencies in cuneus and MT+ has been found to vary not only with motion velocity but also with the contrast by Maruyama, Palomo, and Ioannides (2009). They reported that high contrast stimuli evoked responses peaked in cuneus regions first followed by MT+ peak with a lag between 34 and 55 ms. On the other hand, at low contrast, MT+ showed peak prior to cuneus by 27 ms, and both cuneus and MT+ demonstrated weaker activation amplitude than in high contrast condition. In the current study, we used a field of white dots moving on a black background. Although we did not measure

the contrast between the white moving dots and the black background, the contrast of the stimuli appeared to be fairly high. This particular setting could be a reason of why V1 showed earlier latency than MT+.

Frontoparietal Activation, Decision and Motor Intention

Following the velocity change, a widespread cortical network involving multiple regions in the frontoparietal area was found active at various time points in the correct trials. In contrast, the incorrect trials showed virtually no activations in the frontoparietal region after the velocity change except for the MFG/ACC activation from 50 to 60 ms. In the correct trials, the earliest activation in the parietal region, albeit low in amplitude, was reported at 50 ms after velocity change within the PPC area (Figure 19). According to Bullier's integrated visual processing model (Bullier, 2001), the subregions in parieto-temporal area could be very rapidly activated by visual inputs through the direct M pathway from the magnocellular layers of LGN, which in turn influences the visual signal processing in V1/V2 through feedback connections. If this direct M pathway does function as Bullier (2001) proposed, given the rapid response of the magnocellular layers in the LGN (50% of the population could be activated within approximately 30 ms as shown in Figure 3-B, Schmolesky et al., 1998), the event-related activation in PCC at 50 ms could very likely be the cortical source of the aforementioned rapid attention-related visual signals and thus indicate the higher attention load in the correct trials. In addition, this rapid signal latency at 50 ms in the posterior parietal region was almost identical with the latencies reported in the monkey LIP neurons

during attention-demanding visual tasks (Bisley, Krishna, & Goldberg, 2004; Zhang & Barash, 2000).

From 120 to 280 ms following the velocity change, frontoparietal activation was found only in the correct trials. The left PM and SMC regions were found to be activated at 120 ms. It is well understood that visual targets can be attended to without fixation (Sperling & Melchner, 1978), and the prefrontal regions (such as the frontal eye field) have been shown playing an important role in covert visual attention (Moore & Fallah, 2004; Thompson, Biscoe, & Sato, 2005). In the current study, the frontal activation after the velocity change supported the idea that the frontal and the parietal regions work together in directing covert visual attention during the early processing of the change detection. Although in our experiment only the right hand was used for button press, the left lateralization of the frontoparietal activation after the velocity change implied an overall functional asymmetry in directing visual attention and in forming a perceptual decision for a rule-based response. It has been previously reported that increased activation of the left inferior parietal lobe was correlated with self-paced movements in comparison to externally triggered movements (Ball, Schreiber, Feige, Wagner, Lücking, & Kristeva-Feige, 1999; Wiese et al., 2004), and the activation of left PPC was found to be involved in attention, reaching, and movement selection independent of the hand used in the tasks (Cheyne et al, 2006; Rushworth et al., 2001 & 2003; Vesia, Monteon, Sergio, & Crawford, 2006). Similar left lateralization in the inferior parietal regions was reported when movement was

only imagined (Krams, Rushworth, Deiber, Frackowiak, & Passingham, 1998).

Following the frontal activation, the posterior site of the PPC showed significant task-related activations from 220 to 280 ms only in the correct trials, which suggested its importance in the formation of perceptual decisions and motor intentions as shown in previous neuroimaging and neurophysiology studies (Churchland et al., 2008 & 2011; Desmurget et al., 2009a & 2009b; Gold et al., 2007; Kiani, et al., 2008 & 2009; Roitman et al., 2002; Shadlen et al., 2001). The peak of event-related activities moved from a posterior site in the left IPL to a more anterior site within the left IPL from 220 to 280 ms. The IPL activation observed here may have encoded the population firing rates in the human parietal area that reflected the accumulation of stochastic evidence of the visual input for a decision of motor response. The activation in the posterior site in the PPC was most prominent when subjects are covertly orienting visual attention (Nobre, Gitelman, Dias, & Mesulam, 2000). However, it was restricted to the anterior areas in the left supramarginal gyrus and the adjacent AIP region during hand movement preparation. On the other hand, evidence has shown that the disruptions introduced by TMS in the anterior site of the left PPC (the supramarginal gyrus) impaired the redirecting of motor attention regardless of which hand was used to respond (Rushworth et al., 2001).

Together, the frontal activations and the left inferior parietal (aIPL and pIPL) activations after velocity change in the correct trials showed their importance in directing covert attention and the perception of motion velocity change. Our

findings were consistent with Cisek's action selection model (2007), which could be considered as an elaboration of the action selection process defined in Gold and Shadlen's (2007) generalized decision-making model (see elements in red in Figure 7). With the current paradigm, it could be inferred that the velocity change was processed first in the motion network for specifying the potential actions (pressing left or right button) that were currently available in the motor repertoire as suggested by Cisek (2007). After the stimulus onset, these two potential actions for either left or right button press were competing against each other for further processing until the accumulation of sensory evidence (the velocity change) was captured and reached a crucial level to bias this competition which eventually resulted in a final selection of an action — this very likely was the case for most of the correct trials. Cisek's (2007) model further suggests that the potential actions are competing against each other within the fronto-parietal cortex, while the biasing factors are provided by the prefrontal and subcortical regions such as the basal ganglia. Our data are consistent with this hypothesis by demonstrating the early frontal (PM and SMC) activation approximately at 120 ms followed by the PPC activation from 220 to 280 ms after the velocity change. However, the motion sensitive region MT+ showed no above-threshold activations. This could be due to the fact that the erSAM and the thresholding methods were not sensitive to the activations when the activation latency had a large individual variability, which has been demonstrated and explained in the motion perception data (see Figure 14).

When comparing to the widespread frontoparietal activations observed in the correct trials, however, incorrect trials showed virtually no event-related responses in the frontoparietal network except for an early activation from 50 to 60 ms in the MFG/ACC region. The absence of the activation in the frontoparietal network in the incorrect trials confirmed the idea that a perceptual decision of the velocity change was unlikely to be formed and thus no motor intention for response was specified when a perceptual decision was unavailable (Cisek, 2007). The medial frontal and anterior cingulate cortex (MFG/ACC) connect extensively to multiple regions in the prefrontal cortices, the motor cortex, parietal cortex, midline thalamus, and the brainstem nuclei (for a review see Paus, 2001). Functionally, it has been considered as a key structure for motor control, cognition, emotion, arousal, and drive state. Two unique cognitive functions of the ACC seem to be relevant to the early responses seen in our data as error detection (Falkenstein, Hohnsbein, Hoorman, & Blanke, 1991; Gehring, Goss, Coles, Meyer, & Donchin, 1993) and executive attention and conflict monitoring (Carter, Botvinick, & Cohen, 1999; Posner & DiGirolamo, 1998). In addition, the dorsal ACC is connected with parietal cortex and the frontal eye field (FEF), which have been shown to have fast latency as early as 40 ms (Bullier, 2001). Considering the close functional and anatomical connectivity from the parietal and FEF to the MFG/ACC, this early activation seems plausible. However, it is difficult to deduce what contributed to the MFG/ACC activation observed in the incorrect response in the current paradigm design. The functional role of the MFG/ACC region needs to

be further investigated in the future research by examining the group as well as the individual dynamics in this region after separating responses of "hit", "miss", "false alarm", and "correct reject".

Frontoparietal Oscillatory Activities

The erSAM is an estimate of the evoked responses that are phase-locked to a stimulus, but the MEG data also contains non-phase-locked responses, which is also known as induced responses (Kiebel & Friston, 2004; Kiebel, Tallon-Baudry, & Friston, 2005; Makeig et al., 2002; Tallon-Baudry & Bertrand, 1999). These induced responses, especially at higher frequencies such as high β and γ band, are usually invisible to the event-related averaging methods but could be visualized by using a linear convolution with a Morlet wavelet after bandpass-filtering the single trial data (Tallon-Baudry et al., 1997). We observed noisy evoked responses following the velocity change, but we could differentiate the correct and incorrect responses by examining the oscillatory activities from the virtual sensors localized after the velocity change.

The time-frequency analysis revealed different frontoparietal oscillatory activity patterns between the correct and incorrect responses. One major finding was that the correct trials demonstrated significantly more β band ERD than the incorrect trials from 200 to 400 ms following the velocity change onset (see the first row in Figure 23). We interpret this parietal β band ERD as a neural signature underlying the accumulation of sensory evidence before the selection of a motor response in the parietal region as suggested by Cisek (2007) and Gold et al.

(2007). Moreover, the parietal β band ERD switched to ERS after 400 ms, and we noticed that the beginning of this β band ERS was perfectly aligned with the SMC β band ERD increment at 400 ms (indicated by the black dotted line in Figure 23). We propose that after a motor intention was formed (e.g. which button to press) in the parietal area after the detection of the velocity change, the ensemble that is responsible for decision-making returned to idling state, which was reflect by the initiation of parietal β band ERS and by the lack of difference in oscillatory pattern between correct and incorrect trials after 400 ms. Meanwhile, after the decision for the response was made, the motor command for moving the specified finger for button press was prepared in the SMC area, which was indicated by the increase in β band ERD amplitude after 400 ms. Thus, a motor intention following a visual perception was generated.

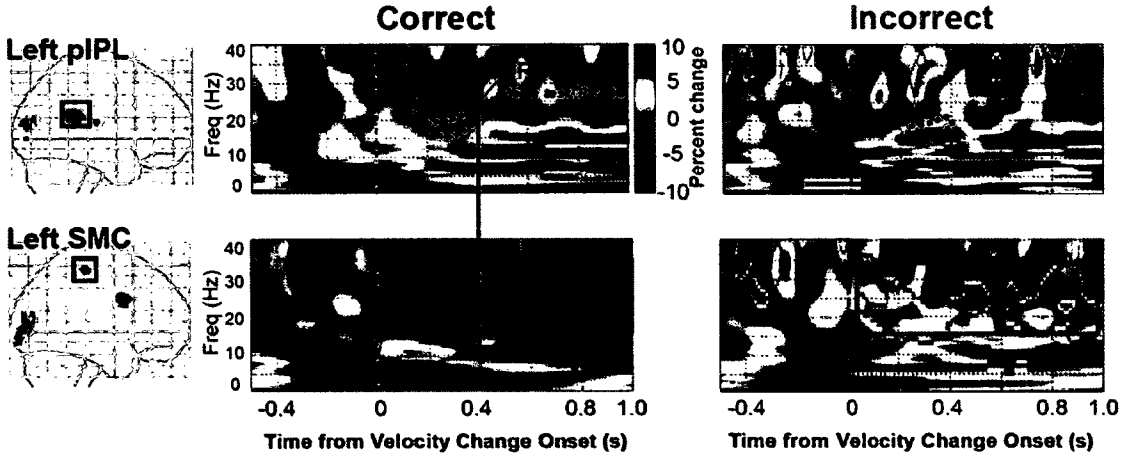

Figure 23. First row: in the correct response, the pIPL showed significantly more β band ERD from 200 to 400 ms as indicated by the area encircled by the dotted line. The pIPL β band ERS was perfectly aligned with the SMC β band ERD increment at 400 ms (indicated by the black dotted line). The significant differences between the correct and incorrect trials were determined by a nonparametric unpaired permutation test ($P<0.05$).

The difference in oscillatory activity patterns between the correct and incorrect responses from the pIPL and SMC sources implies that different neural populations in the frontoparietal ensemble could be recruited simultaneously for the parallel processing of a task related motor response. Supports to this idea are found in a monkey study by Pesaran, Nelson, and Andersen (2008) in which they reported that local field potential activity in dorsal premotor (PMd) and parietal reach region (PRR) showed lower 20 Hz and 10 Hz power respectively when the animals were following instructions (rule-based) than when they were freely making choices. Consistent with Cisek's model (2007), Pesaran et al. (2008) postulated that a sub-population of cells in frontal and parietal cortex form a decision circuit, and they coordinate to exert influences on motor planning by providing a bias towards the general goal of the action. In our data, both the SMC and the MFG/ACC showed prominent β band event-related desynchronization (ERD) after the velocity change onset (see Figures 21 & 22), which implied the preparation of the motor response in the correct trials after the perceptual decision was made. The 20 Hz ERD is an important neural signature of the activation of the motor cortex which is often observed after the motor plan is made and before the execution of the movement, or when the subject is passively viewing other people's movement (Cheyne et al., 2006; Donner, Siegel, Fries, & Engel, 2009; Eimer et al., 1998; Gaetz, MacDonald, Cheyne, & Snead, 2010; Haggard et al., 1999; Hari, Parkkonen, & Nangini, 2010; Libet et al., 1983). The clear termination of the 10 Hz event-related synchronization in MFG/ACC contralateral to the

responding hand prior to the button press in the correct trials (third figure in the right column, Figure 22) implies it may have triggered finger movement by suppressing the inhibitory signal it exerted on the (M1) for the effector as suggested by Ball et al. (1999).

Future Directions

Our result showed that the thresholded velocity change in the motion stimuli evoked very weak neuromagnetic responses in most of our twelve subjects. Considering the low signal-to-noise ratio in these data, we still could localize the event-related sources in the frontoparietal network that were thought to be related to the forming of decision and motor intention. In the current study, we provided two options for a forced-choice response. Although the behavioural data showed that the subjects could detect the velocity change with a correct rate (±SD) of 68.3%±11.7%, there was a relatively high probability (50%) of guessing the correct response even when the subjects were unable to detect the velocity change. This problem can be attenuated in the future experiments by adding a third-button as "did not see change" and inserting trials in which velocity change did not occur. Thus, the "hit" and "miss" trials will become more valid measurements. Moreover, it would be interesting to compare the behavioural output of "hit", "miss", "false alarm", and "correct reject", and to inspect what neural processes differentiate the behavioural output and what correlation are between the behaviour and neural responses. Moreover, in future studies, if responses are made by using different hands (or even with toes, saccades, or other body parts that are far away from hand's representation in the somatosensory homunculus), we will be able to further test the action-selection model (Cisek, 2007) by investigating the temporal and spatial dynamics in the

frontoparietal network or possibly demarcate a somatotopic map in the decision-making circuitry. In addition, the individual evoked response patterns in the frontoparietal network need to be inspected in the near future for better understanding the decision-making and action-selection process.

Synchronization of neuronal activity across brain regions is thought to reflect the distributed computation in the brain, and cross-frequency synchrony and within phase synchrony across the bands is often enhanced during various cognitive tasks. For instance, prestimulus and peristimulus α and β activities in the parietal sources have been shown as an important signature of vigilance, consciousness (Palva & Palva, 2007), active inhibition (Klimesch, Sauseng, & Hanslmayr, 2007), and was reported to be correlated with visual discrimination ability in attention-demanding perceptual tasks (van Dijk, Schoffelen, Oostenveld, & Jensen, 2008). Moreover, α and β power fluctuations were suggested to be correlated with the efficiency of signal processing and thus influence the accuracy of perceptual decision (Donner, Siegel, Oostenveld, Fries, Bauer, & Engel, 2007). The fluctuations in α and β oscillatory power was also implied to reflect the synaptic reverberation and temporal integration of motion signals in the decision-making process (Wang, 2001). The current study applied a Morlet wavelet with the single trial data (Tallon-Baudry et al., 1997) and used a nonparametric unpaired permutation test (Maris et. al., 2007) to compare the oscillatory power between the correct and incorrect responses. However, the temporal resolution in the domain below the α and β bands is relatively low by

using this method (e.g. α band's resolution is approximately from 67 to 125 ms) and thus is not a very ideal tool for analyzing signals across multiple regions, especially when the activation timing and sequence across regions is a research interest. To overcome this problem in the future analyses, we could inspect either the amplitude-independent phase locking (Tass et al., 1998) or the locking of the amplitude fluctuations of faster oscillations to the phase of a slower oscillation (Vanhatalo, Palva, Holmes, Miller, Voipio, & Kaila, 2004) for determining the functional connectivity. A good example of the analyses of functional connectivity with phase coherence across oscillatory sources in the MEG data was demonstrated by Palva, Palva, & Kaila (2005). In addition, although few groups are investigating the prestimulus α and β oscillatory activities, given the importance of prestimulus activities in vigilance and visual attention, this aspect of the data should also be inspected in the future analyses (van Dijk et al., 2008).

Table 1 – Correct response rate (fast and slow velocity)

Percentage (%)		Subjects														
		AB	AK	CM	DA	ES	JD	PD	SL	ST	SW	SX	WW	mean	stdev	sem
Fast	Correct	50.0	87.1	73.8	69.2	58.8	70.0	76.3	55.8	87.5	52.9	90.4	67.9	**70.0**	**13.8**	**4**
	Incorrect	42.1	12.9	26.3	30.8	40.4	30.0	23.8	38.8	11.7	43.8	9.6	28.3	**28.2**	**12**	**3.5**
	No resp	7.9	0.0	0.0	0.0	0.8	0.0	0.0	5.4	0.8	3.3	0.0	3.8	**1.8**	**2.7**	**0.8**
Slow	Correct	49.6	82.1	60.0	63.3	70.4	66.3	76.7	62.1	80.4	52.1	75.8	61.3	**66.7**	**10.6**	**3.1**
	Incorrect	44.6	17.9	40.0	35.8	29.6	32.9	23.3	32.1	19.2	42.5	24.2	36.3	**31.5**	**8.9**	**2.6**
	No resp	5.8	0.0	0.0	0.8	0	0.8	0	5.8	0.4	5.4	0	2.5	**1.8**	**2.5**	**0.7**

Table 2 – Correct response rate (left and right visual display)

Percentage (%)		Subjects														
		AB	AK	CM	DA	ES	JD	PD	SL	ST	SW	SX	WW	mean	stdev	sem
Left	Correct	50.8	85.4	66.7	67.9	63.8	64.2	77.9	60.8	81.3	57.1	85.4	66.3	**69.0**	**11.2**	**3.2**
	Incorrect	42.1	14.6	33.3	31.3	35.4	35.8	22.1	34.6	17.9	39.2	14.6	30.4	**29.3**	**9.6**	**2.8**
	No resp	7.1	0.0	0.0	0.8	0.8	0.0	0.0	4.6	0.8	3.8	0.0	3.3	**1.8**	**2.4**	**0.7**
Right	Correct	48.8	83.8	67.1	64.6	65.4	72.1	75.0	57.1	86.7	47.9	80.8	62.9	**67.7**	**12.7**	**3.7**
	Incorrect	44.6	16.3	32.9	35.4	34.6	27.1	25.0	36.3	12.9	47.1	19.2	34.2	**30.5**	**10.7**	**3.1**
	No resp	6.7	0.0	0.0	0.0	0.0	0.8	0.0	6.7	0.4	5.0	0.0	2.9	**1.9**	**2.7**	**0.8**

Table 3 – MT+ localization (previous and current study)

Current Study	N	Left Peak (Tal)			Right Peak (Tal)		
Fast motion	12	-40	-65	15	35	-72	11
Slow motion	12	-38	-75	7	30	-75	11
Previous Studies	**N**	**COGleft (Tal)**			**COGright (Tal)**		
Giaschi et al., 2007	6	-45	-68	-3	39	-60	-1
Martinez-Trujillo et al., 2006 (MEG)	9	-42	-63	20	51	-50	14
Wilms et al., 2005 (functional)	14	-45	-68	12	51	-66	8
Wilms et al., 2005 (anatomical)	10	-43	-67	8	49	-64	9
Dukelow et al., 2001	5	-	-	-	44	-66	2
Rees et al., 2000	4	-44	-64	2	50	-66	0
Dumoulin et al., 2000	10	-47	-76	2	44	-67	0
Sunaert et al., 1999	12	-42	-66	2	42	-62	6
Goebel et al., 1998	5	-48	-60	2	45	-57	5
Hasnai et al., 1998 (PET)	11	-39	-72	-1	41	-65	2
Smith et al., 1998	15	-46	-70	4	46	-70	4
Beauchamp et al., 1997	8	-42	-70	3	42	-70	3
Dupont et al., 1997	10	-40	-70	-4	40	-64	4
Tootell et al., 1995	6	-45	-76	3	45	-76	3
Dupont et al., 1994 (PET)	14	-46	-72	0	32	-74	8
Watson et al., 1993 (PET)	12	-44	-70	0	40	-68	0
Maximum		-39	-60	20	51	-50	14
Minimum		-48	-76	-4	32	-76	0
Average		-43.9	-68.8	3.3	43.8	-65.3	4.2

COGleft: center of gravity of the activation in the left hemisphere. COGright: center of gravity of the activation in the right hemisphere

List of Abbreviations

aIPL – anterior inferior parietal lobule

ERD – event-related desynchronization

erSAM – event-related synthetic aperture magnetometry (beamformer)

ERS – event-related synchronization

MFG/ACC – medial frontal gyrus and anterior cingulate cortices

MF – motor field

MEFI – first movement-evoked field component

MEFII – second movement-evoked field component

MT – middle temporal region

LIP – lateral intraparietal area

pIPL – posterior inferior parietal lobule

PM –premotor cortex

PPC – posterior parietal cortices

RF – receptive field

RP – readiness potential, (LRP: lateralized RP)

SMC – sensory motor cortices

SC – superior colliculus

TFR – time-frequency analysis

W judgment – willing or wanting to move

Appendix A: Individual Virtual Sensor Data (fast motion in the right visual field)

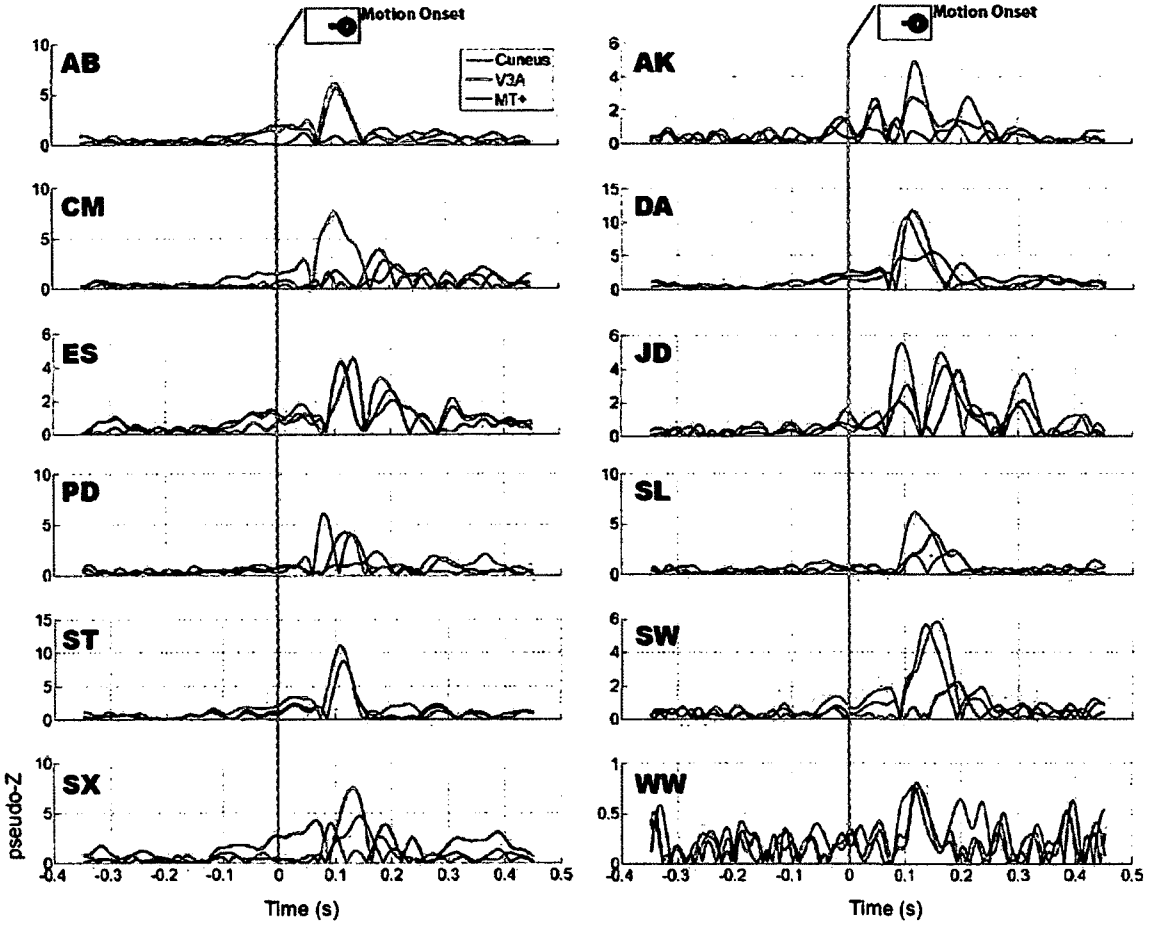

Note: Individual virtual sensor data (pseudo-Z) aligned to the onset of fast motion in the right visual field. Most of the subjects showed clear visually evoked responses, but subject WW demonstrated relatively lower signal-to-noise ratio than the other subjects in this condition. To demonstrate the individual differences in activation amplitude, all the subjects' data were not normalized.

Appendix B: Individual Virtual Sensor Data (slow motion in the right visual field)

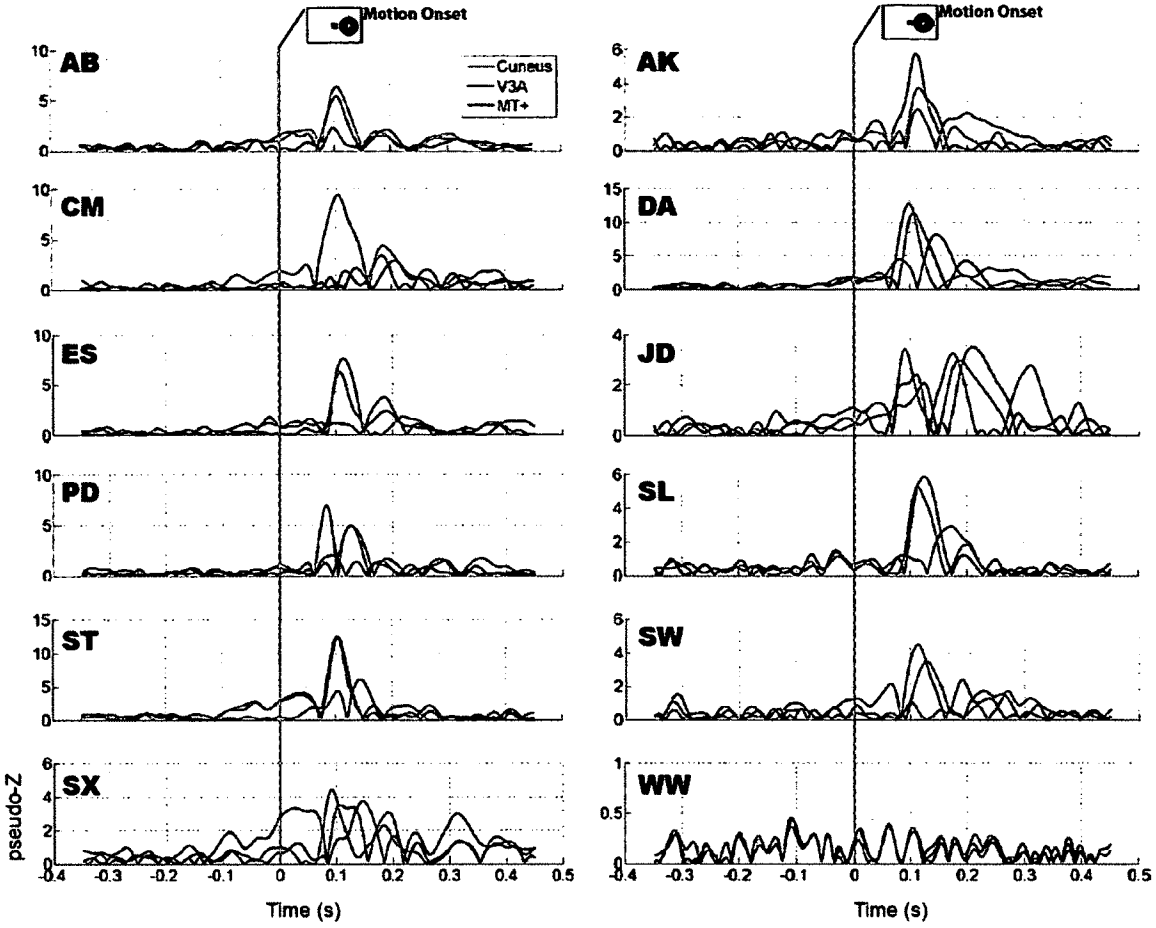

Note: Individual virtual sensor data (pseudo-Z) aligned to the onset of slow motion in the right visual field. Most of the subjects showed clear evoked responses from the cuneus, V3A, and MT+ virtual sensors. However, in this condition, subject WW had noisy virtual sensors, and no evoked responses were found. To demonstrate the individual differences in activation amplitude, all the subjects' data were not normalized.

Note: individual erSAM (pseudo-Z) images are overlaid on the MRI images for the left and right visual displays. The peaks of the MT+ source are marked with green dots, and the peak latencies are shown in the right-bottom corner of the images. All the subjects showed contralateral MT+ peaks except for AK had ipsilateral MT+ when the stimuli were displayed in the left visual field.

Appendix D: Individual MT+ Peaks (Slow Motion)

Note: individual erSAM (pseudo-Z) images are overlaid on the MRI images for the left and right visual displays. The peaks of the MT+ source are marked with green dots, and the peak latencies are shown in the right-bottom corner of the images. All the subjects showed contralateral MT+ peaks except for AK had ipsilateral MT+ when the stimuli were displayed in the left visual field.

References

Adams, M. M., Hof, P. R., Gattass, R., Webster, M. J., & Ungerleider, L. G. (2000). Visual cortical projections and chemoarchitecture of macaque monkey pulvinar. *J. Comp, Neurol, 419,* 377–393.

Albright, T. D. (1984). Direction and orientation selectivity of neurons in visual area MT of the macaque. *J Neurophysiol, 52,* 1106–1130.

Albright, T.D. (1993). Cortical processing of visual motion. *Rev Oculomot Res,5,* 177–201.

Allman, J. M., & Kaas, J. H. (1971). A representation of the visual field in the caudal third of the middle temporal gyrus of the owl monkey (*Aotus trivirgatus*). *Brain Res, 31(1),* 85–105.

Amano, K., Nishida, S., & Takeda, T. (2006). MEG responses correlated with the visual perception of velocity change. *Vis Res, 46(3),* 336-345.

Andersen, R.A. (1987). The role of the inferior parietal lobule in spatial perception and visual-motor integration. *In The Handbook of Physiology. Section I: The Nervous System, Volume V. Higher Functions of the Brain Part 2, F. Plum, V.B.* Mountcastle & S.R. Geiger, eds. (Bethesda, MD: American Physiological Society), pp. 483–518.

Andersen, R.A., & Buneo, C.A. (2002). Intentional maps in posterior parietal cortex. *Annu Rev Neurosci, 25,* 189–220.

Andersen, R. A., & Cui, H. (2009). Intention, action planning, and decision-making in parietal-frontal circuits. *Neuron, 63(5)*, 568-583.

Anderson, S.J., Holliday, I.E., Singh, K.D., & Harding, G.F. (1996). Localization and functional analysis of human cortical area V5 using magneto-encephalography. *Proc R Soc B Biol Sci, 263*, 423–431.

Azzopardi, P., & Cowey, A. (2001). Motion discrimination in cortically-blind patients. *Brain, 124*, 30–46.

Azzopardi, P., Fallah, M., Gross, C. G., & Rodman, H. R. (1998). Responses of neurons in visual areas MT and MST after lesions of striate cortex in macaque monkeys. *Society for Neuroscience Abstracts*, 24, 648.

Azzopardi, P., Fallah, M., Gross, C.G., & Rodman, H.R. (2003). Response latencies of neurons in visual areas MT and MST of monkeys with striate cortex lesions. *Neuropsychologia, 41(13)*, 1738-1756.

Bach, M., & Hoffmann, M. B. (2000). Visual motion detection in man is governed by non-retinal mechanisms. *Vis Res, 40(18)*, 2379-2385.

Bach, M., Ullrich, D. (1994). Motion adaptation governs the shape of motion evoked cortical potentials. *Vision Res, 34*, 1541–1547.

Ball, T., Schreiber, A., Feige, B., Wagner, M., Lücking, C.H., & Kristeva-Feige, R. (1999) The role of higher-order motor areas in voluntary movement as revealed by high-resolution EEG and fMRI. *Neuroimage, 10*, 682–694.

Barbur, J. L., Ruddock, K. H., & Waterfield, V. A. (1980). Human visual responses in the absence of the geniculo-calcarine projection. *Brain 103(4)*, 905-928.

Barbur, J. L., Watson, J. D., Frackowiak, R. S. J., & Zeki, S. (1993). Conscious visual perception without V1. *Brain, 116*, 1293–1302.

Barton, J. J., & Sharpe, J. A. (1997). Motion direction discrimination in blind hemifields. *Ann Neurol, 41*, 255–264.

Baumann, M.A., Fluet, M.-C., & Scherberger, H. (2009). Context-specific grasp movement representation in the anterior intraparietal area. *J Neurosci, 29*, 6436–6448.

Beauchamp, M.S., Cox, R.W., & DeYoe, E.A. (1997) Graded effects of spatial and featural attention on human area MT and associated motion processing areas. *J Neurophysiol, 78*, 516–520.

Beckers, G., & Zeki, S. (1995). The consequences of inactivating areas V1 and V5 on visual motion perception. *Brain, 118(1)*, 49-60.

Behrmann, M., Geng, J.J., & Shomste, S. (2004). Parietal cortex and attention. . *Curr Opin Neurobiol, 14(2)*, 212-217.

Berman, R. A., & Wurtz, R. H. (2008). Exploring the pulvinar path to visual cortex. Progress in Brain Research. K. Christopher and R. J. Leigh, Elsevier. Volume 171: 467-473.

Billino, J., Braun, D. I., Bohm, K. D., Bremmer, F., & Gegenfurtner, K. R. (2009). Cortical networks for motion processing: Effects of focal brain lesions on perception of different motion types. *Neuropsychologia, 47(10),* 2133-2144.

Bisley, J. W., Krishna, B. S., & Goldberg, M. E. (2004). A rapid and precise on-response in posterior parietal cortex. *J Neurosci, 24(8),* 1833-1838.

Borg-Graham, L. J. (2001). The computation of directional selectivity in the retina occurs presynaptic to the ganglion cell. *Nature Neurosci, 4*, 176–183.

Born, R. T., & Bradley, D. C. (2005). Structure and function of visual area MT. *Annu Rev Neurosci, 28(1)*, 157-189.

Boussaoud, D., Ungerleider, L. G., & Desimone, R. (1990). Pathways for motion analysis: Cortical connections of the medial superior temporal and fundus of the superior temporal visual areas in the macaque. *J Comp Neurol, 296,* 462–495.

Bridge, H., Thomas, O., Jbabdi, S., & Cowey, A. (2008). Changes in connectivity after visual cortical brain damage underlie altered visual function. *Brain 131(6)*, 1433-1444.

Bullier, J. (2001). Integrated model of visual processing. *Brain Res Rev, 36(2-3)*, 96-107.

Burnod, Y., Baraduc, P., Battaglia-Mayer, A., Guigon, E., Koechlin, E., Ferraina, S., Lacquaniti, F., & Caminiti, R. (1999). Parieto-frontal coding of reaching: an integrated framework. *Exp Brain Res, 129*, 325–346.

Burr, D. C. (1981). Temporal summation of moving images by the human visual system. *P Roy Soc Lond B Bio, 211*, 321-339.

Calton, J. L., Dickinson, A. R., & Snyder, L.H. (2002). Non-spatial, motor-specific activation in posterior parietal cortex. *Nat Neurosci, 5(6)*, 580-588.

Carter, C. S., Botvinick, M. M., & Cohen, J. D. (1999). The contribution of the anterior cingulate cortex to executive processes in cognition. *Rev Neurosci,*

10, 49–57.

Cavada, C, & Goldman-Rakic, P.S. (1989). Posterior parietal cortex in rhesus monkey. I. Parcellation of areas based on distinctive limbic and sensory corticocortical connections. *J Comp Neurol, 287*,393–421.

Cheyne, D., Bakhtazad, L., & Gaetz, W. (2006). Spatiotemporal mapping of cortical activity accompanying voluntary movements using an event-related beamforming approach. *Hum Brain Mapp, 27(3)*, 213-229.

Cheyne, D., Bostan, A.C., Gaetz, W., & Pang, E. W. (2007). Event-related beamforming: A robust method for presurgical functional mapping using MEG. *Clin Neurophysiol, 118(8)*, 1691-1704.

Churchland, A. K., Kiani, R., Chaudhuri, R., Wang, X. J., Pouget, A., & Shadlen, M. N. (2011). Variance as a signature of neural computations during decision making. *Neuron, 69(4)*, 818-831.

Churchland, A. K., Kiani, R., & Shadlen, M. N. (2008). Decision-making with multiple alternatives. *Nat Neurosci, 11(6)*, 693-702.

Cisek, P. (2007). Cortical mechanisms of action selection: the affordance competition hypothesis. *Philos T Roy Soc B, 362(1485)*, 1585-1599.

Colby, C.L., & Goldberg, M.E., (1999). Space and attention in parietal cortex. *Annu Rev Neurosci*, 22, 319–349.

Corbetta, M. (1998). Frontoparietal cortical networks for directing attention and the eye to visual locations: Identical, independent, or overlapping neural□systems? *P Natl Acad Sci USA, 95(3)*, 831- 838.

Cornette, L., Dupont, P., Rosier, A., Sunaert, S., Van Hecke, P., Michiels, J., Mortelmans, L., & Orban, G.A. (1998). Human brain regions involved in direction discrimination. *J Neurophysiol, 79(5)*, 2749-2765.

Conover, W. J. (1980). *Practical Nonparametric Statistics*. Hoboken, NJ: John Wiley & Sons, Inc.

Cowey, A. (2010). The blindsight saga. *Exp Brain Res, 200(1)*, 3-24.

Cowey, A., & Azzopardi, P. (2001). Is blindsight motion-blind? In B. de Gelder, E. de Haan, & C. Heywood (Eds.), Out of mind: Varieties of unconscious processing. Oxford: Oxford University Press.

Cusick, C. G., Scripter, J. L., Darensbourg, J. G., & Weber, J. T. (1993). Chemoarchitectonic subdivisions of the visual pulvinar in monkeys and their connectional relations with the middle temporal and rostral dorsolateral visual areas, MT and DLr. *J Comp Neurol, 336,* 1–30.

Derrington, A. M., & Lennie, P. (1984). Spatial and temporal contrast sensitivities of neurons in lateral geniculate nucleus of macaque. *J Physiol, 357*, 219-40.

DeSouza, J. F. X., Dukelow, S. P., Gati, J. S., Menon, R. S., Andersen, R. A., & Vilis, T. (2000). Eye position signal modulates a human parietal pointing region during memory-guided movements. *J Neurosci, 20(15)*, 5835-5840.

DeSouza, J. F. X., Menon, R. S., & Everling, S. (2003). Preparatory set associated with pro-saccades and anti-saccades in humans investigated with event-related fMRI. *J Neurophysiol, 89(2)*, 1016-1023.

Desmurget, M., Reilly, K.T., Richard, N., Szathmari, A., Mottolese, C., & Sirigu, A.

(2009a). Movement intention after parietal cortex stimulation in humans. *Science, 324*, 811–813.

Desmurget, M., & Sirigu, A. (2009b). A parietal-premotor network for movement intention and motor awareness. *Trends Cogn Sci, 13(10)*, 411-419.

Donner, T. H., Siegel, M., Fries, P., & Engel, A. K. (2009). Buildup of choice-predictive activity in human motor cortex during perceptual decision making. *Curr Biol, 19(18)*, 1581-1585.

Donner, T. H., Siegel, M., Oostenveld, R., Fries, P., Bauer, M., & Engel, A. K. (2007). Population activity in the human dorsal pathway predicts the accuracy of visual motion detection. *J Neurophysiol, 98(1),* 345-359.

Dubner, R. & Zeki, S.M. (1971). Response properties and receptive fields of cells in an anatomically defined region of the superior temporal sulcus in the monkey, *Brain Res, 35(2)*, 528–532.

Dukelow, S.P., DeSouza, J.F.X., Bhanji, A., Gati, J.S., Menon, R.S., & Vilis, T. (1997). Speed sensitivity in human area MT/V5 as determined by fMRI. *Society for Neuroscience Abstracts*, 23.

Dukelow, S. P., DeSouza J. F. X., Culham, J.C., van den Berg, A.V., Menon, R.S., & Vilis, T. (2001). Distinguishing subregions of the human MT+ complex using visual fields and pursuit eye movements. *J Neurophysiol, 86(4)*, 1991-2000.

Dumoulin, S.O., Bittar, R.G., Kabani, N.J., Baker, C.L. Jr., Le Goualher, G., Pike, G.B., & Evans, A.C. (2000). A new anatomical landmark for reliable

identification of human area V5/MT: a quantitative analysis of sulcal patterning. *Cereb Cortex, 10*, 454–463.

Dupont, P., Orban, G.A., de Bruyn, B., Verbruggen, A., & Mortelmans, L. (1994). Many areas in the human brain respond to visual motion. *J Neurophysiol, 72*, 1420–1424.

Dupont, P., de Bruyn, B., Vandenberghe, R., Rosier, A-M., Michiels, J., Marchal, G., Mortelmans, L., & Orban, G.A. (1997). The kinetic occipital region in human visual cortex. *Cereb Cortex, 7*, 283–292

Egeth, H. E., & Yantis, S. (1997). Visual attention: Control, representation, and time course. *Annu Rev Psychol, 48,* 269–297.

Eimer, M. (1998). The lateralized readiness potential as an on-line measure of central response activation processes. *Behav Res Meth Ins C, 30*, 146–156.

Everling, S., & DeSouza, J. F. X. (2005). Rule-dependent activity for prosaccades and antisaccades in the primate prefrontal cortex. *J Cogn Neurosci, 17(9)*, 1483-1496.

Falkenstein, M., Hohnsbein, J., Hoorman, J. & Blanke, L. (1991). Effects of crossmodal divided attention on late ERP components. II. Error processing in choice reaction tasks. *Electroencephalogr Clin Neurophysiol*, 78, 447–455.

Felleman, D.J. & Van Essen, D.C. (1987). Receptive field properties of neurons in area V3 of the macaque monkey. *J Neurophysiol, 58*, 889–920.

ffytche, D. H., Guy, C. N., & Zeki, S. (1995). The parallel visual motion inputs into

areas V1 and V5 of human cerebral cortex. *Brain, 118*, 1375–1394.

ffytche, D. H., Guy, C. N., & Zeki, S. (1996). Motion specific responses from a blind hemifield. *Brain, 119*, 1971–1982.

Fairchild, M. D. (2005). *Color appearance models*. Chichester, West Sussex, England ; Hoboken, NJ : J. Wiley. ISBN: 0470012161.

Fogassi, L., Ferrari, P.F., Gesierich, B., Rozzi, S., Chersi, F., & Rizzolatti, G. (2005). Parietal lobe: from action organization to intention understanding. *Science, 308*, 662–667.

Fried, I., Katz, A., McCarthy, G., Sass, K.J., Williamson, P., Spencer, S.S., & Spencer, D.D. (1991). Functional organization of human supplementary motor cortex studied by electrical stimulation. *J Neurosci, 11*, 3656–3666.

Fried, S.I., Münch, T.A., & Werblin, F.S. (2002). Mechanisms and circuitry underlying directional selectivity in the retina. Nature, 420, 411–414.

Gaetz, W., MacDonald, M., Cheyne, D. O., & Snead, O.C. (2010). Neuromagnetic imaging of movement-related cortical oscillations in children and adults: Age predicts post-movement beta rebound. *NeuroImage, 51(2),* 792-807.

Gegenfurtner, K.R., Kiper, D.C. & Levitt, J.B. (1997). Functional properties of neurons in macaque area V3. *J Neurophysiol, 77*, 1906–1923.

Gehring, W. J., Goss, B., Coles, M. G. H., Meyer, D. E., & Donchin, E. (1993). A neural system for error detection and compensation. *Psychol, Sci, 4,* 385–390.

Geyer, S., Matelli, M., Luppino, G., & Zilles, K. (2000). Functional neuroanatomy

of the primate isocortical motor system. *Anat Embryol, 202(6)*, 443-474.

Giaschi, D., Zwicker, A., Young, S. A., & Bjornson, B. (2007). The role of cortical area V5/MT+ in speed-tuned directional anisotropies in global motion perception. *Vis Res, 47(7),* 887-898.

Girard, P., Salin, P. A., & Bullier, J. (1992). Response selectivity of neurons in area MT of the macaque monkey during reversible inactivation of area V1. *J Neurophysiol, 67*, 1437–1446.

Gnadt, J.W., & Andersen, R.A. (1988). Memory related motor planning activity in posterior parietal cortex of macaque. *Exp Brain Res, 70*, 216–220.

Goebel, R., Khorram-Sefat, D., Muckli, L., Hacker, H., & Singer, W. (1998). The constructive nature of vision: direct evidence from fMRI studies of apparent motion and motion imagery. *Eur J Neurosci, 10*, 1563–1573.

Gold, J.I., & Shadlen, M.N. (2007). The neural basis of decision making. *Annu Rev Neurosci, 30*, 535–574.

Goodale, M. A., & Milner, A. D. (1992). Separate visual pathways for perception and action. *Trends Neurosci, 15(1),* 20-25.

Gouras, P. (1969). Antidromic responses of orthodromically identified ganglion cells in monkey retina. *J. Physiol, 204*, 407-19.

Greenlee, M.W. (2000). Human cortical areas underlying the perception of optic flow: brain imaging studies. *Int Rev Neurobiol, 44*, 269-292.

Grieve, K.L., Acuna, C, & Cudiero, J. (2000). The primate pulvinar nuclei: vision and action. *Trends Neurosci 23*, 35–39.

Grossberg, S., & Pilly, P. K. (2008). Temporal dynamics of decision-making during motion perception in the visual cortex. *Vision res, 48(12)*, 1345-1373.

Gur, M., & Snodderly, D. M. (2007). Direction selectivity in V1 of alert monkeys: evidence for parallel pathways for motion processing. *J Physiol, 585(2),* 383-400.

Haarmeier, T., Thier, P., Repnow, M., & Petersen, D. (1997). False perception of motion in a patient who cannot compensate for eye movements. *Nature, 389 (6653)*, 849-852.

Haggard, P., & Eimer, M. (1999). On the relation between brain potentials and the awareness of voluntary movements. *Exp Brain Res, 126*, 128–133.

Hari, R., Parkkonen, L., & Nangini, C. (2010). The brain in time: insights from neuromagnetic recordings. *Ann NY Acad Sci,1191(1),* 89-109.

Hasnain, M.K., Fox, P.T., & Woldorff, M.G. (1998). Intersubject variability of functional areas in the human visual cortex. *Hum Brain Map, 6*, 301–315.

Harvey, M, Butler, S. H., Ludwig, C. J. H., Muir, K., Bone, I., Duncan, G., Gilchrist, I. D., & Reeves, I. (2006). Magnocellular impairment drives size distortion in hemispatial neglect. *Perception, (35),* 231.

Heilman, K.M., & van den Abell, T. (1980). Right hemisphere dominance for attention: The mechanism underlying hemispheric asymmetries of inattention (neglect). *Neurology, 30*, 327–330.

Hess, R. F., Baker Jr., C. L., & Zihl, J. (1989). The 'motion-blind' patient: Low-level spatial and temporal filters. *J Neurosci, 9*, 1628–1640.

Hesse, M. D., Thiel, C. M., Stephan, K.E., & Fink, G.R. (2006). The left parietal cortex and motor intention: An event-related functional magnetic resonance imaging study. *Neurosci, 140(4)*, 1209-1221.

Hicks, T. P., Lee, B. B., & Vidyasagar, T. R. (1983). The responses of cells in the macaque lateral geniculate nucleus to sinusoidal gratings. *J Physiol, 337*, 183-200.

Horton, J.C., & Hoyt, W.F. (1991). The representation of the visual field in human striate cortex. A revision of the classic Holmes map. *Arch Ophthalmol, 109*, 816-24.

Hubel, D.H. (1963). The visual cortex of the brain. *Scientific American 1963;209*, 54-62.

Hugh, D., Edward, S., & Perkins, M.D. (2008). *Human eye*. Encyclopedia Britannica.

Hyvärinen, J. (1982). Posterior Parietal Lobe of the Primate Brain. *J Physiol Rev, 62*, 1060.

Ikeda, A., Lüders, H.O., Burgess, R.C., & Shibasaki, H. (1992). Movement-related potentials recorded from supplementary motor area and primary motor area. Role of supplementary motor area in voluntary movements, *Brain, 115 (4)*, 1017–1043.

Itaya, S. K., & Van Hoesen, G. W. (1983). Retinal projections to the inferior and medial pulvinar in the Old-World monkey. *Brain Res. 269*, 223–230.

Johnson, P.B., Ferraina, S., Bianchi, L., & Caminiti, R. (1996). Cortical networks

for visual reaching: physiological and anatomical organization of frontal and parietal lobe arm regions. *Cereb Cortex, 6*, 102–119.

Kaas, J. H., & Lyon, D. C. (2007). Pulvinar contributions to the dorsal and ventral streams of visual processing in primates. *Brain Res Rev, 55(2)*, 285-296.

Kalaska, J.F., Scott, S.H., Cisek, P., & Sergio, L.E. (1997). Cortical control of reaching movements. *Curr Opin Neurobiol.*, *7*, 849–859.

Kandel, E.R., Schwartz, J.H., Jessell, T.M. (2000). *Principles of Neural Science, 4th ed.* McGraw-Hill, New York.

Kaneoke, Y. (2006). Magnetoencephalography: In search of neural processes for visual motion information. *Prog Neurobiol, 80(5)*, 219-240.

Kaplan, E., & Shapley, R. M. (1982). X and Y cells in the lateral geniculate nucleus of macaque monkeys. *J Physiol, 330*, 125- 43.

Khoe, W., Mitchell, J. F., Reynolds, J. H., & Hillyard, S. A. (2005). Exogenous attentional selection of transparent superimposed surfaces modulates early event-related potentials. *Vis Res, 45,* 3004–3014.

Kiani, R., Hanks, T. D., & Shadlen, M. N. (2008). bounded integration in parietal cortex underlies decisions even when viewing duration is dictated by the environment. *J Neurosci, 28(12)*, 3017-3029.

Kiani, R., & Shadlen, M. N. (2009). Representation of Confidence Associated with a Decision by Neurons in the Parietal Cortex. *Science, 324(5928)*, 759-764.

Kiebel, S.J., & Friston, K.J. (2004). Statistical parametric mapping for event-related potentials (II): a hierarchical temporal model. *Neuroimage, 22*,

503–520.

Kiebel, S. J., Tallon-Baudry, C., & Friston, k. J. (2005). Parametric analysis of oscillatory activity as measured with EEG/MEG. *Hum Brain Mapp, 26(3)*, 170-177.

Klimesch, W., Sauseng, P., & Hanslmayr, S. (2007). EEG alpha oscillations: the inhibition-timing hypothesis. *Brain Res Rev, 53,* 63– 88.

Krams, M., Rushworth, M.F., Deiber, M.P., Frackowiak, R.S., & Passingham, R.E., (1998). The preparation, execution and suppression of copied movements in the human brain. *Exp Brain Res, 120*, 386–398.

Krekelberg, B., van Wezel, R.J., & Albright, T.D. (2006a). Adaptation in macaque MT reduces perceived speed and improves speed discrimination. *J Neurophysiol, 95*, 255–270.

Krekelberg, B., van Wezel, R.J., & Albright, T.D. (2006b). Interactions between speed and contrast tuning in the middle temporal area: implications for the neural code for speed. *J Neurosci, 26*, 8988–8998.

Kuba, M., & Kubova, Z. (1992). Visual evoked potentials specific for motion onset. *Doc Ophthalmol, 80*, 83–89.

Kubova, Z., Kuba, M., Hubacek, J., & Vit, F. (1990). Properties of visual evoked potentials to onset of movement on a television screen. *Doc Ophthalmol, 75*, 67–72.

Kubova, Z., Kuba, M., Spekreijse, H., & Blakemore, C. (1995). Contrast dependence of motion-onset and pattern-reversal evoked potentials. *Vis Res,*

35, 197–205.

Kulikowski, J. J., Robson, A. G., & Murray, I. J. (2002). Scalp VEPs and intra-cortical responses to chromatic and achromatic stimuli in primates. *Doc Ophthalmol, 105*, 243–279.

Kurata, K., & Tanji, J. (1986). Premotor cortex neurons in macaques: activity before distal and proximal forelimb movements, *Neurosci, 6*, 403–411.

Lacquaniti, F., Guigon, E., Bianchi, L., Ferraina, S., & Caminiti, R. (1995). Representing spatial information for limb movement: role of area 5 in the monkey. *Cereb Cortex, 5*, 391–409.

Lagnado, L., & Baylor D. (1992). Signal flow in visual transduction. *Neuron, 8,* 955–1002.

Lalancette, M., Quraan, M., & Cheyne, D. (2011). Evaluation of multiple-sphere head models for MEG source localization. *Phys Med Biol, 56*, 5621–5635

Laycock, R., Crewther, D. P., Fitzgerald, P. B., & Crewther, S. G. (2007). Evidence for fast signals and later processing in human V1/V2 and V5/MT+: a TMS study of motion perception. *J Neurophysiol, 98(3)*, 1253-1262.

Libet, B., Gleason, C.A., Wright, E.W., & Pearl, D.K. (1983). Time of conscious intention to act in relation to onset of cerebral activity (readiness-potential). The unconscious initiation of a freely voluntary act. *Brain, 106 (Pt 3)*, 623–642.

Lin, C. S., & Kaas, J. H. (1979). The inferior pulvinar complex in owl monkeys: architectonic subdivisions and patterns of input from the superior colliculus

and subdivisions of visual cortex. *J Comp Neurol, 187*, 655–678.

Liu, J., & Newsome, W.T. (2005). Correlation between speed perception and neural activity in the middle temporal visual area. *J Neurosci, 25*, 711–722.

Livingstone, M., Hubel, D. H. (1987). Connections between layer 4B of area 17 and thick cytochrome oxidase stripes of area 18 in the squirrel monkey. *J Neurosci*, 7, 3371-77.

Lund, J.S. (1988). Anatomical organization of macaque monkey striate visual cortex. *Annu Rev Neurosci, 11*, 253–288.

Luppino, G., Murata, A., Govoni, P., & Matelli, M. (1999). Largely segregated parietofrontal connections linking rostral intraparietal cortex (areas AIP and VIP) and the ventral premotor cortex (areas F5 and F4), *Exp Brain Res, 128*, 181 - 187.

Makeig, S., Westerfield, M., Jung, T., Enghoff, S., Townsend, J., Courchesne, E., & Sejnowski, T. (2002). Dynamic brain sources of visual evoked responses. *Science, 295*, 690–694.

Malikovic, A., Amunts, K., Schleicher, A., Mohlberg, H., Eickhoff, S.B., Wilms, M., Palomero-Gallagher, N., Armstrong, E., & Zilles, K. (2007). Cytoarchitectonic analysis of the human extrastriate cortex in the region of V5/MT+: a probabilistic, stereotaxic map of area hOc5. *Cereb Cortex, 17*, 562 - 574.

Marconi, B., Genovesio, A., Battaglia-Mayer, A., Ferraina, S., Squatrito, S., Molinari, M., Lacquaniti, F., & Caminiti, R. (2001). Eye-hand coordination during reaching. I. Anatomical relationships between parietal and frontal

cortex. *Cereb Cortex, 11*, 513 - 527.

Maris, E., & Oostenveld, R. (2007). Nonparametric statistical testing of EEG- and MEG-data. *J Neurosci Methods, 164(1)*, 177-190.

Marshall, J.C., & Fink, G.R. (2001). Spatial cognition: where we were and where we are. *Neuroimage, 14*, 2–7.

Martinez-Trujillo, J.C., Cheyne, D., William, G., Simine, E., & Tsotsos, J. K. (2006). Activation of area MT/V5 and the right inferior parietal cortex during the discrimination of transient direction changes in translational motion. *Cereb Cortex*, doi:10.1093/cercor/bhl084.

Maruyama, M., Palomo, D. D., & Ioannides, A. A. (2009). Stimulus-contrast-induced biases in activation order reveal interaction between V1/V2 and human MT+. *Hum Brain Mapp, 30(1)*, 147-162.

Matelli, M., Camarda, R., Glickstein, M., & Rizzolatti, G. (1986). Afferent and efferent projections of the inferior area 6 in the macaque monkey. *J Comp Neurol, 251(3)*, 281-298.

Maunsell, J. H. R. (1987). Physiological evidence for two visual subsystems. In Matters of Intelligence, ed. L. Vaina, *Dordrecht, Holland: Reidel.*

Maunsell, J. H. R., & Newsome, W. T. (1987). Visual processing in monkey extrastriate cortex. *Ann Rev Neurosci, 10*, 363–401.

Maunsell, J. H. R., & van Essen, D. C. (1983a). Functional properties of neurons in middle temporal area of the macaque monkey. I. Selectivity for stimulus direction. *J Neurophysiol, 49*, 1127–1147.

Maunsell, J. H. R., & van Essen, D. C. (1983b). The connections of the middle temporal visual area (MT) and their relationship to a cortical hierarchy in the macaque monkey. *J Neurosci, 3*, 2563–2586.

Maus, G. W., Weigelt, S., Nijhawan, R., & Muckli, L. (2010). Does area V3A predict positions of moving objects? *Front Psychology*, 1.

McKeefry, D. J., Burton, M. P., & Morland, A. B. (2010). The contribution of human cortical area V3A to the perception of chromatic motion: a transcranial magnetic stimulation study. *Eur J Neurosci, 31(3),* 575-584.

McKeefry, D.J., Burton, M.P., Vakrou, C., Barrett, B., & Morland, A. (2008). Induced deficits in speed perception by transcranial magnetic stimulation of human cortical areas V5/MT+. *J Neurosci,* 28, 6848–6857.

Medendorp, W.P., Goltz, H.C., Crawford, J.D., & Vilis, T. (2005). Integration of target and effector information in human posterior parietal cortex for the planning of action. *J Neurophysio, 93(2)*, 954-962.

Merigan, W, H., Byrne, C., & Maunsell, J. H. R. (1991). Does primate motion perception depend on the magnocellular pathway? *J Neurosci, 11*, 3422-29.

Merigan, W. H., & Maunsell, J. H. R. (1993). How parallel are the primate visual pathways? *AnnRev Neurosci, 16(1)*, 369-402.

Mishkin, M., & Ungerleider, L.G. (1982). Contribution of striate inputs to the visuospatial functions of parieto-preoccipital cortex in monkeys. *Behav Brain Res*, 6 (1), 57–77.

Moore, T., & Fallah, M. (2004). *Microstimulation of the Frontal Eye Field and Its*

Effects on Covert Spatial Attention. J Neurophysiol, 91(1), 152-162.

Morrone, M.C., Tosetti, M., Montanaro, D., Fiorentini, A., Cioni, G., & Burr, D.C. (2000). A cortical area that responds specifically to optic flow, revealed by fMRI. *Nat Neurosci, 3(12)*, 1322-1328.

Mountcastle, V. B., Lynch, J. C., Georgopoulos, A., Sakata, H., & Acuna, C. (1975). Posterior parietal association cortex of the monkey: command functions for operations within extrapersonal space. *J Neurophysiol, 38*, 871–908.

Murata, A., Gallese, V., Luppino, G., Kaseda, M., & Sakata, H. (2000). Selectivity for the shape, size, and orientation of objects for grasping in neurons of monkey parietal area AIP. *J Neurophysiol, 83(5)*, 2580-2601.

Nakagawa, S., & Tanaka, S. (1984). Retinal projections to the pulvinar nucleus of the macaque monkey: a re-investigation using autoradiography. *Exp. Brain Res, 57*, 151–157.

Nakamura, Y., & Ohtsuka, K. (1999). Topographical analysis of motion triggered visual-evoked potentials in man. *Jpn J Ophthalmol, 43,* 36–43.

Nassi, J. J., & Callaway, E. M. (2006). Multiple circuits relaying primate parallel visual pathways to the middle temporal area. *J Neurosci, 26*, 12789–12798.

Newsome, W. T., & Pare, E. B. (1988). A selective impairment of motion perception following lesions of the middle temporal visual area (MT). *J Neurosci, 8*, 2201–2211.

Newsome, W. T., Wurtz, R. H., & Dürsteler, M. R., (1985). Deficits in visual motion

processing following ibotenic acid lesions of the middle temporal visual area of the macaque monkey. *J Neurosci, 5*, 825–840.

Nichols, T.E., & Holmes, A.P. (2002). Nonparametric permutation tests for functional neuroimaging: a primer with examples. *Hum Brain Mapp, vol 15*, 1-25.

Niedeggen, M., & Wist, E.R. (1999). Characteristics of visual evoked potentials generated by motion coherence onset. *Brain Res Cogn Brain Res, 8,* 95–105.

Nobre, A.C., Gitelman, D.R., Dias, E.C., & Mesulam, M.M., (2000). Covert visual spatial orienting and saccades: overlapping neural systems. *NeuroImage, 11*, 210–216.

O'Brien, B. J., Abel, P. L., & Olavarria, J. F. (2001). The retinal input to calbindin-D28k-defined subdivisions in macaque inferior pulvinar. *Neurosci. Lett, 312*, 145–148.

Ogren, M. P., & Hendrickson, A. E. (1977). The distribution of pulvinar terminals in visual areas 17 and 18 of the monkey. *Brain Res, 137*, 343–350.

Orban, G. A., Lagae, L., Verri, A., Raiguel, S., Xiao, D., Maes, H., & Torre, V., (1992). First-order analysis of optical flow in monkey brain. *P Natl Acad Sci USA, 89*, 2595–2599.

Orban, G.A., Saunders, R.C., & Vandenbussche, E. (1995). Lesions of the superior temporal cortical motion areas impair speed discrimination in the macaque monkey. *Eur J Neurosci, 7,* 2261–2276.

Padberg, J., Franca, J.G., Cooke, D.F., Soares, J.G., Rosa, M.G., Fiorani, Jr. M., Gattass, R., & Krubitzer, L. (2007). Parallel evolution of cortical areas involved in skilled hand use. *J Neurosci, 27,* 10106–10115.

Palva, S., & Palva, J.M. (2007). New vistas for alpha-frequency band oscillations. *Trends Neurosci, 30,* 150 –158.

Palva, J. M., Palva, S., & Kaila, K. (2005). Phase synchrony among neuronal oscillations in the human cortex. *J Neurosci, 25(15),* 3962-3972.

Pasternak, T., & Merigan, W. H. (1994). Motion perception following lesions of the superior temporal sulcus in the monkey. *Cereb Cortex, 4,* 247–259.

Patel, G. H., He, B. J., & Corbetta, M. (2009). Attentional Networks in the Parietal Cortex. *Encyclopedia of Neuroscience. R. S. Larry. Oxford, Academic Press,* 661-666.

Pesaran, B., Nelson, M. J., & Andersen, R. A. (2008). Free choice activates a decision circuit between frontal and parietal cortex. *Nature, 453(7193),* 406-409.

Petrides, M., & Pandya, D. N. (1984). Projections to the frontal cortex from the posterior parietal region in the rhesus monkey. *J Comp Neurol, 228(1),* 105-116.

Pitzalis, S., Di Russo, F., & Spinelli, D. (2005). Loss of visual information in neglect: The effect of chromatic- versus luminance-contrast stimuli in a "what" task. *Exp Brain Res,* 163, 527–534.

Posner, M.I., & DiGirolamo, G.J. (1998). *Executive attention: Conflict, target*

detection, and cognitive control. In Parasuraman, R. *The attentive brain.* Cambridge, Mass: MIT Press.

Prieto, E. A., Barnikol, U. B., Soler, E. P., Dolan, K., Hesselmann, G., Mohlberg, H., Amunts, K., Zilles, K., Niedeggen, M., & Tass, P. A. (2007). Timing of V1/V2 and V5+ activations during coherent motion of dots: An MEG study. *NeuroImage, 37(4)*, 1384-1395.

Purpura, K., Kaplan, E., & Shapley, R. M. (1988). Background light and the contrastgain of primate P and M retinal ganglion cells. *Proc Natl Acad Sci USA, 85*, 534-537.

Paus, T. (2001). Primate anterior cingulate cortex: Where motor control, drive and cognition interface. *Nat Rev Neurosci, 2(6)*, 417-424.

Rees, G., Friston, K., & Koch, C. (2000). A direct quantitative relationship between the functional properties of human and macaque V5. *Nat Neurosci*, 3(7), 716–723

Rizzolatti, G., Fogassi, L., & Gallese, V. (1997). Parietal cortex: from sight to action. *Curr Opin Neurobiol, 7(4)*, 562-567.

Rodman, H.R., & Albright, T.D. (1987). Coding of visual stimulus velocity in area MT of the macaque. *Vision Res, 27*, 2035–2048.

Rodman, H. R., Gross, C. G., & Albright, T. D. (1989). Afferent basis of visual response properties in area MT of the macaque. I. Effects of striate cortex removal. *J Neurosci, 9*, 2033–2050.

Rodman, H. R., Gross, C. G., & Albright, T. D. (1990). Afferent basis of visual

response properties in area MT of the macaque. II. Effects of superior colliculus removal. *J Neurosci, 10*, 1154–1164.

Roitman, J. D. & Shadlen, M. N. (2002). Response of neurons in the lateral intraparietal area during a combined visual discrimination reaction time task. *J Neurosci, 22(21)*, 9475-9489.

Rudolph, K., & Pasternak, T. (1999). Transient and permanent deficits in motion perception after lesions of cortical areas MT and MST in the macaque monkey. *Curr Biol, 9*, 1047–3211.

Rushworth, M.F.S., Ellison, A., & Walsh, V. (2001). Complementary localization and lateralization of orienting and motor attention. *Nat Neurosci, 4*, 656–661.

Rushworth, M. F. S., Johansen-Berg, H., Göbel, S.M., & Devlin, J.T. (2003). The left parietal and premotor cortices: motor attention and selection. *NeuroImage, 20(Supplement 1)*, S89-S100.

Salzman, C. D., Britten, K. H., & Newsome, W. T. (1990). Cortical microstimulation influences perceptual judgments of motion direction. *Nature, 346*, 174–177.

Salzman, C. D., Murasugi, C. M., Britten, K. H., & Newsome, W.T. (1992). Microstimulation in visual area MT: Effects on direction discrimination performance. *J Neurosci, 12*, 2331–2355.

Sakata, H., Taira, M., Kusunoki, M., Murata, A., & Tanaka, Y. (1997). The parietal association cortex in depth perception and visual control of hand action. *Trends Neurosci, 20*, 350–357.

Schenk, T., Mai, N., Ditterich, J., & Zihl, J. (2000). Can a motion-blind patient

reach for moving objects? *Eur J Neurosci, 12(9)*, 3351-3360.

Schiller, P. H., Logothetis, N. K., & Charles, E. R. (1990). Role of the color-opponent and broad-band channels in vision. *Vis Neurosci, 5,* 321~46

Schiller, P.H. (1992). The ON and OFF channels of the visual system. *Trends Neurosci, 15(3)*, 86–92.

Schiller, P. H., & Malpeli, J. G. (1978). Functional specificity of lateral geniculate nucleus laminae of the rhesus monkey. *J Neurophysiol, 41*,788-97.

Schmolesky, M. T., Wang, Y., Hanes, D. P., Thompson, K. G., Leutgeb, S., Schall, J. D., & Leventhal, A. G. (1998). Signal timing across the macaque visual system. *J Neurophysiol, 79(6)*, 3272-3278.

Schoenfeld, M.A., Heinze, H.J., & Woldorff, M.G. (2002). Unmasking motion processing activity in human brain area V5/MT+ mediated by pathways that bypass primary visual cortex. *Neuroimage, 17(2)*, 769-779.

Schoenfeld, M.A., Woldorff, M., Duzel, E., Scheich, H., Heinze, H.J., & Mangun, G.R. (2003). Form-from-motion: MEG evidence for time course and processing sequence. *J Cogn Neurosci, 15(2)*, 157-172.

Sclar, G., Maunsell, J. H. R., & Lennie, P. (1990). Coding of image contrast in central visual pathways of the macaque monkey. *Vis Res, 30*, 1-10.

Seiffert, A.E., Somers, D.C., Dale, A.M., & Tootell, R.B.H. (2003). Functional MRI studies of human visual motion perception: texture, luminance, attention and after-effects. *Cereb Cortex, 13,* 340–349.

Shadlen, M. N., & Newsome, W. T. (2001). Neural basis of a perceptual decision

in the parietal cortex (area lip) of the rhesus monkey. *J Neurophysiol, 86(4)*, 1916-1936.

Shapley, R., Kaplan, E., & Soodak, R. (1981). Spatial summation and contrast sensitivity of X and Y cells in the lateral geniculate nucleus of the macaque. *Nature, 292*, 543-545.

Shapley, R., & Perry, V.H. (1986). Cat and monkey retinal ganglion cells and their visual functional roles. *Trends Neurosci, 9*, 229-235.

Shipp, S. (2003). The functional logic of cortico-pulvinar connections. Philos Trans R Soc Lond B Biol Sci, 358, 1605–24.

Silveira, L. C. L., & Perry, V. H. (1991). The topography of magnocellular projecting ganglion cells (M ganglion cells) in the primate retina. *Neurosci, 40*, 217-37.

Sincich, L. C., Park, K. F., Wohlgemuth, M. J., & Horton, J. C. (2004). Bypassing V1: a direct geniculate input to area MT. *Nat Neurosci 7(10)*, 1123-1128.

Smith, A.T., Greenlee, M.W., Singh, K.D., Kraemer, F.M., & Hennig, J. (1998). The processing of first- and second-order motion in human visual cortex assessed by functional magnetic resonance imaging (fMRI). *J Neurosci, 18(10)*, 3816-3830.

Snyder, L.H., Batista, A.P., & Andersen, R.A. (1997). Coding of intention in the posterior parietal cortex. *Nature, 386*, 167–170.

Sperling, G., & Melchner, M.J. (1978). The attention operating characteristic: examples from visual search. *Science, 202,* 315–318.

Steinman, B., Steinman, S., & Lehmkuhle, S. (1997). Transient visual attention is dominated by the magnocellular stream. *Vis Res, 37,* 17–23.

Stepniewska, I., (2003). *The pulvinar complex.* In: Kaas, J.H., Collins, C.E. (Eds.), The Primate Visual System. *CRC Press, Boca Raton.*

Stepniewska, I., Qi, H. X., & Kaas, J. H. (1999). Do superior colliculus projection zones in the inferior pulvinar project to MT in primates? *Eur J Neurosci, 11,* 469–480.

Strick, P.L. & Kim, C.C. (1978). Input to primate motor cortex from posterior parietal cortex (Area 5). 1. Demonstration by retrograde transport, *Brain Res, 157,* 325–330.

Sunaert, S., van Hecke, P., Marchal, G., & Orban, G.A. (1999). Motion responsive regions of the human brain. *Exp Brain Res, 127,* 355–370.

Talairach, J., & Tournoux, P. (1988). *Co-planar stereotaxic atlas of the human brain.* Thieme, New York.

Tallon-Baudry, C., & Bertrand, O. (1999). Oscillatory gamma activity in humans and its role in object representation. *Trends Cogn Sci, 3,* 151–162.

Tallon-Baudry, C., Bertrand, O., Delpuech, C., & Permier, J. (1997). Oscillatory gamma-band (30-70 Hz) activity induced by a visual search task in humans. *J Neurosci, 17,* 722–734.

Tanne-Gariepy, J., Boussaoud, D., & Rouiller, E.M. (2002). Parietal inputs to dorsal versus ventral premotor areas in the macaque monkey: evidence for largely segregated visuomotor pathways. *Exp Brain Res, 145,* 91–103.

Tass, P., Rosenblum, M.G., Weule, J., Kurths, J., Pikovsky, A., Volkmann, J., Schnitzler, A., & Freund, H.-J. (1998). Detection of n:m phase locking from noisy data: application to magnetoencephalography. *Phys Rev Lett, 81*, 3291–3294.

Thompson, K. G., Biscoe, K. L., & Sato, T. R. (2005). Neuronal basis of covert spatial attention in the frontal eye field. *J Neurosci, 25(41)*, 9479-9487.

Toni, I., D. Thoenissen, & Zilles, K. (2001). Movement preparation and motor intention. *Neuroimage, 14(1),* S110-S117.

Tootell, R. B. H., Mendola, J. D. Hadjikhani, N. K., Ledden, P. J., Liu, A. K., Reppas, J. B., Sereno, M. I., & Dale, A. M. (1997). Functional Analysis of V3A and Related Areas in Human Visual Cortex. *J Neurosci, 17(18)*, 7060-7078.

Tootell, R.B.H., Reppas, J.B., Kwong, K.K., Malach, R., Born, R.T., Brady, T.J., Rosen, B.R., & Belliveau, J.W. (1995). Functional analysis of human MT and related visual cortical areas using magnetic resonance imaging. *J Neurosci, 15(4)*, 3215–3230.

Ungerleider, L. G., Desimone, R., Galkin, T. W., & Mishkin, M. (1984). Subcortical projections of area MT in the macaque. *J Comp Neurol, 222,* 368–386.

Ungerleider LG, & Mishkin M. (1982). *Two cortical visual systems.* In: DJ Ingle, Goodale, M.A., Mansfield, R.J.W. (eds). Analysis of Visual Behavior, pp. 549-586. Cambridge, MA: MIT Press.

van Dijk, H., Schoffelen, J. M., Oostenveld, R., & Jensen, O. (2008). Prestimulus

oscillatory activity in the alpha band predicts visual discrimination ability. *J Neurosci, 28(8)*, 1816-1823.

Van Essen, D. C., & Gallant, J. L. (1994). Neural mechanisms of form and motion processing in the primate visual system. *Neuron, 13(1),* 1-10.

Vanhatalo, S., Palva, J.M., Holmes, M.D., Miller, J.W., Voipio, J., & Kaila, K. (2004). Infraslow oscillations modulate excitability and interictal epileptic activity in the human cortex during sleep. *Proc Natl Acad Sci USA, 101,* 5053–5057.

Vesia, M., Monteon, J.A., Sergio, L.E., & Crawford, J. D. (2006). Hemispheric asymmetry in memory-guided pointing during single-pulse transcranial magnetic stimulation of human parietal cortex. *J Neurophysio, 96(6)*, 3016-3027.

Vesia, M., Yan, X.G., Henriques, D.Y., Sergio, L.E., & Crawford, J. D. (2008). Transcranial magnetic stimulation over human dorsal–lateral posterior parietal cortex disrupts integration of hand position signals into the reach plan. *J Neurophysio, 100(4)*, 2005-2014.

Villeneuve, M. Y., Kupers, R., Gjedde, A., Ptito, M., & Casanova, C. (2005). Pattern-motion selectivity in the human pulvinar. *NeuroImage, 28(2),* 474-480.

Wandell, B.A., Dumoulin, S.O., & Brewer, A.A. (2007). Visual field maps in human cortex. *Neuron, 56*, 366–383.

Wang, X.J. (2001). Synaptic reverberation underlying mnemonic persistent

activity. *Trends Neurosci, 24*, 455–463.

Warner, C. E., Goldshmit,Y., & Bourne,J. A. (2010). Retinal afferents synapse with relay cells targeting the middle temporal area in the pulvinar and lateral geniculate nuclei. *Frontn Neuroanatomy, 4, 8.*

Watamaniuk, S. N. J., & Sekuler, R. (1992). Temporal and spatial integration in dynamic random-dot stimuli. *Vis Res, 32(12)*, 2341-2347.

Watson, J.D., Myers, R., Frackowiak, R.S., Hajnal, J.V., Woods, R.P., Mazziotta, J.C., Shipp, S., & Zeki, S. (1993). Area V5 of the human brain: evidence from a combined study using positron emission tomography and magnetic resonance imaging. *Cereb Cortex, 3*, 79–94.

Watson, A. B., & Nachmias, J. (1977). Patterns of temporal interaction in the detection of gratings. *Vis Res, 17*, 893-902.

Wiese, H., Stude, P., Nebel, K., de Greiff, A., Forsting, M., Diener, H. C., & Keidel, M. (2004). Movement preparation in self-initiated versus externally triggered movements: an event-related fMRI-study. *Neurosci Lett, 371(2-3)*, 220-225.

Williams, D, Phillips, G., & Sekuler, R. (1986). Hysteresis in the perception of motion direction as evidence for neural cooperativity. *Nature, 324*, 253–255.

Wilms, M., EEickhoff, S. B., Specht, K., Amunts, K., Shah, N.J., Malikovic, A., Fink, G.R. (2005). Human V5/MT+: comparison of functional and cytoarchitectonic data. *Anat Embryol (Berl), 210(5)*, 485-495.

Wise, S.P., Boussaoud, D., Johnson, P.B., & Caminiti, R. (1997). Premotor and parietal cortex: corticocortical connectivity and combinatorial computations.

Annu Rev Neurosci, 20, 25 - 42.

Wong-Riley, M. T. T. (1972). Neuronal and synaptic organization of the normal dorsal lateral geniculate nucleus of the squirrel monkey, Saimiri sciureus. *J Comp Neurol, 144*, 25–59.

Zeki, S. M. (1974). Functional organization of a visual area in the posterior bank of the superior temporal sulcus of the rhesus monkey. *J Physiol, 236*, 549–573.

Zeki, S.M. (1978) The third visual complex of rhesus monkey pre-striate cortex. *J Physiol, 277,* 245–272.

Zeki, S. M. (1998). Parallel processing, asynchronous perception, and a distributed system of consciousness in vision. *Neuroscientist, 4*, 365–372.

Zeki, S. M., Friston, K.J., Kennard, C., & Frackowiak, R.S. (1991). A direct demonstration of functional specialization in human visual cortex. *J Neurosci, 11*, 641–649.

Zeki, S.M., Perry, R.J., & Bartels, A. (2003) The processing of kinetic contours in the brain. *Cereb Cortex, 13*, 189–202.

Zihl, J., von Cramon, D., & Mai, N. (1983). Selective disturbance of movement vision after bilateral brain damage. *Brain, 106*, 313–340.

Zhang, M., & Barash, S. (2000). Neuronal switching of sensorimotor transformations for antisaccades. *Nature, 408(6815)*, 971-975.